University of Torino, Doctorate School of Life Science
PhD Course in Complex Systems for Life Sciences
XXXIII Cycle

PhD Thesis

Cerebral Cavernous Malformation disease: characterization of new pathogenic mechanisms and development of nanotechnology-based therapeutic approaches

Tutor: Prof. Saverio Francesco Retta

Candidate: Andrea Perrelli

Abstract

Cerebral cavernous malformation (CCM) is a cerebrovascular disease of genetic origin affecting 0,5% of the general population. It is characterized by clusters of abnormally dilated and leaky capillaries that predispose to seizures, focal neurological deficits and intracerebral hemorrhage. CCM is caused by loss-of-function mutations in three genes: *KRIT1*, *CCM2* and *CCM3*. Growing evidence demonstrates that KRIT1 protein has pleiotropic effects in cellular homeostasis and defense against oxidative stress and inflammatory conditions, including cell-cell and cell-matrix adhesion, cytoskeleton dynamics, autophagy, redox homeostasis and signaling, and antioxidant and anti-inflammatory responses, pointing to multiple and complex pathogenic effects of KRIT1 loss-of-function. Among others, we demonstrated that KRIT1-loss induces a redox-sensitive sustained upregulation of Nrf2 and Glo1, and a reduction in intracellular levels of MG-modified Hsp70 and Hsp27 proteins. Moreover, it affects the glutathione (GSH) redox system, causing a deficit in the GSH-mediated antioxidant capacity. Overall, these effects lead to a chronic adaptive redox homeostasis that counteracts intrinsic oxidative stress but increases susceptibility to oxidative DNA damage and apoptosis, thus sensitizing cells to further oxidative challenges. Consistently, redox proteomic analyses showed an increased S-glutathionylation of distinct proteins involved in adaptive responses to oxidative stress, including redox-sensitive chaperonins, metabolic enzymes, and cytoskeletal proteins. In addition, we investigated the signaling pathway that regulates KRIT1 functions, including its nucleocytoplasmic shuttling, identifying a key role for protein kinase C (PKC). In particular, we found that PKC activation promotes the cytoplasmic localization of KRIT1, whereas its inhibition leads to KRIT1 nuclear accumulation. Moreover, we demonstrated that the N-terminal region of KRIT1 is crucial for its PKC-dependent nucleocytoplasmic shuttling , and may be a target for PKC-dependent regulatory phosphorylation events. Regarding the therapeutic approaches, which are currently lacking, we developed and tested the efficacy of two alternative combinatorial drug delivery strategies based on platinum and lipid nanoparticles conjugated with different drugs known to rescue molecular and cellular phenotypes of CCM disease. Our results show that the combinatorial targeting of redox signaling and autophagy dysfunctions is effective in rescuing major hallmarks of CCM disease, suggesting its potential for the treatment of this disease. Taken together, our results suggest a major role for redox-sensitive mechanisms in KRIT1 pleiotropic functions and CCM disease pathogenesis, and provide a novel framework for the development of innovative pharmacological strategies to prevent or reverse adverse clinical outcomes of CCM lesions.

Keywords: Cerebral Cavernous Malformation; CCM; cavernous angioma; antioxidant responses; oxidative stress; inflammation; nanoparticles.

1. Introduction

Cerebral Cavernous Malformation (CCM, OMIM 116860), also known as cavernous angioma or cavernoma, is a major vascular dysplasia with a prevalence of 0.5% in the general population, thus affecting approximately 35 million people worldwide (Rigamonti 2011, Fontanella 2015, Flemming 2017). It consists of closely clustered, abnormally dilated and leaky sinusoidal capillaries (caverns) lined by a thin endothelium and devoid of normal vessel structural components, such as pericytes and astrocyte foot processes, that histologically appear as multilobate "mulberry-like" vascular lesions (Zhang, Clatterbuck et al. 2001, Tanriover, Sozen et al. 2013). Diagnosis is commonly made by standard spin-echo magnetic resonance imaging (MRI) at 1.5-, 3- or 7-Tesla, which can effectively detect well circumscribed CCM lesions; however, the unmasking of small lesions is far more likely via gradient-echo (GRE) or susceptibility-weighted imaging (SWI) (Cooper, Campeau et al. 2008, de Souza, Domingues et al. 2008, Campbell, Jabbour et al. 2010). Notably, the prevalence of CCM disease continues to rise worldwide due to the increased detection of CCM lesions by the widespread use of MRI (Moore, Brown et al. 2014). CCM lesions are predominantly found in the central nervous system (CNS), including brain and spinal cord, but are also known to affect retina, skin and liver. Within the brain, CCM can occur as single or multiple lesions (up to hundreds), ranging in size from a few millimeters to a few centimeters, which can remain clinically silent for a lifetime or unpredictably give rise to clinical symptoms of various type and severity at any age, including recurrent headaches, focal neurological deficits, seizures, stroke, and even fatal intracerebral hemorrhage (ICH) (Batra, Lin et al. 2009, Rigamonti 2011, Fontanella 2015, Flemming 2017). Indeed, despite the high prevalence of CCM lesions, only approximately 30% of affected people will eventually develop clinical symptoms, which are extremely variable and highly unpredictable, suggesting that CCM disease onset and severity may depend on the combinatorial contribution of multiple genetic and environmental risk factors (Trapani and Retta 2015, Retta and Glading 2016, Flemming 2017).

CCM is a disease of proven genetic origin that may arise sporadically or is inherited as an autosomal dominant condition with incomplete penetrance and highly variable expressivity (Cavalcanti, Kalani et al. 2012, Choquet, Pawlikowska et al. 2015). The sporadic form (sCCM) accounts for up to 80% of cases and is characterized by a lack of family history of the disease and the general presence of a single lesion on MRI. On the other hand, the familial form (fCCM) accounts for at least 20% of cases and is often characterized by the presence of multiple CCM lesions in the brain, which may show progression in both number and size over time (Choquet, Pawlikowska et al. 2015, Zafar, Quadri et al. 2019). Notably, while in sCCM cases a CCM lesion is frequently observed in close association with a developmental venous anomaly (DVA), such association has never been observed in fCCM

cases, suggesting the possibility of a different developmental mechanism (Petersen, Morrison et al. 2010, Meng, Bai et al. 2014, Brinjikji, El-Masri et al. 2017). Human genetic studies have so far identified three genes whose heterozygous loss-of-function mutations are linked to CCM disease: *CCM1* (*KRIT1*), *CCM2* (*MGC4607*) and *CCM3* (*PDCD10*) (Choquet, Pawlikowska et al. 2015). In particular, *KRIT1* mutations have been associated with over 50% of all familial cases (Choquet, Nelson et al. 2014). However, both clinical reports and accumulating evidence in animal models clearly demonstrate that homozygous loss of CCM genes is not fully sufficient to cause CCM lesion formation and disease progression, suggesting the necessary contribution of additional determinants, including microenvironmental stress events and interindividual variability in stress responses (Retta and Glading 2016, Retta, Perrelli et al. 2020). Consistently, the clinical behavior in individual patients, including the development of numerous and large lesions, and the risk of serious complications, such as ICH, remains highly unpredictable even among family members carrying the same CCM mutation (Trapani and Retta 2015). Indeed, although advances in the understanding of CCM disease pathophysiology have been significant, to date there are no direct therapeutic approaches besides the surgical removal of accessible lesions (Fontanella and Bacigaluppi 2015). A comprehensive understanding of the physiopathological functions of CCM proteins remains therefore a major research challenge for the effective development of preventive and therapeutic strategies. Accumulated evidence points to KRIT1 (Krev-interaction trapped protein 1) as a major regulator of endothelial cell homeostasis and function. KRIT1 is a multidomain scaffold protein shown to form functional complexes with distinct proteins, including CCM2 and CCM3 – the other two proteins associated with CCM disease – as well as ICAP1, Rap1, Heg1, and Nd1-L (Zhang, Clatterbuck et al. 2001, Zhang, Rigamonti et al. 2007). Indeed, there is evidence that KRIT1 forms a signaling platform that plays a key role in the maintenance of endothelial cell-cell junction stability and blood-brain barrier (BBB) integrity by regulating multiple mechanisms (Retta and Glading 2016, Retta, Perrelli et al. 2020). Among others, KRIT1 has been shown to regulate cadherin-mediated cell–cell junctions (Glading, Han et al. 2007), integrin-mediated cell-matrix adhesion (Faurobert, Rome et al. 2013, Liu, Draheim et al. 2013, Macek Jilkova, Lisowska et al. 2014), Rho GTPase-mediated cytoskeleton dynamics (Whitehead, Chan et al. 2009, Stockton, Shenkar et al. 2010), Delta-Notch signaling (Wüstehube, Bartol et al. 2010, Schulz, Wieland et al. 2015, Vieceli Dalla Sega, Mastrocola et al. 2019), vascular endothelial growth factor (VEGF) signaling (DiStefano, Kuebel et al. 2014), and mechano-transduction pathways mediated by blood flow-sensitive transcription factors of the Krüppel-like factor (KLF) family (Renz, Otten et al. 2015). On the other hand, original findings by our group have clearly demonstrated that these pleiotropic functions are a consequence of the main role that KRIT1 plays in the modulation of intracellular redox homeostasis and signaling, including

the regulation of redox-sensitive signaling pathways and mechanisms involved in cellular adaptive responses to oxidative stress and inflammation, such as pro-oxidant and antioxidant pathways and autophagy (Goitre, Balzac et al. 2010, Goitre, De Luca et al. 2014, Marchi, Corricelli et al. 2015, Marchi, Retta et al. 2016, Marchi, Trapani et al. 2016, Retta and Glading 2016, Goitre, DiStefano et al. 2017, Antognelli, Trapani et al. 2018, Antognelli, Trapani et al. 2018, Cianfruglia, Perrelli et al. 2019, Antognelli, Perrelli et al. 2020, Retta, Perrelli et al. 2020). In particular, it was found that KRIT1 loss of function induces an increase in intracellular levels of reactive oxygen species (ROS) via downregulation of FOXO1, a master transcriptional regulator of major antioxidant genes, such as superoxide dismutase 2 (SOD2, also known as MnSOD) (Goitre, Balzac et al. 2010). Furthermore, it was demonstrated that KRIT1 loss of function leads to defective autophagy, and here we show that it also induces a sustained Nrf2-mediated adaptive redox homeostasis, resulting in cellular dysfunctions and enhanced sensitization to oxidative stress and inflammatory insults (Marchi, Corricelli et al. 2015, Antognelli, Trapani et al. 2018, Antognelli, Trapani et al. 2018, Cianfruglia, Perrelli et al. 2019, Antognelli, Perrelli et al. 2020). These findings have thus pointed towards a novel unifying mechanistic scenario based on redox homeostasis and signaling, which reconciles all the pleiotropic physiopathological functions of KRIT1 proposed so far (Marchi, Trapani et al. 2016, Retta and Glading 2016, Retta, Perrelli et al. 2020).

Useful insights into molecular mechanisms underlying the biological roles of KRIT1 have been derived from the functional characterization of its structural motifs and domains, including the identification of specific interacting proteins. In particular, KRIT1 is a 736 amino acid protein that contains distinct protein-protein interaction domains, including a Nudix domain and three NPXY/F motifs within the N-terminal region, four central ankyrin repeats, and a C-terminal clover-shaped FERM domain (Fisher and Boggon 2014, Zhang, Li et al. 2015). This FERM domain is composed of three structurally unrelated subdomains (lobes F1, F2, and F3) featuring a ubiquitin-like fold, a four-helix bundle, and a phosphotyrosine binding (PTB)-like domain, respectively. Collectively, these multiple motifs, domains, and subdomains form various binding sites for distinct interaction partners (Draheim, Fisher et al. 2014, Fisher and Boggon 2014, Zhang, Dubey et al. 2017). As mentioned above, known binding partners of KRIT1 include integrin cytoplasmic domain–associated protein 1α (ICAP1α) (Zhang, Clatterbuck et al. 2001, Zawistowski, Serebriiskii et al. 2002, Liu, Draheim et al. 2013), CCM2 (Zawistowski, Stalheim et al. 2005, Zhang, Rigamonti et al. 2007, Fisher, Liu et al. 2015), sorting nexin 17 (SNX17) (Czubayko, Knauth et al. 2006, Stiegler, Zhang et al. 2014), the actin cytoskeleton-stabilizing protein Nd1-L (Guazzi, Goitre et al. 2012), the membrane anchor protein heart of glass 1 (HEG1) (Kleaveland, Zheng et al. 2009, Gingras, Liu et al. 2012, Gingras,

Puzon-McLaughlin et al. 2013), and the small GTPase Rap1 (Serebriiskii, Estojak et al. 1997, Li, Zhang et al. 2012, Gingras, Puzon-McLaughlin et al. 2013).

KRIT1 has been found in multiple cellular and subcellular compartments, including microtubules, cell boundaries and cell–cell junctions, and the nucleus (Béraud-Dufour, Gautier et al. 2007, Glading, Han et al. 2007, Glading and Ginsberg 2010, Liu, Rigamonti et al. 2011, Draheim, Huet-Calderwood et al. 2017). Indeed, the interactions between KRIT1 and corresponding binding partners appear to regulate KRIT1 trafficking between microtubules and the plasma membrane (Béraud-Dufour, Gautier et al. 2007, Liu, Rigamonti et al. 2011), or between the cytoplasm and the nucleus (Zawistowski, Stalheim et al. 2005, Zhang, Rigamonti et al. 2007, Francalanci, Avolio et al. 2009, Draheim, Huet-Calderwood et al. 2017, Su, Simon et al. 2020), respectively. Furthermore, we and others have also shown that KRIT1 can form intramolecular interactions between its N-terminal NPXY/F motifs and the C-terminal FERM domain (Béraud-Dufour, Gautier et al. 2007, Francalanci, Avolio et al. 2009). Specifically, it has been found that KRIT1 may adopt a closed conformation through a head-to-tail intramolecular interaction involving the third NPXY/F motif at the N-terminus and the PTB subdomain of the FERM domain at the C-terminus (Francalanci, Avolio et al. 2009). This suggested a novel mechanism whereby a signal-regulated conformational switch from the closed to the open state dictates KRIT1 nucleocytoplasmic shuttling and intermolecular interactions, thus presumably impacting its functions (Francalanci, Avolio et al. 2009). Nevertheless, the upstream regulatory proteins and signaling mechanisms that control the subcellular localization of KRIT1 remain to be defined. Among the potential upstream regulators of KRIT1 nucleocytoplasmic shuttling, we focused our attention on members of the protein kinase C (PKC) family of serine/threonine kinases, including PKC isoforms known to play pleiotropic roles in the control of physiological and pathological responses to oxidative stress and inflammation (Gopalakrishna and Jaken 2000, Inoguchi, Sonta et al. 2003, Yan, Li et al. 2008, Giorgi, Agnoletto et al. 2010, Scoditti, Nestola et al. 2014, Steinberg 2015).

Despite the knowledge of different CCM disease phenotypes and pathogenic mechanisms, to date neurosurgical removal of accessible lesions is the only direct therapeutic approach (Fontanella and Bacigaluppi 2015). On the other hand, novel therapeutic approaches aimed at rescuing major molecular and cellular dysfunctions underlying CCM disease pathogenesis and severity are currently emerging, being based mainly on compounds endowed with either antioxidant or autophagy stimulating properties or both. Specifically, well-established antioxidant compounds, such as resveratrol (Carrizzo, Forte et al. 2013), statins (Vaughan and Delanty 1999, Di Napoli 2004), and the SOD-mimetic Tiron (Antognelli, Trapani et al. 2018), display powerful ROS scavenging and pro-autophagic activities (Wang, Li et al. 2018, Ashrafizadeh, Ahmadi et al. 2020). Furthermore, well-

known autophagy stimulators, including rapamycin and Torin1 (Marchi, Corricelli et al. 2015), have been shown to rescue defective autophagy in cellular models of CCM disease, reducing mitochondrial dysfunction and significantly decreasing oxidative stress (Lesniewski, Seals et al. 2017, De Luca, Pedone et al. 2018, Di Domenico, Tramutola et al. 2019, Zhuang, Wang et al. 2020). Recently, also vitamin D and avenanthramides have been suggested as potential innovative therapeutic approaches for CCM disease (Gibson, Zhu et al. 2015, Goitre, DiStefano et al. 2017, Finetti, Moglia et al. 2018, Perrelli, Goitre et al. 2018, Kim, Perrelli et al. 2020). Indeed, the health benefits of natural avenanthramide from oats have been attributed to their antioxidant, anti-inflammatory, and anti-proliferative activities, suggesting their potential implication for prevention and treatment of different human diseases, including cardiovascular and cerebrovascular pathologies, inflammation- and oxidative stress-related diseases, and cancer (Moglia, Goitre et al. 2015, Finetti, Moglia et al. 2018, Perrelli, Goitre et al. 2018). Also, the effectiveness of vitamin D is related to its ability to promote endothelial barrier function and inhibit peripheral vascular diseases by stimulating autophagy and reducing oxidative stress and inflammatory events, including the production of ROS, lipopolysaccharides, and inflammatory cytokines (Gibson, Davis et al. 2015, Kim, Perrelli et al. 2020). These findings opened novel preventive and therapeutic perspectives for CCM disease treatment, suggesting that a promising possibility is the development of a multitargeted combinatorial treatment that simultaneously and synergistically counteract both increased oxidative stress and defective autophagy. To address this possibility, we exploited rapamycin-functionalized platinum nanoparticles (Pt NPs) to develop a multifunctional nanocarrier (De Luca, Pedone et al. 2018), which combines the intrinsic antioxidant activity of Pt NPs (Moglianetti, De Luca et al. 2016, Pedone, Moglianetti et al. 2017) with the autophagy-stimulating activity of rapamycin (Marchi, Corricelli et al. 2015). Furthermore, we focused on an alternative combinatorial drug delivery approach based on solid lipid nanoparticles (SLN, also known as intralipid -IL-). Indeed, there is evidence that lipid nanoparticles, including ILs, are well-suited for the nose-to-brain delivery of therapeutic compounds (Gastaldi, Battaglia et al. 2014, Battaglia, Panciani et al. 2018). In particular, lipid nanoparticulate systems are characterized by high biocompatibility, drug payload, controlled drug release, solvent-free and easy to scale-up preparation methods, and could therefore be employed for the targeted nose-to-brain delivery of therapeutic candidates for CCM disease (Mulder, Strijkers et al. 2004, Saraiva, Praça et al. 2016, Tapeinos, Battaglini et al. 2017, Teixeira, Lopes et al. 2020). A preliminary multitarget combinatorial therapy approach based on the formulation of biocompatible lipid nanoparticles loaded with distinct therapeutic candidates for CCM disease, including avenanthramide, rapamycin and bevacizumab, has already been carried out, leading to promising results.

Overall, the major aims of this thesis were to extend the knowledge of the intricate mechanistic scenario underlying CCM disease pathogenesis, including the emerged major role of the redox-dependent pleiotropic effects associated with KRIT1 loss-of-function, by exploiting the availability of specific cellular models. Furthermore, we attempted to develop innovative nanomedicine strategies based on combinatorial and targeted therapeutic approaches.

2. Results

2.1 KRIT1 loss-of-function induces a chronic Nrf2-mediated adaptive homeostasis that sensitizes cells to oxidative stress

To gain further insights into the role of KRIT1 in redox-sensitive pathways and mechanisms underlying cell defense against oxidative stress, we tested the effects of KRIT1 loss-of-function on the expression levels of Glyoxalase 1 (Glo1), a major redox-dependent cytoprotective enzyme involved in distinct cellular responses to oxidative stress, including induction of epithelial-to-mesenchymal transition (EndMT) and apoptosis (Antognelli, Gambelunghe et al. 2014, Antognelli, Palumbo et al. 2014, Antognelli, Gambelunghe et al. 2015, Antognelli, Gambelunghe et al. 2016). To this end, we took advantage of established cellular models of CCM disease, including KRIT1-knockout MEF cells and KRIT1-silenced human brain microvascular endothelial cells (hBMEC), which previously allowed the identification of new molecules and mechanisms involved in KRIT1 physiopathological functions, opening novel therapeutic perspectives for CCM disease (DiStefano, Kuebel et al. 2014, Gibson, Zhu et al. 2015, Moglia, Goitre et al. 2015, Moglianetti, De Luca et al. 2016). Compared with wild-type (K+/+) and KRIT1–/– MEFs re-expressing KRIT1 (K9/6) cells, KRIT1–/– (K–/–) cells displayed a significantly higher expression of Glo1 both at protein and mRNA levels, suggesting that KRIT1 loss induces the upregulation of Glo1 expression (Fig. 1a-c). Glo1 plays a key role in limiting intracellular accumulation of methylglyoxal (MG), thereby modulating the formation and effects of MG-derived protein glycation adducts. Among these, argpyrimidine (AP) has been shown to play a dual role in the regulation of important cellular processes, including opposite effects on the apoptotic process, depending on its concentration and the cell context. Specifically, high levels of AP can promote cell death, whereas physiological levels are required to drive major cell survival mechanisms (Sakamoto, Mashima et al. 2002, Schalkwijk, van Bezu et al. 2006). Thus, we addressed the possibility that the KRIT1 loss-dependent increase in Glo1 expression was accompanied by a decrease in the intracellular levels of AP adducts. To this end, AP levels in protein extracts from K–/–, K+/+ and K9/6 cells were analyzed by Western Blot with an antibody specifically directed against AP adducts. As a result, we detected two major bands with an approximate molecular

weight of 70 and 27 kDa, whose intensity was lower in K–/– compared to K+/+ and K9/6 cells, indicating that the KRIT1 loss-dependent increase in Glo1 expression and activity was indeed accompanied by a drop in the intracellular levels of AP adducts (Fig. 1d) (Antognelli, Trapani et al. 2018, Antognelli, Trapani et al. 2018). Moreover, in line with experimental observations in K–/– MEF cells, we found that Glo1 was significantly upregulated in KRIT1-silenced versus control hBMEC cells both at protein (Fig. 2a), mRNA (Fig. 2b), and specific activity (Fig. 2c) levels. Furthermore, these events were accompanied by an increase in intracellular levels of oxidative species (Fig. 2d), and a reduced formation of MG-derived AP adducts (Fig. 2e), demonstrating that the upregulation of Glo1 and the downregulation of AP adducts induced by the loss-of-function of KRIT1 can occur in different cellular models, including brain microvascular endothelial cells. Then, to clarify the molecular mechanism underlying the KRIT1 loss-dependent and redox-sensitive upregulation of Glo1, we investigated the possible involvement of Nrf2, the master transcription factor that coordinately regulates cellular defenses against oxidative stress through the induction of genes coding for antioxidant and detoxification enzymes, including Glo1. To this end, nuclear and cytoplasmic extracts of K–/–, K+/+ and K9/6 cells were analyzed to examine the activation of Nrf2 by WB assessment of its nuclear translocation. Indeed, an increased accumulation in the nucleus is a key part of the Nrf2 activation mechanism in stress conditions (Kaspar, Niture et al. 2009, Bryan, Olayanju et al. 2013). The outcomes of these experiments demonstrated that the nuclear to cytoplasmic ratio of Nrf2 was significantly higher in K–/– than K+/+ and K9/6 cells, suggesting that Nrf2 is activated in response to the loss-of-function of KRIT1. Furthermore, consistent with the established transcriptional control of Glo1 by Nrf2 (Xue, Rabbani et al. 2012), the increased nuclear translocation of Nrf2 in K–/– versus K+/+ and K9/6 cells reflected the upregulation of Glo1 mRNA and protein levels (Fig. 3a), suggesting that KRIT1 loss-of-function leads to a sustained upregulation of the Nrf2-Glo1 antioxidant pathway. To test whether the observed activation of Nrf2 was a consequence of the increase in intracellular ROS levels associated with KRIT1 loss-of-function, we analyzed the effects of cell treatment with the ROS scavenger Tiron, using nuclear c-Jun and phospho-c-Jun (P-c-Jun) as controls (Goitre, De Luca et al. 2014). Indeed, we previously demonstrated that nuclear levels of the phosphorylated active form of c-Jun, a critical component of the redox-sensitive dimeric transcription factor complex AP-1 (activating protein 1), are upregulated by KRIT1 loss-of-function in a redox-dependent manner (Goitre, De Luca et al. 2014). Data showed that the antioxidant Tiron rescued both c-Jun and Nrf2 activation occurring in K–/– cells near to levels of K+/+ and K9/6 cells, demonstrating that these activations were redox-sensitive events linked to KRIT1 loss-of-function. Notably, the Tiron-mediated reduction of Nrf2 nuclear levels (Fig. 3b) reflected a correspondent downregulation of Glo1, which is consistent with the reported redox-sensitive transcriptional regulation of Glo1

expression mediated by Nrf2 (Xue, Rabbani et al. 2012). Furthermore, consistent with the activation of Nrf2, we found that the increased nuclear translocation of Nrf2 induced by KRIT1 loss-of-function was associated with the upregulation of heme oxygenase-1 (HO-1) (Fig. 3c), an established Nrf2/ARE-regulated phase II antioxidant and detoxification enzyme that is primarily involved in cytoprotection against oxidative stress-induced cellular damage and apoptosis in various tissues, including the vasculature (Morse, Lin et al. 2009, Loboda, Damulewicz et al. 2016, McSweeney, Warabi et al. 2016). Specifically, Western blot analysis showed a marked increase in the expression levels of HO-1 in K–/– cells as compared with K9/6 cells (Fig. 3c), which was significantly reduced upon cell treatment with the antioxidant Tiron (Fig. 3c). Taken together, these findings suggest that KRIT1 loss-of-function leads to the redox-sensitive activation of Nrf2 and consequent upregulation of its downstream targets (Antognelli, Trapani et al. 2018, Antognelli, Trapani et al. 2018, Antognelli, Perrelli et al. 2020, Retta, Perrelli et al. 2020). Furthermore, we addressed the possibility that the redox-sensitive phosphorylation and activation of JNK associated with KRIT1 loss-of-function (Goitre, De Luca et al. 2014) could reside upstream of the upregulation of Nrf2 and its targets HO-1 and Glo1. Consistently, treatment of K–/– cells with the SP600125 JNK inhibitor under the same conditions previously shown to normalize phospho-c-Jun levels (Goitre, De Luca et al. 2014) resulted in a significant inhibition of the increased nuclear localization of Nrf2 (Fig. 4a), and accompanying upregulation of HO-1 (Fig. 4b) and Glo1 (Fig. 4c,d) observed in untreated K–/– cells, indicating that these effects are indeed influenced by the redox-sensitive activation of JNK. Therefore, our results suggest that defective autophagy and redox-dependent activation of JNK induced by KRIT1 loss-of-function contribute to the redox-sensitive activation of Nrf2 and consequent upregulation of its downstream effectors HO-1 and Glo1. In turn, the activation of these Nrf2-mediated stress response pathways could represent an adaptive mechanism by which cells sense and respond to the increased intracellular levels of oxidative species and consequent redox changes caused by KRIT1 loss-of-function (Antognelli, Trapani et al. 2018, Antognelli, Trapani et al. 2018, Retta, Perrelli et al. 2020).

2.2 KRIT1 loss-of-function affects the glutathione redox state leading to enhanced S-glutathionylation of distinct proteins

To further investigate the regulatory role of KRIT1 in cellular redox homeostasis and redox-sensitive mechanisms, we addressed the putative involvement of glutathione (GSH), the most abundant cellular antioxidant and major modulator of the intracellular redox status. The intracellular concentration of GSH, which usually range from 1 to 10 mM, and the ratio of GSH to its oxidized form, glutathione disulfide (GSSG), reflect the redox potential of the cell and thereby influence redox homeostasis, whereas their decrease is generally considered a marker of oxidative stress. Accordingly, under

normal conditions, the GSH/GSSG ratio is closely regulated and maintained at high levels, exceeding 100:1, while in various models of oxidative stress, this ratio has been demonstrated to decrease to values of 10:1 and even 1:1 (Zitka, Skalickova et al. 2012, Giustarini, Galvagni et al. 2015). Furthermore, it is now established that decreased GSH levels and GSH/GSSG ratio correlate with increased cellular susceptibility to oxidative stress and can contribute to some human diseases, including cardiovascular diseases (Ballatori, Krance et al. 2009, Giustarini, Galvagni et al. 2015). The reduced glutathione (GSH) and oxidized glutathione (GSSG) levels, and the GSH/GSSG ratio were comparatively evaluated in K–/– and K9/6 MEF cells. In particular, total glutathione (GSH+GSSG), and GSSG were quantified by specific analytical methods, including an optimized recycling assay that spectrophotometrically measures the reduction of DTNB to TNB in the presence of glutathione reductase (GR) (Akerboom and Sies 1981). The outcomes of these analyses demonstrated that GSH levels were significantly lower in K–/– as compared to K9/6 cells (Fig. 5a,b), suggesting that KRIT1 loss-of-function is associated with a depletion of intracellular glutathione levels, which in turn is indicative of a compromised redox homeostasis. Consistently, the GSH/GSSG ratio resulted significantly reduced in K–/– cells (Fig. 5c), highlighting a detriment of the cellular antioxidant capacity and consequent shift of the intracellular redox state toward a more-oxidizing environment. Furthermore, treatment of K–/– cells with a GSH supply (5 mM final concentration for 4h) determined a significant increase of GSSG levels along with the increase of total GSH (Fig. 5a,b), confirming that depletion of cellular thiols, including GSH, contributes to the redox imbalance associated with KRIT1 loss-of-function. However, a significant rescue of the GSH/GSSG ratio was also observed (Fig. 5c). Given that cellular thiol content is the main determinant of total antioxidant capacity (TAC) (Balcerczyk and Bartosz 2003), we then evaluated TAC levels in K–/– and K9/6 cells using a total oxyradical scavenging capacity (TOSC) assay. As compared to K9/6 cells, TAC levels resulted significantly reduced in K–/– cells (Fig. 5d), suggesting that KRIT1 loss-of-function causes a concomitant depletion of cellular thiols and antioxidant defenses (Cianfruglia, Perrelli et al. 2019, Antognelli, Perrelli et al. 2020). The increased levels of GSSG and decreased ratio of GSH to GSSG observed in K–/– cells clearly indicated a cellular redox imbalance toward a mild oxidative stress condition, raising the possibility that changes in protein S-glutathionylation (PSSG), a highly conserved oxidative post-translational modification (OPTM) consisting of the reversible formation of mixed disulfides between the thiol of GSH and a thiol group of a target protein (Dalle-Donne, Rossi et al. 2007, Dalle-Donne, Rossi et al. 2009, Gallogly, Starke et al. 2009), may also occur. To verify this possibility, the formation of protein-GSH mixed disulfides was examined in K–/– and K9/6 cells by a comparative immunoblotting analysis of total cell extracts with an anti-GSH antibody. Along with S-glutathionylated proteins present in K9/6 cell extracts, immunoblotting analysis of K–

/– cell extracts showed some novel S-glutathionylated protein bands (Fig. 6a), which were abolished by cell pre-treatment with a GSH supply (Fig. 6a, K–/– plus GSH), suggesting that the changes in PSSG associated with KRIT1 loss-of-function are redox-dependent and reversible upon GSH supplementation (Cianfruglia, Perrelli et al. 2019). To further investigate and identify proteins undergoing differential S-glutathionylation in K–/– versus K9/6 cells, protein extracts were separated by two-dimensional polyacrylamide gel electrophoresis (2-D PAGE) and analyzed by mass spectrometry. Analysis of 2-D blots with an anti-GSH antibody showed a higher number of S-glutathionylated proteins in K–/– cells (Fig. 6b), as compared to K9/6 cells (Fig. 6c), suggesting that KRIT1 loss-of-function causes a significant increase in S-glutathionylation of several proteins. To identify these S-glutathionylated proteins, digitized images from Western blot were matched to counterparts from colloidal Coomassie stained gels (Fig. 6d,e), and protein spots corresponding to immunoreactive signals were excised and subjected to mass spectrometry analysis. Twenty out of twenty-six analyzed protein spots were unequivocally identified, as reported in Table 1. The outcomes of these analyses demonstrated that KRIT1 loss-of-function has a striking impact on the pattern of protein S-glutathionylation. Indeed, most of the immunoreactive signals in K–/– cells had no counterparts in K9/6 cells, and corresponded mainly to proteins involved in key processes of cellular homeostasis, stress response, and adaptation, including redox-sensitive enzymes of the energy metabolism, chaperonins, and cytoskeletal proteins (Table 1). Overall, these findings demonstrate that loss-of-function of KRIT1 leads to S-glutathionylation of distinct structural, metabolic, and regulatory proteins involved in cell functions, suggesting important physiopathological implications (Cianfruglia, Perrelli et al. 2019, Antognelli, Perrelli et al. 2020, Retta, Perrelli et al. 2020). Since the redox-dependent changes in PSSG play important roles in endothelial biology, and, in particular, is emerging as a novel redox mechanism of vascular barrier dysfunction implicated in the etiology of human diseases (Galougahi, Liu et al. 2014, Han, Weisbrod et al. 2016), we also investigated whether the upregulation of PSSG adducts observed in K−/− MEF cells could be recapitulated in a different cellular model, more strictly connected to CCM disease, taking advantage of human brain microvascular endothelial cells (hBMEC) (Marchi, Corricelli et al. 2015, Antognelli, Trapani et al. 2018). In line with experimental observations in K−/− MEF cells, we found that PSSG adducts were significantly upregulated in KRIT1-silenced versus control hBMEC cells (Fig. 7), showing that the upregulation of PSSG adducts induced by the loss-of-function of KRIT1 can occur in brain microvascular endothelial cells. Furthermore, and remarkably, this effect was significantly rescued by cell treatment with the antioxidant Tiron, a mitochondria-permeable ROS scavenger previously shown to be effective in rescuing major molecular hallmarks of KRIT1 dysfunctions and CCM disease (Antognelli, Trapani et al. 2018, Antognelli, Trapani et al. 2018), demonstrating that the

accumulation of PSSG adducts is indeed a reversible, redox-dependent phenomenon triggered by KRIT1 loss-of-function (Fig. 7).

2.3 Protein Kinase Cα (PKCα) regulates the nucleocytoplasmic shuttling of KRIT1

Previous structural analyses found that KRIT1 may adopt a closed conformation through a head-to-tail intramolecular interaction involving the third NPXY/F motif at the N-terminus and the PTB subdomain of the FERM domain at the C-terminus (Béraud-Dufour, Gautier et al. 2007, Francalanci, Avolio et al. 2009). These findings suggested a novel mechanism whereby a signal-regulated conformational switch from the closed to the open state dictates KRIT1 nucleocytoplasmic shuttling and intermolecular interactions, thus presumably impacting its functions (Francalanci, Avolio et al. 2009). Nevertheless, the upstream regulatory proteins and signaling mechanisms that control the subcellular localization of KRIT1 remained to be defined. Therefore, we investigated the potential upstream regulation of KRIT1 nucleocytoplasmic shuttling by members of PKC family of serine/threonine kinases, including PKC isoforms known to play pleiotropic roles in the control of physiological and pathological responses to oxidative stress and inflammation (Gopalakrishna and Jaken 2000, Inoguchi, Sonta et al. 2003, Yan, Li et al. 2008, Giorgi, Agnoletto et al. 2010, Scoditti, Nestola et al. 2014, Steinberg 2015). PKC enzymes are structurally defined by a highly conserved C-terminal catalytic domain and an N-terminal regulatory domain, which contains the binding sites for allosteric activators, including diacylglycerol (DAG) and tumor-promoting phorbol esters such as phorbol 12-myristate 13-acetate (PMA) (Mellor and Parker 1998, Newton 2001). Among their established pleiotropic functions, there is also evidence that PKCs are redox-sensitive kinases that phosphorylate Ser and Thr residues in many target proteins to regulate their molecular interactions and subcellular compartmentalization, including cytoplasmic and nuclear distribution and nucleocytoplasmic shuttling, in an isozyme-specific manner (Valovka, Verdier et al. 2003, Goyal, Pandey et al. 2005, Doller, Schlepckow et al. 2010, Giorgi, Agnoletto et al. 2010, Aisiku, Dowal et al. 2011).

To assess the potential role of PKC in regulating KRIT1 nucleocytoplasmic shuttling, non-confluent HeLa cells transiently transfected with an EGFP-tagged KRIT1 cDNA construct (GFP-KRIT1) (Francalanci, Avolio et al. 2009) were either vehicle-treated (vehicle alone) or treated with phorbol 12-myristate 13-acetate (PMA), a well-established activator of cPKCs and nPKCs (Castagna, Takai et al. 1982), and analyzed by fluorescence microscopy to assess GFP-KRIT1 subcellular distribution. As compared to the prevalent nuclear localization of GFP-KRIT1 in vehicle-treated cells (Fig. 8a-c), cell treatment with PMA resulted in a drastic shift in GFP-KRIT1 subcellular distribution towards an almost exclusively cytoplasmic localization (Fig. 8d-f), suggesting that KRIT1 is responsive to PMA-

induced PKC activation. To assess whether the observed effect was indeed due to PKC activation, cells were pre-treated with bisindolylmaleimide I (BIM), a PKC inhibitor that acts as a competitive inhibitor for the ATP binding site of PKC and shows high selectivity for PKCα, β1, β2, γ, δ, and ε isozymes, before treatment with PMA. In contrast to cell treatment with PMA alone (Fig. 8d-f), BIM+PMA treatment did not affect the nuclear localization of GFP-KRIT1 (Fig. 8g-i), confirming a specific role for PKC activation in the regulation of KRIT1 nucleocytoplasmic shuttling.

To investigate whether the PKC-dependent nucleocytoplasmic shuttling of KRIT1 observed in HeLa cells could be recapitulated in an endothelial cellular model, which is more strictly related to CCM disease, we tested the effects of PMA and BIM+PMA treatments on primary human pulmonary artery endothelial cells (HPAECs) transiently transduced with adenoviral mCherry-KRIT1. To make an accurate comparison with the data obtained with HeLa cells, only cells without cell–cell contacts were analyzed. Consistent with our observations in HeLa cells, HPAECs treated with PMA exhibited a significantly enhanced cytoplasmic localization of mCherry-KRIT1 (Fig. 9A, panels g-i) as compared to their vehicle-treated counterparts (Fig. 9A, panels a-c), while mCherry-KRIT1 nuclear localization was not affected in HPAECs treated with either BIM alone (Fig. 9A, panels d-f) or BIM+PMA (Fig. 9A, panels j-l), suggesting that PKC activation induces KRIT1 nucleocytoplasmic shuttling in both epithelial and endothelial cells. The ratio of nuclear-to-cytoplasmic localization was quantified by comparison of fluorescence intensities (Fig. 9B) (De Luca, Perrelli et al. 2020). Previously, we identified KRIT1B, a KRIT1 isoform characterized by the alternative splicing of the 15th coding exon, which accounts for the deletion of the 39 amino acid segment forming the distal β-sheet of the F3/PTB-like subdomain of the FERM domain (Retta, Avolio et al. 2004). Remarkably, it has been previously demonstrated that this isoform exhibits an exclusive cytoplasmic localization despite the presence of a true nuclear localization sequence (NLS) at the N-terminus of the protein (residues 46–51), suggesting that the C-terminal PTB-like subdomain enables the nucleocytoplasmic shuttling of KRIT1, while its alteration confers a restricted cytoplasmic localization (Francalanci, Avolio et al. 2009). Indeed, by taking advantage of the KRIT1B isoform and performing site-directed mutagenesis, my group previously demonstrated that an intact FERM domain is necessary and sufficient for KRIT1 nuclear translocation, whereas the KRIT1 N-terminal region acts mainly as a regulatory arm that counterbalances the constitutive nuclear translocation property of the C-terminal region (Francalanci, Avolio et al. 2009). Consistently, a KRIT1 deletion mutant lacking the N-terminal arm (207 amino acids) showed a constitutive and exclusive localization into the nucleus (Francalanci, Avolio et al. 2009). To evaluate the role of this N-terminal arm in the observed PKC-mediated nucleocytoplasmic shuttling of KRIT1, we transiently transfected HeLa cells with a construct encoding a GFP-tagged KRIT1 deletion mutant devoid of the N-terminal 207 amino acids

(GFP-KRIT1Δ207) and performed fluorescence microscopy analysis to assess its subcellular localization in response to PMA-induced PKC activation. In agreement with previous results (Francalanci, Avolio et al. 2009), the expression of the N-terminal deletion mutant GFP-KRIT1Δ207 in HeLa cells resulted in its constitutive nuclear accumulation (Fig. 10a-c). However, in contrast to full length KRIT1 (Fig. 8d-f), this N-terminal truncated mutant showed only very little, if any, change in its prevalent nuclear localization upon cell treatment with PMA (Fig. 10d-f), with a consequently almost undetectable effect of cell pre-treatment with BIM (Fig. 10g-i). While this evidence does not exclude that KRIT1 C-terminal domains may be partially responsive to PKC activation, it clearly demonstrates that the N-terminal regulatory domain plays a major role in PKC-dependent nucleocytoplasmic shuttling of KRIT1.

Moreover, accumulated evidence demonstrates that distinct PKC isoforms regulate subcellular compartmentalization and nucleocytoplasmic shuttling of various proteins by triggering a simultaneous phosphorylation of different phosphorylation sites within their regulatory domains (Valovka, Verdier et al. 2003, Goyal, Pandey et al. 2005, Doller, Schlepckow et al. 2010, Aisiku, Dowal et al. 2011). In this light, we sought to determine whether the observed nucleus-to-cytoplasm translocation of KRIT1 in response to PKC activation by PMA could be associated with any PKC-mediated phosphorylation of KRIT1. To this end, HeLa cells transiently transfected with EGFP-tagged KRIT1 (GFP-KRIT1) (Francalanci, Avolio et al. 2009) and mCherry-KRIT1 expressing HPAEC were treated with PMA, BIM, BIM+PMA or vehicle (CTRL), and then lysed for subsequent immunoprecipitation and Western blotting analysis of Ser/Thr phosphorylation. Specifically, to assess potential changes in Ser/Thr phosphorylation levels, GFP-KRIT1 and mCherry-KRIT1 were immunoprecipitated from cell lysates with anti-GFP and anti-KRIT1 antibodies, respectively, and analyzed by Western blotting with pan-phospho-Ser/Thr antibodies. As compared to the almost undetectable Ser/Thr phosphorylation of both GFP-KRIT1 and mCherry-KRIT1 in vehicle-treated HeLa cells (CTRL; Fig. 11a) and HPAEC (CTRL; Fig. 11b), respectively, treatment of these cell types with PMA resulted in a significant increase in Ser/Thr phosphorylation levels (PMA; Fig. 11a,b). Ser/Thr phosphorylation was rescued by cell pre-treatment with the PKC inhibitor BIM (BIM+PMA; Fig. 11a,b), suggesting that KRIT1 undergoes Ser/Thr phosphorylation in response to PMA-induced PKC activation in both epithelial and endothelial cells. Consistent with our findings, various high-throughput proteomic studies have indeed demonstrated that KRIT1 can undergo phosphorylation at multiple sites, including Tyr11 (1), Thr20 (2), Ser22 (29), Tyr28 (1), Ser32 (3), Tyr33 (1), Tyr125 (1), Thr147 (1), Thr151 (14), Tyr230 (3), Tyr240 (1), Tyr252 (3), Tyr260 (8), Ser261 (2), Ser274 (7), Ser276 (13), Ser391 (1), Ser430 (1), Tyr431 (1), Ser592 (4), Tyr605 (1), Tyr659 (1), and Thr732 (1), where in parentheses is indicated the number of studies referring to a

specific phosphorylated amino acid residue, as resulting from available phosphorylation databases. Therefore, considering the evidence that PKC activity-dependent regulation of nucleocytoplasmic shuttling of target proteins may require simultaneous phosphorylation of different phosphorylation sites (Doller, Schlepckow et al. 2010), additional KRIT1 phosphorylation sites of lower-stoichiometry might play a role in the modulation of KRIT1 nucleocytoplasmic shuttling. Anyway, further site-directed mutagenesis studies are necessary to address these possibilities, and to determine the effect of phosphorylation in different site in KRIT1.

2.4 Multifunctional Platinum@BSA−Rapamycin Nanocarriers for the combinatorial therapy of CCMs

Despite the significant progress in understanding CCM pathogenesis, a complete knowledge of the pathogenetic mechanisms of CCM disease and a defined therapeutic approach to treat CCM lesion remains an important question. Indeed, at date there are no direct therapeutic strategies for CCM disease besides the surgical removal of accessible lesion in patients with recurrent hemorrhages or intractable seizures or strokes (Fontanella and Bacigaluppi 2015, Fontanella, Panciani et al. 2015, Awad and Polster 2019). However, based on the great multidisciplinary research advances in the identification of pathobiological mechanisms of CCM disease made in the last decade, some imaging and plasma biomarkers of prognostic value and distinct promising pharmacological strategies for preventing or limiting symptomatic disease onset and severity in susceptible individuals have been recently proposed and tested in animal models and pilot small clinical trials (Retta and Glading 2016, Awad and Polster 2019, Mabray, Caprihan et al. 2019). In particular, to address the possibility of developing a combinatorial treatment, simultaneously targeting different molecular dysfunctions associated with CCM disease phenotype, including oxidative stress and defective autophagy, we developed a multifunctional nanocarrier, composed of rapamycin-functionalized platinum nanoparticles (PtNPs) (De Luca, Pedone et al. 2018). The multifunctional nanocarrier was prepared using biocompatible, endotoxin-free, and highly catalytic citrate-capped PtNPs of 5 nm, synthesized as previously reported by Moglianetti and colleagues (Moglianetti, De Luca et al. 2016). The radical scavenging activity of PtNPs was recently proved to restore intracellular redox homeostasis in a cellular model of CCM disease. Although the small size of these NPs may limit their drug loading capacity, their superior antioxidant nanozyme properties (due to their high surface-to-volume ratio) are particularly promising for the combinatorial treatment of CCM (Moglianetti, De Luca et al. 2016). On the other hand, rapamycin was selected for its proven efficacy in rescuing defective autophagy in CCM cells (Marchi, Corricelli et al. 2015, Retta and Glading 2016). Because this drug has low bioavailability (Simamora, Alvarez et al. 2001), we exploited Bovine Serum Albumin (BSA) to

incorporate rapamycin within the hydrophobic pockets of the protein in the attempt to improve its solubilization and delivery, as well as to protect it from degradation (Karimi, Bahrami et al. 2016). To test the activity of our multifunctional platinum@BSA−rapamycin nanocarrier (Pt5@Rapa NPs), we took advantage of KRIT1-knockout mouse embryonic fibroblast (MEF) cells (KRIT1-KO MEFs), which is a well suited *in vitro* model for testing combination approaches based on multifunctional nanocarriers. We first assessed the toxicological profile of the Pt5@Rapa nanocarriers on KRIT1-KO MEF cells. Specifically, the cytocompatibility of Pt5@Rapa NPs was tested at concentrations up to 50 μg/mL for 24 and 48 h, by WST-1 assay. Pt5@Rapa NPs were cytocompatible on MEFs (Fig. 12a), indicating that Pt5 NP conjugation with rapamycin-loaded BSA does not alter their toxicological profile. Moreover, we assessed Pt5@Rapa NP cellular uptake and their intracellular fate by confocal microscopy. Confocal images showed an efficient internalization of Pt5@Rapa NPs and their compartmentalization within lysosomes (Fig. 12b), confirming that NP uptake occurs by endocytosis, as previously demonstrated for nonfunctionalized citrate-capped Pt5 NPs (Moglianetti, De Luca et al. 2016). It has been demonstrated that also rapamycin–polymer conjugates are taken up by the endocytic pathway and compartmentalized within the lysosomes, where the release of the drug takes place (Tai, Chen et al. 2014). Accordingly, it is possible to speculate that, once endocytosed, the attack of peptidases to Pt5@Rapa NPs within lysosomes may induce the release of rapamycin from BSA, leading to rapamycin therapeutic action. Furthermore, growing evidence demonstrate that treatments of the employed cellular model with distinct compounds, endowed with antioxidant properties, were able to reduce intracellular ROS levels and altered redox signaling (Goitre, Balzac et al. 2010, Goitre, De Luca et al. 2014, Moglia, Goitre et al. 2015, Moglianetti, De Luca et al. 2016, Goitre, DiStefano et al. 2017, Antognelli, Trapani et al. 2018, Antognelli, Trapani et al. 2018, Perrelli, Goitre et al. 2018, Cianfruglia, Perrelli et al. 2019, Kim, Perrelli et al. 2020), whereas its treatment with rapamycin was effective in rescuing also defective autophagy. The efficacy of Pt5@Rapa NPs as rapamycin delivery system was tested by quantifying the expression of p62, a typical autophagic marker that accumulates when autophagy is inhibited. The total level of p62 was quantified in lysates of KRIT1-KO MEFs treated with Pt5 or Pt5@Rapa NPs. In parallel, cells were treated with free rapamycin, at a concentration known to restore the physiological p62 expression of wild-type cells (Marchi, Corricelli et al. 2015). Western blot analysis revealed that the accumulation of p62 significantly decreased upon cell treatment with Pt5@Rapa NPs (Fig. 12c,d), indicating that rapamycin delivered by the nanocarrier is able to restore cell autophagy with similar efficiency as the free drug. Conversely, no change in the level of p62 expression was detected in cells treated with nonfunctionalized Pt5 NPs, demonstrating that Pt5 NPs itself does not interfere with autophagy. Citrate-capped Pt5 NPs were recently found to restore ROS homeostasis in KRIT1-KO MEFs

(Moglianetti, De Luca et al. 2016). To assess the ROS scavenging activity of Pt5@Rapa NPs, KRIT1-KO MEFs were treated with citrate-capped Pt5, Pt5, Pt5@Rapa NPs, or free rapamycin and ROS levels were quantified by the dichloro-dihydro-fluorescein diacetate (DCFH-DA) assay. Both Pt5 NPs and the multifunctional nanocarrier citrate-capped exhibited high ROS scavenging potential, which was comparable to that of non-functionalized Pt5 NPs, even though their surface is partially covered by thiols and BSA (Fig. 12e). This suggests that the coating does not interfere with the catalytic reactions. Within the intracellular environment, Pt5@Rapa NPs exert significant antioxidant activity, directly reducing the ROS species, unlike free rapamycin that indirectly regulates the ROS levels by acting on autophagy pathways that control the clearance of ROS-generating dysfunctional mitochondria (Choi, Ryter et al. 2013). Therefore, the drug itself has a weak antioxidant activity. Furthermore, by impairing autophagy and dysregulating ROS homeostasis, loss-of-function of CCM genes, including KRIT1, causes EndMT (Guan and Couldwell 2013, Marchi, Corricelli et al. 2015, Bravi, Malinverno et al. 2016), a process whereby endothelial cells lose their specific markers and cell−cell contacts, weakening their barrier function (Kovacic, Mercader et al. 2012). In light of this mechanism, we tested the efficacy of our multifunctional nanocarrier to attenuate or reverse EndMT and re-establish physiological angiogenesis of KRIT1-depleted endothelial cells, comparing its effect with that of rapamycin alone or PtNPs, by an *in vitro* angiogenesis assay (Fig. 13a). Interestingly, KRIT1-KO HUVECs exposed to Pt5 NPs developed some capillary-like structures, demonstrating that PtNPs can promote the partial recovery of the endothelial phenotype of KRIT1-silenced HUVECs. This might be attributed to the intrinsic property of Pt5 NPs to act as antioxidant nanozymes, being ROS homeostasis crucial for normal endothelial cell function and signaling (Panieri and Santoro 2015). As expected, also rapamycin treatment was found to be effective in reactivating some *in vitro* angiogenesis. Indeed, treatment with rapamycin was previously demonstrated to reverse EndMT by increasing the expression of key endothelial cell markers in KRIT1-KO endothelial cells (Marchi, Corricelli et al. 2015). However, neither the antioxidant treatment with bare nanoparticles nor autophagy induction with rapamycin alone was sufficient to fully inhibit EndMT and restore physiological *in vitro* angiogenesis, further supporting the requirement of a combined treatment with antioxidants and autophagy inducers. Remarkably, KRIT1-KO HUVECs treated with Pt5@Rapa NPs were able to undergo *in vitro* angiogenesis almost comparably to unsilenced cells, thus demonstrating the synergistic effect of the combination of the two therapeutic activities. In conclusion, the loss-of-function of KRIT1 strongly affects autophagy, leading to the aberrant accumulation of p62 and causing an increase in intracellular ROS and the EndMT switch (Fig. 14a). Cell treatment with rapamycin reactivates autophagy, thereby decreasing p62 accumulation, partially reducing the ROS levels and reverting the EndMT switch (Fig. 14b). On

the other hand, given the intrinsic ROS scavenging activity of the Pt5 NPs core and the pro-autophagic activity of the conjugated rapamycin, Pt5@Rapa NPs can directly counteract both increased intracellular ROS levels and defective autophagy, thus exerting synergistic effects that efficiently limit the major molecular and cellular dysfunctions associated with CCM disease phenotype. Such a combined action allows endothelial cells to reacquire their specific phenotype and function (Fig. 14c).

2.5 Solid lipid nanoparticles for drug delivery

Along with synthetic polymers and inorganic materials, also natural polymers and natural lipids are increasingly employed for nanodrug formulations with either diagnostic or therapeutic purposes due to their particular physicochemical and biological properties (Mulder, Strijkers et al. 2004, Battaglia, Panciani et al. 2018, Teixeira, Lopes et al. 2020). Accordingly, we also developed another kind of combinatorial treatment based on lipid nanoparticles (ILs), characterized by good biocompatibility, lower cytotoxicity, easy scale-up preparation, controlled drug release, the avoidance of organic solvents in the preparation methods (Battaglia and Gallarate 2012, Gastaldi, Battaglia et al. 2014, Battaglia, Panciani et al. 2018). Thanks to their size that range from 50 to 1000 nm, ILs in water or oil solution are able to incorporate different drugs without forming aggregate or precipitates, and, consequently, exploited as drug delivery system with a wide potential application spectrum. To analyze the efficacy of drug-loaded lipid nanoparticles as combinatorial treatment, in order to rescue the major molecular dysfunctions associated with CCM disease phenotype, we took advantage of our well established cellular model as previously described (Goitre, Balzac et al. 2010, Goitre, Fornelli et al. 2020). As first step, we analyzed the toxicological profile of lipid nanoparticles at different time by an MTT vitality assay on KRIT1-KO (K–/–) and KRIT1-overexpressing (K9/6) MEF cells, exploiting specific concentrations previously shown to be safe and effective in different *in vitro* models, thus optimizing the concentration of lipid nanoparticles for cell treatments in order to avoid cytotoxic effects, which might be attributed to the suspension in which lipid nanoparticles are dispersed (data not shown). Once established the cytocompatible concentration of our functionalized lipid nanoparticles, we tested their effectiveness in rescuing major molecular phenotypes associated with KRIT1 loss-of-function. To this end, we treated either K–/– and K9/6 MEF cells for 12 hours with lipid nanoparticles conjugated with rapamycin (Rapa), avenanthramide (Avn), bevacizumab (Bvz), or with a mixture of all three compounds (herein indicated as Mix), and analyzed the expression levels of biomarkers of KRIT1 loss-of-function, including oxidative stress-related protein (such as SOD2), endothelial growing factor (VEGF, and its receptor VEGFR), and autophagy (LC3, p62). The results were compared with cells treated with free rapamycin, bevacizumab and avenanthramide, and a mixture of the three compounds, at concentrations known to completely or

partially restore the expression level of markers associated with molecular dysfunctions linked to CCM disease. The outcomes of these experiments showed that SOD2 expression level significantly increased upon treatment with drug-conjugated lipid nanocarriers in K–/– cells, underlying a good intracellular delivery and effectiveness of antioxidant compounds (Fig. 15). On the other hand, no significative change in SOD2 expression was observed in K9/6 cells, and a little increase was observed in cells treated with unfunctionalized lipid nanocarriers, demonstrating that ILs were not completely inert and can play a role during treatments (Fig. 15). Moreover, we found positive effects of cell treatment with drug-conjugated lipid nanocarriers also by analyzing and quantifying the expression levels of the autophagic marker p62. As shown in Fig. 16, p62 expression level importantly decreased after treatment with rapamycin-loaded lipid nanocarriers, indicating that rapamycin delivered by these nanocarriers is able to restore cell autophagy similarly to the free drug (Marchi, Corricelli et al. 2015). Differently from the first two markers, no significant differences were observed in VEGF expression levels in cells treated with nanoparticles carrying bevacizumab (data not shown). Further studies are needed to better understand the variations in VEGF expression and the effects that this marker exerts on cells, as well as the effects that bevacizumab plays in our *in vitro* model. Indeed, whereas few data in literature clearly report the function of VEGF *in vitro* and *in vivo* models of CCM disease (Kar, Samii et al. 2015), little is known about the efficacy of bevacizumab in the treatment of cavernomas. The outcomes of these experiments underline the significant efficacy of potential therapeutic compounds in rescuing major molecular dysfunctions that characterize KRIT1 loss-of-function (Marchi, Corricelli et al. 2015, Moglia, Goitre et al. 2015, Perrelli, Goitre et al. 2018). These results also emphasize the importance of developing a new preventive or even therapeutic treatment for CCM disease, with the specific aim of reducing the risk of onset or decreasing the size of cavernomas, trying to inhibit or completely revert the multiple molecular dysfunctions that characterize the pathogenesis and progression of CCM disease. In particular, the use of biocompatible nanoparticles would allow the conjugated drugs to act directly in the lesion areas. Moreover, a strong advantage is given also by the possibility of combining nanoparticles loaded with different pharmacological compounds within a single treatment, thus creating a mixture endowed with an even more positive effect for disease treatment. Indeed, the efficacy of the combination of different therapeutic properties is clearly visible in the expression levels of the aforementioned markers in K–/– cells treated with the mixture of the three drug-conjugated lipid nanoparticles. However, some experimental procedures have yet to be optimized, including the concentrations of both lipid nanocarriers and loaded drugs for *in vivo* treatments, and the delivery of functionalized nanoparticles into the brain of CCM mouse models.

3. Materials and methods

3.1 Cell culture, lentiviral vector production, and cell transduction

KRIT1 –/– (K–/–) and KRIT1 +/+ (K9/6) Mouse Embryonic Fibroblast (MEF) cell lines were established from KRIT1 –/– and KRIT1 +/+ E8.5 mouse embryos, respectively, using the 3T3 protocol, and cultured at 37°C and 5% CO_2 in DMEM supplemented with 10% FCS, 2 mM glutamine and 100 U/ml penicillin/streptomycin. Human Umbilical Vein Endothelial Cells (HUVECs), purchased from Lonza (CC-2519, Lonza Group Ltd, Switzerland), were cultured on gelatine-coated dishes in M199 medium (Sigma) supplemented with 10% FCS, 10 mg/ml heparin, endothelial cell growth supplement (ECGS, Sigma), glutamine and antibiotics. HeLa cells (ATCC) were cultured in Dulbecco's modified Eagle's medium (DMEM) supplemented with 10% Fetal Bovine Serum (FBS; Life Technologies), 2 mM L-glutamine, 100 U/mL penicillin and 100 mg/mL streptomycin (EuroClone). Primary human pulmonary artery endothelial cells (HPAEC) were cultured in DME/F-12 medium containing 5% FBS, 1X endothelial cell growth supplement (ECGS, ScienCell), 15 U/mL heparin, 100 U/mL penicillin, 100 µg/mL streptomycin, and 0.25 µg/mL amphotericin b. HEK293 cells were cultured for viral particle propagation in complete DMEM/High modified containing 10% FBS, 1x non-essential amino acids, 100 U/mL penicillin, 100 µg/mL streptomycin, and 292 µg/mL L-glutamine. All cell lines were cultured at 37 °C and 5% CO_2 in a humidified incubator.A KRIT1A-expresssing lentiviral construct was generated from the HIV-derived self-inactivating transfer construct pCCLsin.PPT.PGK.EGFP.Wpre by replacing the GFP cassette with the murine KRIT1A cDNA. Lentiviral vector particles were produced in 293T packaging cells, transiently cotransfected with a mix of transfer, envelope, and core-packaging constructs. To obtain KRIT1-null and KRIT1-expressing MEF cells with uniform genetic backgrounds to be used for comparative molecular and cellular biology studies, distinct KRIT1 –/– MEF clones were infected with a lentiviral vector encoding either KRIT1 (pCCLsin.PPT.PGK.KRIT1.Wpre), to restore KRIT1 expression, or GFP (pCCLsin.PPT.PGK.EGFP.Wpre) as a control. The efficiency of distinct infections, evaluated as percentage of GFP positive cells, was always greater that 80%.

3.2 Gene silencing experiments

The expression of KRIT1 in HUVEC cells was silenced by the RNA interference (RNAi) technology using two distinct short interfering double stranded RNA oligomers (siRNAs), Silencer Validated #15655 (siK655) and #15469 (siK469) siRNAs (Ambion), corresponding to exon 12 and exon 9 sequences (GenBank accession nu NM_194455), respectively. The BLOCK-iT™ Alexa Fluor Red Fluorescent Oligo (Invitrogen) was used for determination of efficiency of siRNA transfection as well as RNAi negative control along with the Silencer Negative Control #1 siRNA (Ambion). Cells were

reverse transfected with 30 nM KRIT1-specific or Negative Control siRNAs using the Amaxa HUVEC Nucleofector Kit and electroporation device (Lonza) according to the optimized manufacturer's reverse transfection protocol. Briefly, cells were harvested by trypsinization and cell density was determined using the Countess automated cell counter (Invitrogen). 56105 cells per sample were pelleted, resuspended in 100 ml of supplemented HUVEC Nucleofector solution, combined with the appropriate dilution of siRNAs, electroporated using the U-001 Nucleofector program, and seeded in 6-well plates containing complete culture medium. 48–72 hours post-transfection, cells were lysed and analyzed by real-time quantitative PCR (RT-qPCR).

3.3 RNA isolation, reverse transcription, and quantitative real time PCR analysis (qRT-PCR)

RNA was isolated using Direct-Zol^{TM} RNA Mini-Prep Plus or Trizol extraction accorded to the manufacturer's instructions. Total RNA was reverse-transcribed to single stranded cDNA (cDNA) using the commercially available High-Capacity cDNA Reverse Transcription Kit (Applied Biosystems, Foster City, CA, USA), according to the manufacturer's instructions. Each reaction consisted in RT buffer, deoxy-ribonucleotide triphosphate mixture, random primers, and Multiscribe RT enzyme. Samples were incubated at 25° C for 10 min and then at 37° C for 2 h in a PTC-100 Thermal Cycler (MJ Research, Waltham, MA, USA). Negative controls of the RT were performed by omitting the enzyme or by substituting the RNA for sterile RNAse-free water, to control for genomic DNA and RNA contamination, respectively. cDNA samples were stored at −20°C. Quantitative real-time PCR was carried out using the StepOne Plus Instrument PCR System (Applied Biosystem) in combination with commercial Taqman gene expression assays, consisting in the specific mouse primers and the fluorogenic internal probe. PCR amplifications were performed in Optical 96-well plates (Applied Biosystems) on cDNA samples. PCR was performed in a total volume of 50 µl containing 25 µl of 2× Taqman Universal PCR Master mix (Applied Biosystems), 2.5 µl of 20× Taqman gene expression assays and 22.5 µl of the properly diluted cDNA. Blank controls consisting in no template (water) or RT negative reactions were performed for each. Each value was calculated using the comparative Ct method and normalized to α-tubulin internal control.

3.4 Cell culture and treatment

KRIT1–/– mouse embryonic fibroblast (MEF) cell lines were established from KRIT1–/– E8.5 mouse embryos, respectively, whereas KRIT1 9/6 MEFs were obtained by infecting KRIT1–/– cells with a lentiviral vector encoding KRIT1(Goitre, Balzac et al. 2010). Cells were cultured at 37° C and 5% CO_2 in Dulbecco's modified Eagle's medium (DMEM) supplemented with 10% fetal bovine serum (FBS), 2 mM glutamine, and 1% penicillin/streptomycin (100 U/ml). Human Umbilical Vein Endothelial Cells (HUVECs, Thermo Fisher Scientific, Waltham, MA, USA) were grown on 1.5%

gelatin-coated tissue culture dishes and maintained in medium M200 (Thermo Fisher Scientific) containing 2% fetal bovine serum (FBS) and growth factors (EGM-2, Thermo Fisher Scientific) at 37 °C with 5% CO_2. For GSH treatment, cells were subcultured in 6-well plates at a concentration of 3×10^5 cells/well, and then incubated with 5 mM GSH-encapsulated liposomes for 4 h. Cell treatment with antioxidant compounds, including the mitochondria-permeable Tiron (4,5-dihydroxy-1,3-benzenedisulfonic acid disodium salt monohydrate, Sigma-Aldrich, Milan, Italy) (5 mM for 24 h) and the JNK inhibitor SP600125 (Calbiochem-Merck, Darmstadt, Germany) (25 μM for 1 h), was performed as previously described (Antognelli, Trapani et al. 2018, Antognelli, Trapani et al. 2018). The concentrations and timing of GSH and Tiron used for rescue experiments were based on preliminary dose-response and time course experiments performed in previous works (Armeni, Cianfruglia et al. 2014), which showed an optimal efficacy of the indicated concentration and time of treatment. MEFs were treated for 15 h with 50 μg/mL of Pt5, Pt5@Rapa NPs, or 500 nM rapamycin. KRIT1-ko and KRIT1-overexpressing MEFs were also treated for 12 hours with solid lipid nanoparticles conjugated with rapamycin, bevacizumab, avenanthramide, or with a mixture of all three compounds (herein indicated as MIX) to a final concentration of: AVN = 15 μg/mL (50 μM), RAPA = 0.46 μg/mL (500 nM), BVZ = 10 μg/mL (70 nM). Then, we analyzed the expression levels of biomarkers of KRIT1 loss-of-function, including SOD2, VEGF, and autophagy (p62), through Western blot analysis. The results were compared with cells treated with free rapamycin, bevacizumab and avenanthramide, and a mixture of the three compounds, at concentrations known to restore the expression level of markers associated with molecular dysfunctions linked to CCM disease. The given concentrations of these compounds were based on the outcomes of previous works (Goitre, De Luca et al. 2014, Marchi, Corricelli et al. 2015), and preliminary optimization experiments, showing no significant toxicity to cells and optimal efficacy in specific biochemical assays.

3.5 Quantitative determination of glutathione and glutathione disulfide levels

Total glutathione (GSH+GSSG) and oxidized glutathione (GSSG) were measured spectrophotometrically (at 412 nm) using the glutathione reductase (GR) recycling assay in the presence of 5,50-dithiobis(2-nitrobenzoic acid) (DTNB), with a calibration line based upon known concentrations of GSH and GSSG. To prevent GSH artificial oxidation during sample processing, cells were washed twice (1 min each) at room temperature with PBS containing 5 mM N-ethylmaleimide (NEM) (Sigma Aldrich, Milan, Italy) immediately after culture medium removal, according to an optimized protocol for the reliable measurement of GSH, GSSG, and PSSG in cell cultures. Cells were then trypsinized, washed twice in cold PBS containing 5 mM NEM, and quickly

centrifuged. For total GSH/GSSG determination, the pellet was resuspended with 1% sulfosalicylic acid, vortexed, and incubated 30 min at 4 °C. Samples were then centrifuged at 2300× g for 2 min, and the supernatant was separated in two aliquots: one was maintained at 4 °C for GSH quantification, and the other was treated with 2-vinilpiridin (Cf = 5%) and 20% v/v triethanolamine (Cf = 1%) to mask the GSH present in the extract and prevent its measurement. Finally, the pellet was resuspended with 1 M NaOH for recovery and quantification of proteins.

3.6 Protein extraction and Western blotting

Extraction of total proteins was performed by lysing cells in precooled lysis buffer (RIPA). Protein concentration in cell extracts was determined spectrophotometrically using the BCA protein assay kit (Pierce, Waltham, MA, USA). For WB, cell extract supernatants containing an equal amount of proteins (30 μg) were treated with Laemmli buffer, boiled for 5 min, resolved on either 10 or 12% SDS-PAGE, and then blotted onto a nitrocellulose membrane using iBlot Dry Blotting System (Invitrogen, Carlsbad, CA, USA). Unoccupied protein-binding sites were blocked by incubation with nonfat dry milk 5% in TBS for 1 h at room temperature, and membranes were then incubated overnight at 4°C with appropriate dilutions of specific primary antibodies. Subsequently, membranes were washed three times with TBS/0.3% Tween-20 (TBST) for 15 min each, and incubated for 1 h at room temperature with the appropriate horseradish peroxidase (HRP)-conjugated secondary antibody (Abcam) diluted 1:5000 in TBST. After two washes with TBST for 10 min each, antigen-antibody complexes were then visualized by chemiluminescent detection of peroxidase activity using the ChemiDoc Touch Imaging System (Bio-Rad Laboratories, Milan, Italy). As an internal control for protein loading, all membranes were subsequently re-probed with the antibody for α-tubulin, vinculin, and actin housekeeping proteins. Protein bands from Western blots were quantified by densitometry using the ImageJ software, and their relative amounts were normalized to the levels of housekeeping protein serving as internal loading control.

3.7 Confocal Microscopy

MEFs (10 000 cells/well) cells were seeded in an 8-well chamber (VWR) and incubated at 37 °C and 5% CO2. After 24 h, the cellular medium was removed and replaced with 50 μg/mL Pt5@Rapa NPs containing Alexa Fluor 647 conjugated BSA diluted in fresh FluoroBrite DMEM medium (Thermo Fisher Scientific). After 30 min, the cells were imaged with Leica TCS SP8 confocal microscope using a 63× oil immersion objective. Pt5@Rapa NPs were imaged using a 647 nm excitation wavelength. For lysosomes imaging, the cells were incubated with 75 nM LysoTracker Green DND-26 (Molecular probes). After 10 min of incubation, the medium was removed, cells were washed

three times with PBS, and imaged using a 488 nm excitation wavelength for LysoTracker Green signal detection.

3.8 In Vitro angiogenesis assay

Seventy-two hours after transfection with negative control siRNA or 4× predesigned KRIT1 siRNA, the HUVECs were incubated with 50 μg/mL Pt5, Pt5@Rapa NPs, or 500 nM rapamycin. After 15 h, the In Vitro Angiogenesis Assay (Millipore) was performed following the manufacturer's instructions. Briefly, untreated or treated HUVECs (10 × 103) were plated in each well of a 96-well plate precoated with 50 μL of ECMatrix (Millipore) in complete Medium 200. After 4 h of incubation, the samples were stained with Calcein AM (Thermo Fisher Scientific) for 20 min at 37 °C and the formation of capillary-like structures was analyzed under an EVOS Cell Imaging microscope (Thermo Fisher Scientific) at 4× magnification. To evaluate the degree of angiogenesis progression, the number of closed polygons formed in eight replicates was counted using ImageJ software (NIH).

3.9 Antibodies

Primary antibodies, used in the present study, include the following: rabbit anti-KRIT1 mAb [ab196025] (Abcam, San Francisco, CA, USA); mouse anti-α-tubulin mAb [B-5-1-2] (Sigma-Aldrich, Milan, Italy); mouse anti-actin [C4] mAb [ab14128] (Abcam); rabbit anti-SQSTM1/p62 mAb [D1Q5S] (Cell Signaling, Danvers, MA, USA); mouse anti-SOD2 [2A1] mAb [ab16956] (Abcam); rabbit anti-VEGF pAb [ab46154] (Abcam); mouse anti-Methylglyoxal-AGE (Arg-Pyrimidine) mAb (clone 6B) (BioLogo, Hamburg, Germany); rabbit anti-Nrf2 pAb (C-20) (Santa Cruz Biotechnology); rabbit anti-Nrf2 pAb (ab31163, Abcam); rabbit antiNrf2 mAb [EP1808Y] (AB62352, Abcam); rabbit anti-c-Jun pAb (H-79) (Santa Cruz Biotechnology); mouse anti-phospho-c-Jun mAb (KM-1) (Santa Cruz Biotechnology); mouse anti-Heme Oxygenase 1 mAb [HO1-1] (Abcam); rat anti-Glyoxalase 1 mAb (6F10) (Santa Cruz Biotechnology); mouse anti-p-JNK mAb (G-7) (Santa Cruz Biotechnology); rabbit anti Caspase3 pAb (9662, Cell Signaling Technology); mouse anti-β-actin mAb (C4) (Santa Cruz Biotechnology) or [A5441] (Sigma Aldrich); rabbit anti-lamin β1 pAb (H-90) (Santa Cruz Biotechnology); anti-phospho Ser/Thr antibodies [ab17464] (Abcam) or [22A] (BD Biosciences, San Jose, CA); rabbit anti-PKCδ pAb [9374S] (Cell Signaling); rabbit anti-PKCα pAb [sc-208] (Santa Cruz Biotechnology).

Secondary antibodies conjugated with horseradish peroxidase (HRP) or fluorescent dyes are the following: goat anti-Rabbit IgG [ab6721] (Abcam); rabbit anti-Mouse IgG [ab6728] (Abcam); Hoechst (H33342, Sigma) or ToPro-3 (Thermo Fisher Scientific, Waltham, MA, USA) were used for the staining of the nuclei.

3.10 Immunofluorescence and pharmacological treatments

Pharmacological compounds used for cell treatments were phorbol-12-myristate-13-acetate (PMA; Santa Cruz Biotechnology, Santa Cruz, CA, or Sigma-Aldrich, St. Louis, MO), or PKC inhibitors, including bisindolylmaleimide-1 (BIM) and Gö6976 (Calbiochem, Bad Soden, Germany, or Cayman Chemical, Ann Arbor, MI). Immunoprecipitation of GFP-KRIT1 and mCherry-KRIT1 was performed using rabbit polyclonal anti-GFP (ab290, Abcam) and Mab15.B2 (Millipore, Burlington, MA) antibodies, respectively. HeLa cells were treated with 20 ng/mL PMA for 2 h, with or without a 30 min pre-treatment with 1 μM BIM. DMSO was used a vehicle control. After treatments, cells were fixed in 3% paraformaldehyde or cold methanol for 10 min, nuclei were stained with Hoechst or ToPro-3, and coverslips were mounted with Mowiol (Calbiochem) on microscope slides. Digital images were acquired with either an Axio-Observer-Z1 microscope (Zeiss) equipped with ApoTome system for optical sectioning or a 3-channel TCS SP2 laser scanning confocal microscope (Leica Microsystems, Wetzlar, Germany). HPAEC were plated on fibronectin-coated coverslips (10 μg/mL) and transduced in growth media, then changed to serum-free DME/F-12 medium (HyClone GE Healthcare, Piscataway, NJ) for 30 min. Cells were then treated with 20 ng/mL PMA for 2 h, with or without a 30 min pre-treatment with 1 μM BIM. DMSO was used as vehicle control. At the end of the treatment period, cells were fixed in 10% formalin and washed with 0.001% Tritonx-100 in PBS. Cells were counterstained with Hoechst 33258 (VWR, Radnor, PA) to label nuclei, then mounted on glass slides with ProLong Gold Antifade (Invitrogen, Carlsbad, CA). Images were acquired on an Olympus IX70 fluorescent microscope using a Hamamatsu digital imaging system. Fluorescence was quantified by calculating the ratio of pixel intensity in the nucleus to the average pixel intensity of four cytoplasmic regions halfway between the nucleus and cell edge. Both the concentrations of pharmacological compound and the time of treatment used were selected according to data found in literature and the outcomes of our preliminary experiments.

3.11 Immunoprecipitation and Western blotting

GFP-KRIT1 transfected HeLa cells treated with PMA or BIM+PMA were lysed in NP-40 buffer containing protease and phosphatase inhibitors (P8340 and P2850, Sigma). GFP-KRIT1 was immunoprecipitated from cell lysates using the rabbit polyclonal anti-GFP antibody (ab290, Abcam), and analyzed by Western blotting with a pan-phospho-Ser/Thr antibody (1:1000). Western blotting analysis was performed as previously described (Balzac, Avolio et al. 2005). mCherry-KRIT1 expressing HPAEC treated with PMA, BIM, and BIM+PMA were lysed in buffer containing 20 mM HEPES-KOH pH 7.5, 1.5 mM $MgCl_2$, 5 mM KCl, protease and phosphatase inhibitors, supplemented

with 1% TritonX-100. KRIT1 was immunoprecipitated (Mab15.B2, Millipore, Burlington, MA) from total lysate and blotted with pan-phospho-Ser/Thr antibody 22A (1:1000).

3.12 In silico prediction of putative post-translation modification sites

Putative phosphorylation sites were predicted using GPS 3.0 (Group-based Prediction System, version 3.0, http://gps.biocuckoo.org/). For the analysis, medium level threshold was chosen and ACG kinases were selected as Ser/Thr phosphorylation kinases. Prediction results were then sorted for PKC specific predicted sites.

3.13 Two-Dimensional polyacrylamide gel electrophoresis (2D PAGE) analysis

Cells were harvested and resuspended in 8 M urea, 40 mM Tris and 2% CHAPS to allow the recovery of total protein extracts. Protein content was quantified by the Bradford assay. Isoelectrofocusing (IEF) (first dimension) was performed using a 7 cm Immobiline™DryStrip NL (GE Healthcare, Milan, Italy), pH 3–10. Each strip was actively rehydrated in the presence of proteins (200 µg) within an IPG-Phor system (Amersham Pharmacia, Macclesfield, UK) at 30 V, for 12 h. After rehydration, IEF runs were carried out at 20 ◦C, based on a current limit of 50 µA/IPG-strip: 300 V for 1 h; 4000 V for 3.75 h (gradient); and 4000 V until 15,000 V/h was reached in total. After IEF, IPG-strips were equilibrated in a buffer containing 50 mM Tris-HCl, pH 8.8, 6 M urea, 30% v/v glycerol, 2% w/v SDS, for 30 min. SDS-PAGE (second dimension) was performed at 90 V for 130 min using 10% acrylamide/bis-acrylamide gels. First and second dimensions were carried out in nonreducing conditions to avoid reduction of PSSG derivatives. Gels were then blotted onto PVDF membranes, and then Western blotting with a mouse monoclonal anti-GSH antibody was performed to analyze protein S-glutathionylation levels, as previously described. Parallel 2-DE gels were directly stained with colloidal Coomassie Blue. Digitalized gel images of Western blotting membranes and colloidal Coomassie-stained gels were acquired using an Image Scanner II (GE Healthcare, Bronx, NY, USA) apparatus and analyzed with the Image Master Platinum 6.0 software (GE Healthcare) for spot matching and relative quantization. Protein spots corresponding to immunoreactive signals were manually excised from 2D-gels and further subjected to mass spectrometric analysis (Cianfruglia, Perrelli et al. 2019).

3.14 Mass spectrometry analysis

Bands corresponding to proteins of interest were excised, in-gel alkylated with iodoacetamide, digested with endoprotease LysC or endoprotease AspN (Roche), and extracted as previously reported (Salzano, Novi et al. 2013). Peptide mixtures were directly subjected to peptide mapping experiments or further enriched for phosphopeptides by using Ga3+-immobilized metal ion affinity

chromatography (Ga3+-IMAC) (Phosphopeptide Isolation Kit, Pierce, USA) (D'Ambrosio, Arena et al. 2006). All samples were analyzed by nLC-ESI-LIT-MS/MS using a LTQ XL mass spectrometer (ThermoFisher, San Jose, CA), equipped with a Proxeon nanospray source (Proxeon, Denmark) connected to an Easy-nanoLC (Proxeon). Peptide mixtures were separated on an Easy C18 column (10 x 0.075 mm, 3 μm) (Proxeon). Mobile phases consisted of 0.1% v/v aqueous formic acid (solvent A) and 0.1% v/v formic acid in acetonitrile (solvent B), running at flow rate of 300 nL/min. Solvent B ramped from 5% to 35% over 45 min, from 35% to 60% over 10 min, and from 60% to 95% over 20 min. Spectra were acquired in the range of m/z 400-2000. Acquisition was controlled by a data-dependent product ion scanning procedure over the three most abundant ions, enabling dynamic exclusion (repeat count 2 and exclusion duration 60 s); the mass isolation window and collision energy values were set to m/z 3 and 35%, respectively. Raw data were searched by using Sequest (ThermoFisher) and Mascot (Matrix Science, UK) within the Proteome Discoverer software package version 1.0 SP1 (ThermoFisher) against an indexed database containing the GFP-KRIT1, LysC endoprotease, endoprotease AspN and common keratin sequences. Database searching was performed by selecting Cys carbamidomethylation as static and Met oxidation and Ser/Thr/Tyr phosphorylation as dynamic modifications, respectively. A mass tolerance value of 2 Da and 0.8 Da (for precursor ion and MS/MS fragments, respectively), endoprotease LysC or endoprotease AspN as proteolytic enzymes, and a missed cleavages maximum value of two were used as searching parameters. Definitive assignment of peptide phosphorylation site(s) was associated with manual spectral visualization and verification.

3.15 WST-1 Assay

In vitro toxicological profile of Pt5 and Pt5@Rapa NPs on MEFs and HUVECs was evaluated by WST-1 assay (Sigma-Aldrich) according to the previously described method (Brunetti, Chibli et al. 2013). Briefly, MEFs (25 000 cells/well) were plated in a 96-well tissue culture plate in a final volume of 100 μL. After 24 h of adhesion, the culture medium was removed and replaced with medium containing Pt5 or Pt5@Rapa NPs at a concentration of 50 μg/mL, up to 24 or 48 h. Afterward, the cells were washed three times with PBS and incubated for 1 h with medium containing 10% WST. The HUVECs (50 000 cells/well) were plated in a 96-well tissue culture plate in a final volume of 100 μL. After 24 h of adhesion, the culture medium was removed and replaced with medium containing a series of Pt5 NPs dilutions ranging from 10 to 50 μg/mL, and the cells were cultured for other 24 h. Afterward, the cells were washed three times with PBS and incubated for 1 h with a medium containing 10% WST. An Infinite 200 Pro Tecan microplate reader was used for reading the cell viability results.

3.16 DCFH-DA Assay

Assessment of cellular levels of reactive oxidative species, including levels of general reactive oxygen species (ROS) and reactive nitrogen species (RNS), was performed as previously described (Perrelli and Retta 2020) using the membrane permeable 2′–7′-dichlorofluorescin-diacetate (DCFH-DA) fluorogenic dye (Invitrogen). Following cleavage of the acetate groups by intracellular esterases, the resultant dichlorofluorescin (DCFH) is trapped intracellularly due to its hydrophilicity, and oxidized by various ROS/RNS to form the highly fluorescent 2′,7′-dichlorofluorescein (DCF), which can be detected by fluorescence spectrophotometry or microscopy, thus serving as an effective indicator of generalized cellular oxidative stress. Briefly, MEF and hBMEC cellular models described above were grown to confluence in complete medium, washed twice with PBS, incubated with DCFH-DA at a final concentration of 5 µM in PBS at 37 °C for 30 min, and analyzed by image-based cytometry with a Tali® Image-Based Cytometer (Invitrogen). Raw data were processed using the Flowing software (v.2.5.0, by Perttu terho, University of Turku, Finland). Fluorescence readings were expressed as either relative fluorescence units (RFU) or relative ROS/RNS level units. MEFs (25 000 cells/well) were also plated in 96-well microplates (Constar) and exposed to 50 µg/mL of citrate-capped Pt5, Pt5, Pt5@Rapa NPs, and 500 nM rapamycin. After 15 h, the cells were washed three times with PBS with Ca2+ and Mg2+ and incubated at 37 °C for 10 min with 5 µM DCFH-DA (Sigma) in PBS. An Infinite 200 Pro Tecan microplate reader was used for reading the DCF fluorescence intensity, setting the excitation filter at 480 nm and the emission filter at 520 nm. The results were normalized with respect to untreated control cells.

3.17 Total Oxyradical Scavenging Capacity Assay

The total antioxidant capacity (TAC) of cell extracts was evaluated using the total oxyradical scavenging capacity (TOSC) assay, which measures the capacity of cellular antioxidants to inhibit the oxidation of α-keto-γ-methiolbutyric acid (KMBA) to ethylene gas in the presence of different forms of oxyradicals, artificially generated at a constant rate. Reactions were performed on 50 µL of cell extracts and 2 mM KMBA; hydroxyl radicals were generated from the Fenton reaction of iron-EDTA (1.8 µM Fe^{3+}, 3.6 µM EDTA) plus ascorbate (180 µM) in potassium phosphate buffer (100 mM, pH 7.4). TOSC values were quantified using the equation $TOSC = 100 - (SA/CA \times 100)$ and referred to the protein concentration of each sample. Specifically, SA and CA represent the integrated area calculated under the least squares kinetic curve produced during the reaction for the sample and the control, respectively.

3.18 Statistical analysis

Data were generated from three independent experiments and expressed as means±standard deviation (SD). Statistical significance, determined by Student's t-test, was set at $p<0.05$.

4. Discussion and future perspective

In recent years, it has become clear that the three known CCM genes play important roles in controlling signaling pathways involved in cell responses against oxidative stress, pointing to novel pathogenic mechanisms for CCM disease. In particular, KRIT1 protein, encoded by *CCM1* gene, has been found to have pleiotropic functions, modulating multiple signaling pathways and mechanisms involved in cellular homeostasis and responses to oxidative stress and inflammatory conditions (Marchi, Trapani et al. 2016, Retta and Glading 2016, Antognelli, Trapani et al. 2018). Indeed, previous works demonstrated that KRIT1 loss induces both the downregulation of major antioxidant pathways, including the FOXO1/SOD2 axis (Goitre, Balzac et al. 2010), and the upregulation of pro-oxidant and pro-inflammatory pathways, such as JNK/c-Jun/Cox2 and NF-kB pathways (Goitre, Balzac et al. 2010, Goitre, De Luca et al. 2014, Choquet, Trapani et al. 2016, Antognelli, Trapani et al. 2018, Antognelli, Trapani et al. 2018), leading to altered redox homeostasis and enhanced endothelial permeability and inflammatory response (Retta and Glading 2016, Goitre, DiStefano et al. 2017). Furthermore, it has been shown that KRIT1 loss of function affects a major cytoprotective process, such as autophagy (Marchi, Corricelli et al. 2015, Marchi, Retta et al. 2016, Marchi, Trapani et al. 2016), and causes abnormal post-translational modifications of distinct structural and regulatory proteins (Antognelli, Trapani et al. 2018, Antognelli, Trapani et al. 2018, Cianfruglia, Perrelli et al. 2019), leading to a sustained upregulation of adaptive redox homeostasis mechanisms that sensitizes cells to oxidative stress and inflammatory insults (Antognelli, Trapani et al. 2018, Antognelli, Trapani et al. 2018, Antognelli, Perrelli et al. 2020). Consistently, the emerged pleiotropic redox-dependent functions of KRIT1 justify its involvement in the regulation of multiple fundamental cellular structures and mechanisms, including cell-cell and cell-matrix junctions (Glading, Han et al. 2007, Liu, Draheim et al. 2013), cytoskeleton dynamics (Whitehead, Chan et al. 2009, Stockton, Shenkar et al. 2010), and blood vessel development and homeostasis (Wüstehube, Bartol et al. 2010, DiStefano, Kuebel et al. 2014, Renz, Otten et al. 2015, Schulz, Wieland et al. 2015, Vieceli Dalla Sega, Mastrocola et al. 2019). Our findings show that KRIT1 loss-of-function leads to the persistent upregulation of critical cytoprotective proteins that govern cell adaptive responses to oxidative stress, including the master redox-sensitive transcription factor Nrf2 and the anti-glycation enzyme Glo1, a transcriptional target of Nrf2 that plays a critical role in the enzymatic defense against MG-mediated glycative and oxidative stress. Moreover, a significant nuclear accumulation of Nrf2, occurring in

both cellular models of CCM disease and endothelial cells lining the lumen of human CCM vessels (Antognelli, Trapani et al. 2018), suggests that the abnormally sustained activation of Nrf2 caused by KRIT1 loss-of-function may have an important role on CCM disease onset and progression, likely representing an either insufficient or aberrant cellular adaptive response to cope with a focal increase in oxidative challenges induced by local stressful events affecting the neurovascular unit. Furthermore, these data support the possibility that the redox-sensitive upregulation of HO-1 induced by KRIT1 loss-of-function contributes to Nrf2-mediated adaptive defense mechanisms that limit a vicious cycle of ROS production and oxidative stress (Fig. 17a). However, the chronic activation of this adaptive stress response mechanism could cause HO-1 activity to be ineffective or insufficient for cytoprotective responses to additional stressful events occurring over time, leading to homeostasis imbalance and cellular dysfunction that may become irreversible (Fig. 17b). Remarkably, in cellular models of CCM disease, glycative and oxidative post-translational modifications of proteins, such as MG-mediated glycation and S-glutathionylation, affect the modulation of protein biological activity and stability (Nass, Vogel et al. 2010, Sun, Eriksson et al. 2012, Bansode, Chougale et al. 2013) involved in cellular homeostasis and adaptive responses to stressful conditions. The target proteins include prominent members of the heat-shock protein (HSP) family functioning as molecular chaperones, such as HSP70, HSP27, and HSP60, enzymes of energy metabolism, and cytoskeleton proteins, suggesting that they play an important role in the chronic adaptive redox homeostasis and enhanced cell susceptibility to oxidative stress and inflammation that have been associated with loss-of-function mutations of CCM genes (Fig. 17a, Fig. 18) (Antognelli, Trapani et al. 2018, Antognelli, Trapani et al. 2018, Cianfruglia, Perrelli et al. 2019, Antognelli, Perrelli et al. 2020). In this light, it is plausible that MG-mediated glycation and S-glutathionylation of distinct target proteins involved in cellular stress responses, and consequent downstream effects, including endothelial cell dysfunction, may occur simultaneously, thus raising the possibility that these two mechanisms of protein post-translational modifications can influence the pathogenesis of CCM disease in a synergistic manner (Cianfruglia, Perrelli et al. 2019, Antognelli, Perrelli et al. 2020). Consistently, there is evidence that both mechanisms are affected by KRIT1 loss-of-function in the same cellular models and surgical samples of CCM disease, as well as that they are significantly implicated in distinct vascular dysfunctions and diseases. In addition, it is also possible to glimpse potential upstream regulatory mechanisms that could orchestrate a putative molecular crosstalk between MG-mediated glycation and S-glutathionylation and coordinate their downstream effects. Indeed, both mechanisms have been shown to be influenced by the abnormal alteration of cellular redox homeostasis that occurs upon KRIT1 loss-of-function (Fig. 18). Moreover, given the evidence that MG can cause dysfunction of thiol-disulfide oxidoreductase systems, which protect endothelial cells

against oxidative stress, including the thioredoxin/thioredoxin reductase system (Tatsunami, Oba et al. 2009), it is also possible to hypothesize that dicarbonyl stress may decrease the GSH:GSSG ratio and, thereby, stimulate S-glutathionylation. Conversely, there is evidence that S-glutathionylation may contribute to ROS production and altered redox homeostasis by affecting the activity of eNOS (Chen, Wang et al. 2010). Furthermore, it has been reported that S-glutathionylation of Keap1, an endogenous repressor of Nrf2, can be implicated in the activation of Nrf2 (Carvalho, Marques et al. 2016), suggesting a potential mechanistic contribution to the sustained activation of this antioxidant transcription factor that occurs upon KRIT1 loss-of-function and, in consequence, to the upregulation of Nrf2 downstream targets, including Glo1 and HO-1.

We found that KRIT1 loss causes a significant decrease in total GSH and increase in GSSG levels, with a consequent deficit in the GSH/GSSG redox ratio and GSH-mediated antioxidant capacity. Moreover, we observed also a significant reduction in glutathione-S-transferase (GST) activity, which catalyzes the conjugation of GSH to a wide variety of endogenous and exogenous electrophilic compounds to aid in their detoxification, thereby contributing in protecting cells from oxidative damage (Um, Kim et al. 2006). Notably, all these molecular alterations could be rescued by providing cells with exogenous GSH, suggesting that they were interconnected with alterations in the thiol-redox homeostasis (Fig. 18) (Cianfruglia, Perrelli et al. 2019). Indeed, they were consistent with our previous findings demonstrating that KRIT1 loss-of-function causes intracellular redox imbalance and sustained mild oxidative stress conditions, suggesting that changes in the GSH redox status and GST activity contribute to these effects (Goitre, Balzac et al. 2010, Goitre, De Luca et al. 2014, Marchi, Corricelli et al. 2015). Overall, these potential mechanisms of molecular crosstalk between the ROS/Nrf2/Glo1/MG-mediated glycation and the S-glutathionylation pathways might contribute to the chronic adaptive redox homeostasis and enhanced cell susceptibility to oxidative stress associated with KRIT1 loss-of-function mutations (Fig. 19) (Antognelli, Trapani et al. 2018, Antognelli, Trapani et al. 2018, Cianfruglia, Perrelli et al. 2019, Antognelli, Perrelli et al. 2020). While the specific effects of glycative and oxidative post-translational modifications of proteins triggered by loss-of-function mutations of KRIT1, including MG-dependent glycation and S-glutathionylation of important structural and regulatory proteins, remain to be defined, the comprehensive characterization of their upstream regulatory mechanisms and functional interplay should provide novel insights into CCM disease pathogenesis and enable the development of targeted, safe, and effective synergistic drug combination therapies.

Our finding that KRIT1 nucleocytoplasmic shuttling is regulated by PKC is corroborated by several studies showing that PKC plays indeed a major role in regulating subcellular localization of a diverse variety of proteins, often as the result of direct phosphorylation (Represa, Deloulme et al. 1990,

Topham, Bunting et al. 1998, Andreeva, Krause et al. 2001, van Balkom, Savelkoul et al. 2002, Doller, Huwiler et al. 2007). Specifically, our results suggest that KRIT1 is phosphorylated by PKCα, and provide preliminary information on the putative phosphorylation sites required for PMA/PKC-induced nuclear-to-cytoplasmic translocation of KRIT1. Dedicated studies based on site-directed mutagenesis are necessary to assign the specific contribution of each phosphorylation site present in KRIT1 with respect to protein nucleocytoplasmic shuttling. Indeed, given the existence of multiple phosphorylation sites in KRIT1 (Fig. 11D), and the evidence that more than one phosphorylation event may be required for PKC-mediated regulation of protein nucleocytoplasmic shuttling (Doller, Schlepckow et al. 2010), it is likely that distinct PKC-dependent phosphorylation sites contribute to a fine-tuned regulation of KRIT1 nucleocytoplasmic shuttling. Regardless, our observations clearly established a role for PKCα in regulating nuclear-to-cytoplasmic translocation of KRIT1, thus opening a novel research avenue for a comprehensive characterization of the underlying molecular mechanisms and functional consequences. Among others, it would be interesting to address whether the established capacity of PKCα to translocate from the cytosol into the nucleus upon various stimuli, including phorbol esters and redox changes (Schmalz, Kalkbrenner et al. 1996, Giorgi, Agnoletto et al. 2010), is somehow related to its ability to regulate KRIT1 nucleocytoplasmic shuttling. Moreover, given our original findings that KRIT1 plays a major role in cellular defenses against oxidative stress and inflammation (Retta and Glading 2016, Antognelli, Perrelli et al. 2020), and considering the established relationship between PKC functions and oxidative stress (Gopalakrishna and Jaken 2000, Giorgi, Agnoletto et al. 2010), it is tempting to hypothesize that our novel findings disclose a bridge between PKC-dependent regulation of KRIT1 nucleocytoplasmic shuttling and cellular responses to oxidative stress. While further studies are required to build up such a bridge, the novel findings reported in this thesis and in our works opened the way (Francalanci, Avolio et al. 2009, De Luca, Perrelli et al. 2020).

Given the established major role of oxidative stress and inflammation in the pathogenesis of CCM disease, it was tempting to hypothesize that the development of specific antioxidant and anti-inflammatory nanosystems may represent a promising therapeutic strategy for CCM treatment (Retta and Glading 2016, De Luca, Pedone et al. 2018, Antognelli, Perrelli et al. 2020). Consistently, my group demonstrated the reliability and effectiveness of both Pt- and Pd-NPs in rescuing increased intracellular ROS levels and oxidative stress in cellular models of CCM disease (Moglianetti, De Luca et al. 2016, De Luca, Pedone et al. 2018, Moglianetti, Pedone et al. 2020). Furthermore, this possibility was strongly supported and extended by the demonstration that a multitargeted therapy approach based on a composite nanosystem endowed with both antioxidant and pro-autophagic activities was effective in rescuing major molecular and cellular mechanisms of CCM disease

pathogenesis, suggesting its potential for the treatment of this and other oxidative stress-related diseases (De Luca, Pedone et al. 2018, Perrelli, Fatehbasharzad et al. 2020). Specifically, this composite multifunctional nanosystem was developed by combining the intrinsic ROS scavenging activity of PtNPs with the autophagy-stimulating activity of rapamycin, and was tested in distinct cellular models of CCM disease, including KRIT1 knockout mouse embryonic fibroblasts (MEF) (Goitre, Balzac et al. 2010) and KRIT1-silenced human endothelial cells (Marchi, Corricelli et al. 2015). The experimental outcomes highlighted the advantages of composite platinum/rapamycin nanosystems (Rapa@Pt-NPs), including the enhancement of rapamycin physicochemical properties, such as solubility, permeability, stability and bioavailability. Furthermore, they showed that cellular uptake of Rapa@Pt-NPs occurred via endocytosis and resulted in synergistic biological effects, including the rescue of established hallmarks of CCM disease, such as altered redox homeostasis and signaling (Goitre, Balzac et al. 2010, Goitre, De Luca et al. 2014), mitochondrial and autophagy dysfunctions (Goitre, Balzac et al. 2010, Marchi, Corricelli et al. 2015, Marchi, Retta et al. 2016, Marchi, Trapani et al. 2016), and endothelial to mesenchymal transition (EndMT) (Maddaluno, Rudini et al. 2013, Marchi, Corricelli et al. 2015) (Figure 14). Overall, the outcomes of these *in vitro* studies stimulate their further implementation for precision nanomedicine approaches in animal models of CCM disease, thus paving the way for the development of advanced combinatorial nanotherapeutic and nanotheranostic strategies to overcome current diagnostic and therapeutic limitations (De Luca, Pedone et al. 2018). Moreover, besides inorganic and metal-based nanoparticles, lipid-based nanoformulations, such as micelles, liposomes, nanoemulsions and, in particular, solid lipid nanoparticles (SLN), have become very attractive for their unique size dependent properties, as well as for their potential to improve performance of pharmaceuticals, and reach the goal of controlled and site specific drug delivery to the brain. Indeed, they are highly biocompatible and can enhance drug transport through the BBB by targeting specific transport processes in the brain vasculature (Saraiva, Praça et al. 2016, Tapeinos, Battaglini et al. 2017). Our findings also demonstrate that rapamycin delivery, within lipid nanoparticles, is effective to elicit a therapeutic effect comparable to the free drug, even at a lower drug concentration, also showing that rapamycin encapsulation within ILs might also have contributed to its efficacy by protecting it from the degradation and improving its internalization within the cells. Moreover, ILs showed a significant antioxidant activity within the intracellular environment, directly increasing the antioxidant marker SOD2, similarly to free rapamycin, which indirectly regulates the ROS homeostasis by acting on autophagy pathways that control the clearance of ROS-generating dysfunctional mitochondria (Choi, Ryter et al. 2013, Marchi, Corricelli et al. 2015), and avenanthramide, which directly scavenges ROS and prevents oxidative stress (Moglia, Goitre et al. 2015, Goitre, DiStefano et al. 2017, Perrelli, Goitre

et al. 2018). Therefore, the outcomes of our experiments demonstrate that the IL itself has a weak antioxidant activity, and this nanocarrier is also able to regulate ROS homeostasis in a cellular model of CCM disease, confirming its potential as multifunctional nanovector for combination therapy.

These results emphasize the importance of developing a new preventive or even therapeutic treatment for CCM disease, with the specific aim of reducing the risk of onset or decreasing the size of cavernomas, trying to inhibit or completely revert the multiple molecular dysfunctions that characterize the pathogenesis and progression of CCM disease. In particular, the use of biocompatible nanoparticles would allow the conjugated drugs to act directly in the lesion areas. Moreover, a strong advantage is given also by the possibility of combining nanoparticles loaded with different pharmacological compounds within a single treatment, thus creating a mixture endowed with an even more positive effect for disease treatment (Fig. 20). Consistent with these data, different nanosystems currently developed for the prevention and treatment of cerebrovascular diseases are based on antioxidant and anti-inflammatory properties (Yoshitomi and Nagasaki 2011, Kim, Kim et al. 2012, Baranoski and Ducruet 2019). Furthermore, given the emerging molecular links between cerebrovascular and neurological diseases (Lendahl, Nilsson et al. 2019, Sivandzade, Prasad et al. 2019), these advanced nanomedicine approaches may also prevent or limit neurological comorbidities. Finally, additional biological benefits may result from multitargeted, combinatorial nanotherapies that simultaneously and synergistically target distinct molecular dysfunctions underlying the complex pathogenetic mechanisms of cerebrovascular diseases (Perrelli, Fatehbasharzad et al. 2020). Accordingly, whereas the effectiveness of multidisciplinary strategies of precision medicine and combination therapies has been clearly demonstrated (Woodcock, Griffin et al. 2011, Iyengar 2013, Chen and Lahav 2016, Cai, Zhang et al. 2018, Qian, Li et al. 2020), the combinatorial targeting of oxidative stress and defective autophagy by a composite nanosystem endowed with both antioxidant and pro-autophagic activities has recently emerged as a potential nanomedicine strategy for an efficacious treatment of CCM disease (De Luca, Pedone et al. 2018).

In conclusion, our results extend the understanding the complex molecular mechanisms underlying KRIT1 functions and CCM disease pathogenesis, suggesting an important contribution of several major proteins involved in blood vessel development and homeostasis, including adaptive responses to stressful conditions, thus providing a novel framework for a better characterization of KRIT1 physiopathological functions and the development of targeted and effective therapeutic strategies. Further studies in animal models of CCM disease will be necessary to confirm the role of different KRIT1-dependent pathways in CCM lesion genesis and progression, exploiting this intriguing novel perspective toward a more comprehensive understanding of CCM disease pathogenesis, the identification of new disease biomarkers, and the development of targeted and effective therapeutic

strategies. Taken together, the great progress toward a comprehensive characterization of disease mechanisms, and the rapidly growing variety of precisely manufactured composite and effective diagnostic, therapeutic and theranostic nanosystems allow to foresee significant improvements of existing diagnostic and therapeutic approaches for CCM disease, pointing to precision risk stratification and personalized nanomedicine strategies as the most promising avenues of translational care for affected patients. With this growing trend, the future for an early and more effective treatment of CCM disease and associated comorbidities looks bright.

Figures and legends

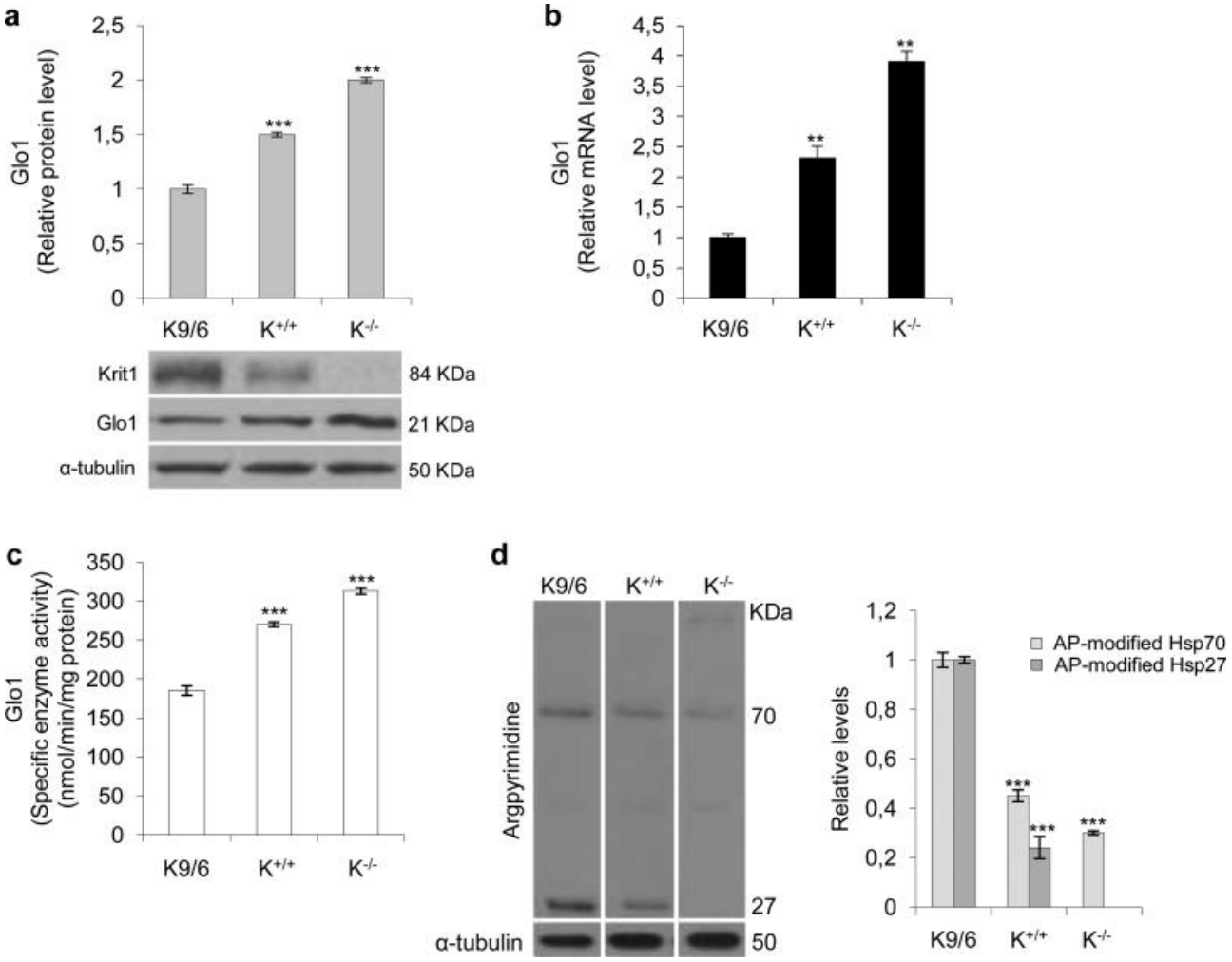

Figure 1. KRIT1 modulates the expression of the anti-glycation enzyme Glyoxalase 1 (Glo1) and the formation of MG-derived argpyrimidine protein adducts. Wild type (K+/+), KRIT1 –/– (K–/–), and KRIT1–/– re-expressing KRIT1 (K9/6) MEF cells grown to confluence under standard conditions were lysed and analyzed by Western blotting (a,d), qRT-PCR (b), and spectrophotometric enzymatic assay (c). Representative Western blot and quantitative histogram of the relative KRIT1 and Glo1 protein expression levels. α-tubulin was used as internal loading control for WB normalization. The WB bands of Glo1 were quantified by densitometric analysis, and normalized optical density values were expressed as relative protein level units referred to average value obtained for K9/6 samples (a). Glo1 mRNA expression levels were analyzed in triplicate by qRT-PCR and normalized to the amount of an internal control transcript (GAPDH). Results are expressed as relative mRNA level units referred to the average value obtained for K9/6 cells, and represent the mean (± SD) of n ≥ 3 independent qRT-PCR experiments (b). Glo1 enzyme activity was measured in cytosolic extracts

according to a spectrophotometric method monitoring the increase in absorbance at 240 nm due to the formation of S-D- lactoylglutathione. Glo1 activity is expressed in milliunits per mg of protein, where one milliunit is the amount of enzyme that catalyzes the formation of 1 nmol of S-D-lactoylglutathione per min under assay conditions. Results represent the mean (± SD) of $n \geq 3$ independent experiments performed in triplicate (c). Representative WB and quantitative histogram of argpyrimidine (AP) adducts as detected using a specific mAb. α-tubulin was used as internal loading control for WB normalization. Western blots are representative of three separate experiments (d). **$p \leq 0.01$ versus K9/6 cells, ***$p \leq 0.001$ versus K9/6 cells. Notice that KRIT1 loss-of-function leads to a significant increase in Glo1 expression and activity, and a decrease in the intracellular levels of major AP adducts of 70 and 27 kDa.

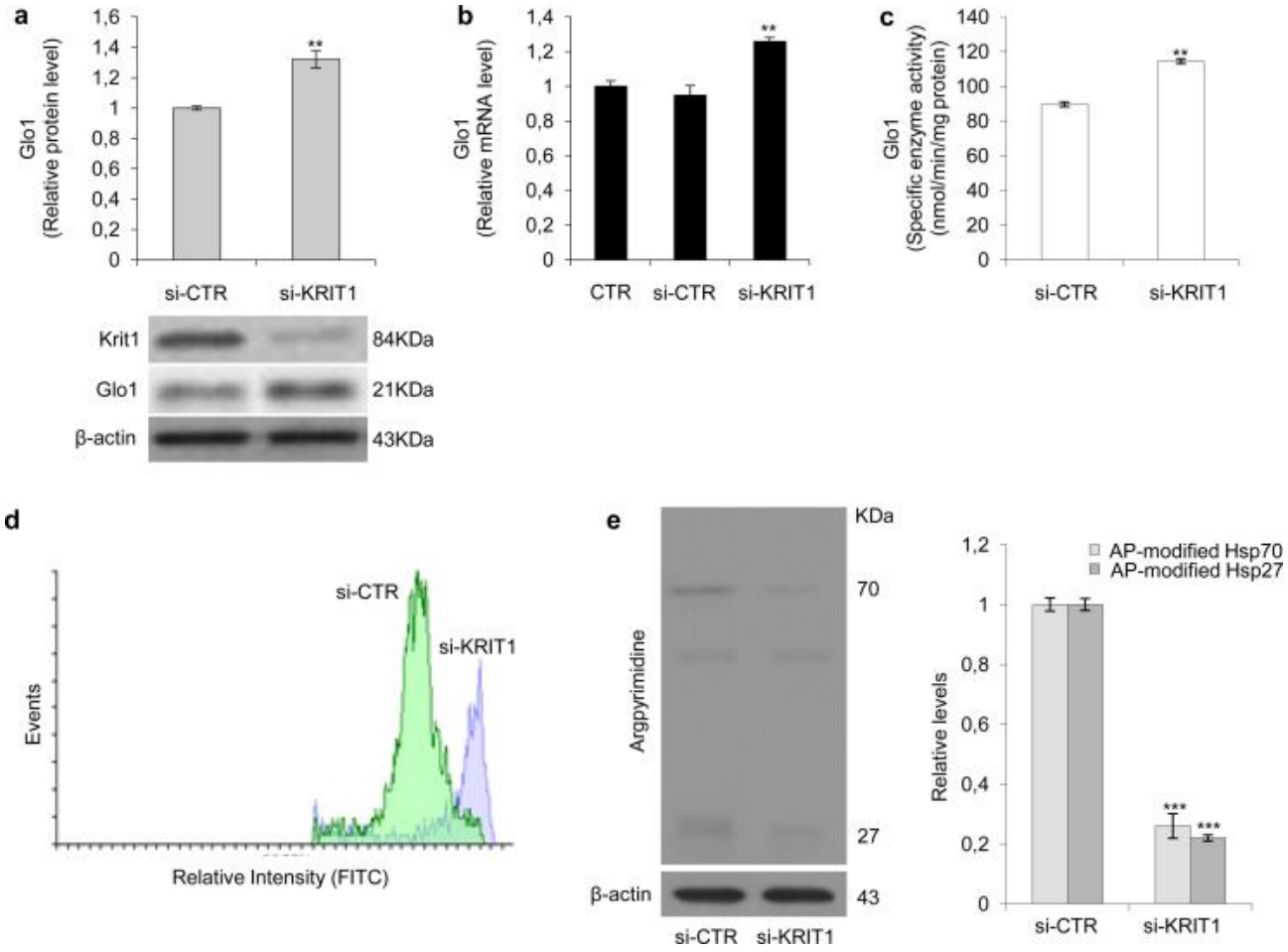

Figure 2. The upregulation of Glyoxalase 1 (Glo1) and the downregulation of argpyrimidine adducts occur also in human brain microvascular endothelial cells upon KRIT1 knockdown. Human brain microvascular endothelial cells (hBMEC) grown under standard conditions were mock transfected (CTR) or transfected with either KRIT1-targeting siRNA (siKRIT1) or a scrambled control (siCTR). Cells were then either lysed and analyzed by Western blotting (a,e), qRT-PCR (b), and spectrophotometric enzymatic assay (c), or treated with DCFH-DA for measurement of cellular levels of general reactive oxidative species by image-based cytometry (d), as described in Materials and Methods. Representative WB and quantitative histogram of the relative KRIT1 and Glo1 protein expression levels in si-CTR and si-KRIT1 cells. β-actin was used as internal loading control for WB normalization (a). The WB bands of Glo1 were quantified by densitometric analysis, and normalized optical density values were expressed as relative protein level units referred to the average value obtained for si-CTR samples. Glo1 mRNA expression levels were analyzed in triplicate by qRT-PCR and normalized to the amount of an internal control transcript (human β-actin). Results are expressed as relative mRNA level units referred to the average value obtained for control cells (CTR), and represent the mean (± SD) of $n \geq 3$ independent qRT-PCR experiments (b). Glo1 enzyme activity was measured in cytosolic extracts of si-CTR and si-KRIT1 cells according to a spectrophotometric

method monitoring the increase in absorbance at 240 nm due to the formation of S-D-lactoylglutathione (c). Glo1 activity is expressed in milliunits per mg of protein, where one milliunit is the amount of enzyme that catalyzes the formation of 1 nmol of S-D-lactoylglutathione per min under assay conditions. Results represent the mean (± SD) of $n \geq 3$ independent experiments performed in triplicate (c). Measurement of cellular levels of general reactive oxidative species. si-CTR and si-KRIT1 endothelial cells were left untreated or treated with DCFH-DA, and DCF fluorescence intensity was analyzed by a Tali® Image-Based Cytometer. The representative cytometer profile shows the increase in DCF fluorescence intensity in si-KRIT1 cells as compared to the control (si-CTR) (d). Representative WB and quantitative histogram of argpyrimidine (AP) adducts in si-CTR and si-KRIT1 endothelial cells as detected using a specific mAb. β-actin was used as internal loading control for WB normalization (e). Western blots are representative of three separate experiments. **$p \leq 0.01$ compared to control (CTR or si-CTR) cells. Notice that KRIT1 knockdown in human brain microvascular endothelial cells leads to a significant increase in Glo1 expression and activity, and a decrease in the intracellular levels of major AP adducts of 70 and 27 kDa.

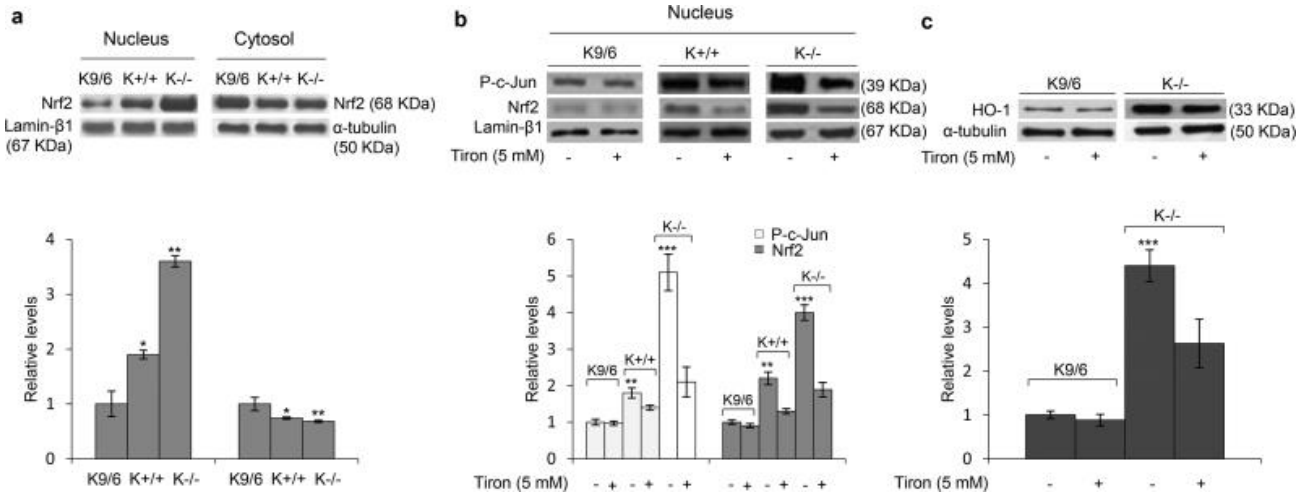

Figure 3. KRIT1 loss-dependent upregulation of Glo1 is part of a cell adaptive response to oxidative stress involving the master redox-sensitive transcriptional regulator Nrf2. Wild type (K+/+), KRIT1–/– (K–/–), and KRIT1 –/– re-expressing KRIT1 (K9/6) MEF cells grown to confluence under standard conditions were left untreated (a) or either mock-pretreated (-) or pretreated (+) with the ROS scavenger Tiron (b,c). Nuclear and cytoplasmic fractions (a,b) or total cell extracts (c) were then obtained and analyzed by Western blotting for the indicated proteins. Nuclear levels of p-c-Jun were used as a control of redox-dependent effect of KRIT1 loss-of-function. Lamin-β1 and α-tubulin were used as internal loading controls for WB normalization of nuclear and total/cytoplasmic proteins, respectively. The histograms below their respective Western blots (a-c) represent the mean (± SD) of the densitometric quantification of three independent experiments. *$p < 0.05$ versus K9/6 cells, **$p \leq 0.01$ versus K9/6 cells, ***$p \leq 0.001$ versus K9/6 cells. Notice that the upregulation of c-Jun and p-c-Jun nuclear levels induced by KRIT1 loss-of-function is paralleled by a marked nuclear accumulation of Nrf2 (a,b) and the upregulation of its downstream effector HO-1 (c), both of which are significantly reverted by cell treatment with the ROS scavenger Tiron (b,c).

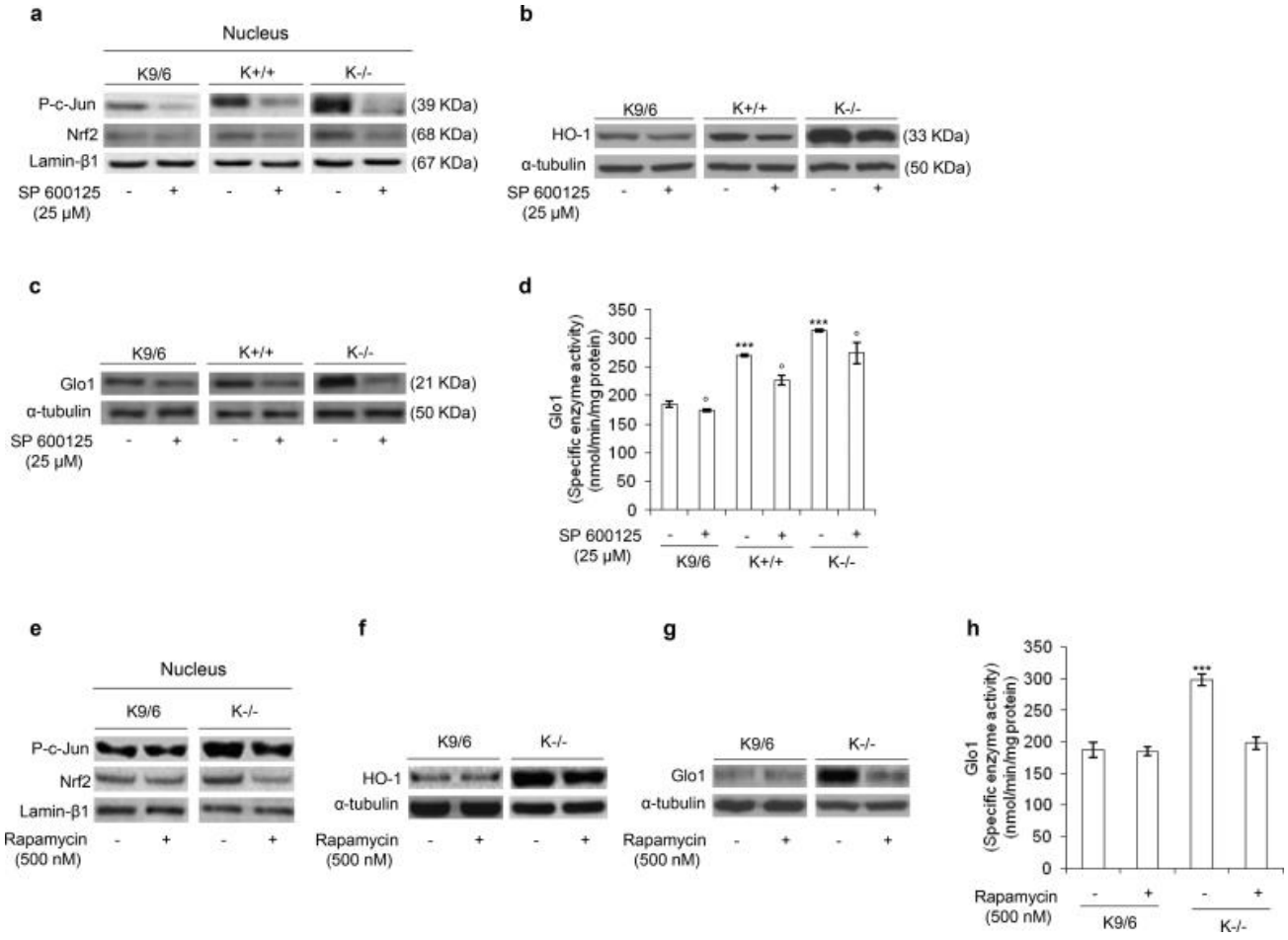

Figure 4. Defective autophagy and JNK activation associated with KRIT1 loss-of-function contribute to the sustained upregulation of Nrf2 and its downstream effectors HO-1 and Glo1. Wild type (K+/+), KRIT1 –/– (K–/–), and KRIT1 –/– re-expressing KRIT1 (K9/6) MEF cells grown to confluence under standard conditions were either mock-pretreated (-) or pretreated (+) with the JNK inhibitor SP600125 (a-d), or the autophagy inducer Rapamycin (e-h). Nuclear and cytoplasmic fractions or total cell extracts were then obtained and analyzed by Western blotting (a-c, e-g) and spectrophotometric enzymatic assay (d,h) for the indicated proteins, as described in Fig. 1a-c. Nuclear levels of p-c-Jun were used as a control of redox-dependent effect of KRIT1 loss-of-function. Lamin-β1 and α-tubulin were used as internal loading controls for WB normalization of nuclear and total/cytoplasmic proteins, respectively. Histograms represent the mean (± SD) of $n \geq 3$ independent experiments performed in triplicate. **$p \leq 0.01$ and ***$p \leq 0.001$ versus K9/6 cells; °$p \leq 0.05$ and °°$p \leq 0.01$ versus mock-pretreated (-) cells. Notice that the redox-sensitive nuclear accumulation of Nrf2 and upregulation of its downstream effectors HO-1 and Glo1 induced by KRIT1 loss-of-function were significantly reverted by cell treatment with either the JNK inhibitor SP600125 (a-d) or the autophagy inducer Rapamycin (e-h).

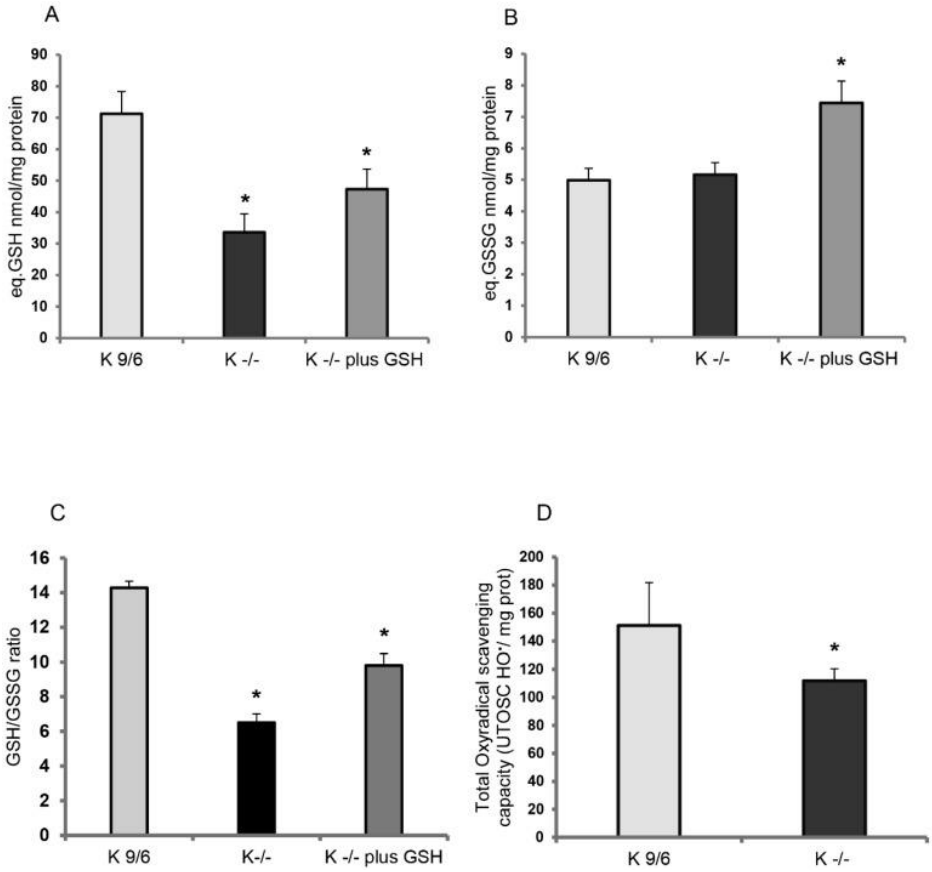

Figure 5. KRIT1 loss-of-function induces GSH depletion. (A,B) The amounts of total glutathione (GSH+GSSG in GSH equivalents) (A) and oxidized glutathione (GSSG) (B) were quantified in K−/− cells left untreated or treated for 4 h with liposome-encapsulated GSH (5 mM final concentration) by an established enzymatic recycling assay. K9/6 cells were used as control. (C) Histogram representing the GSH/GSSG ratio. (D) Total antioxidant capacity for peroxyl radicals in K9/6 and K−/− cells, as determined by the total oxyradical scavenging capacity (TOSC) assay described in Materials and Methods. For all measurements, TOSC values were referred to protein concentration counterparts. Results are reported as mean values ± standard deviation (S.D.) of six different experiments. Asterisks above histogram bars indicate significant differences ($p \leq 0.05$) between groups of means (post hoc comparison).

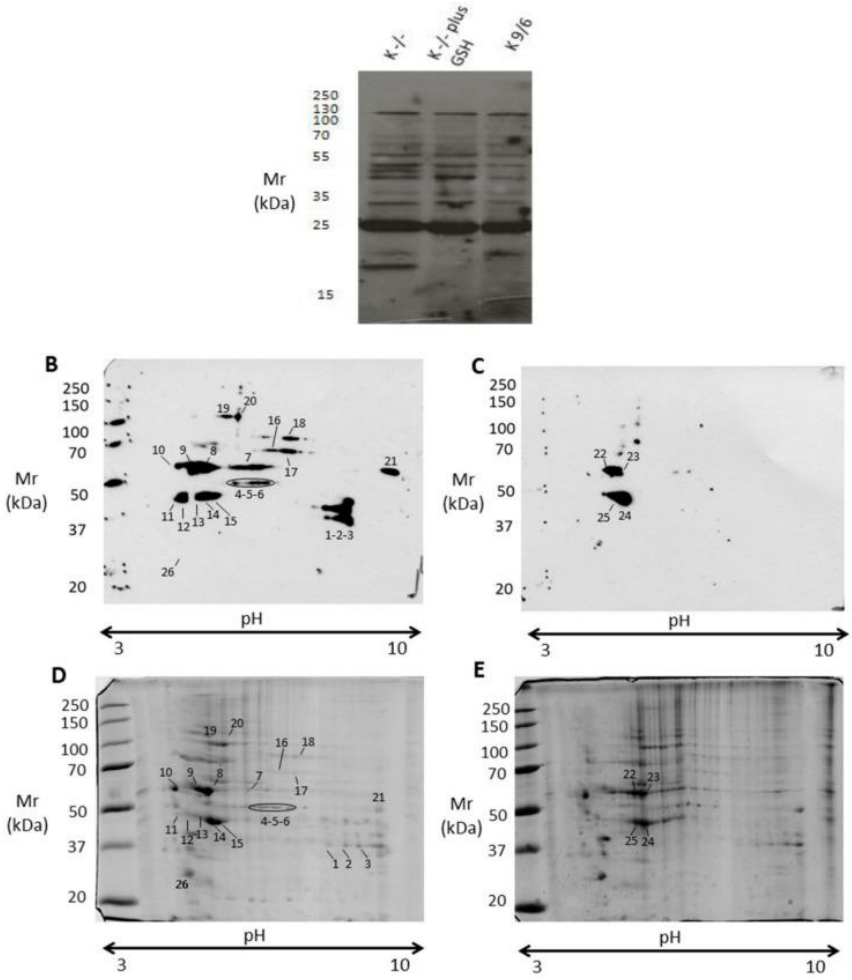

Figure 6. KRIT1 loss-of-function induces changes in protein S-glutathionylation pattern. Total protein extracts of K−/− cells left untreated or treated for 4 h with 5 mM GSH encapsulated within liposomes were separated by monodimensional (A) and two-dimensional electrophoresis (B–E) under nonreducing conditions, and analyzed by immunoblotting with an anti-GSH antibody to detect protein S-glutathionylation adducts (A–C), or by colloidal Coomassie staining to identify protein spots by mass spectrometry analysis (D,E). K9/6 cells were used as control. (A) Equal amounts of protein extracts (30 μg) of the indicated cells were analyzed by SDS-PAGE and Western blotting under nonreducing conditions. (B–E) Equal amounts of protein extracts (200 μg) of K−/− (B,D) and K9/6 (C,E) cells were analyzed by two-dimensional (2-D) electrophoresis and Western blotting. Parallel experiments were performed for Western blotting (B,C) and colloidal Coomassie staining (D,E) analyses. Digitalized images of PVDF membranes and colloidal Coomassie-stained gels were acquired and analyzed with a dedicated software that ensured spot matching and relative quantitation. Gel spots corresponding to immunoreactive signals were manually excised from 2D-gels and further subjected to mass spectrometric analysis. Experiments were performed in technical duplicate on two biological replicates.

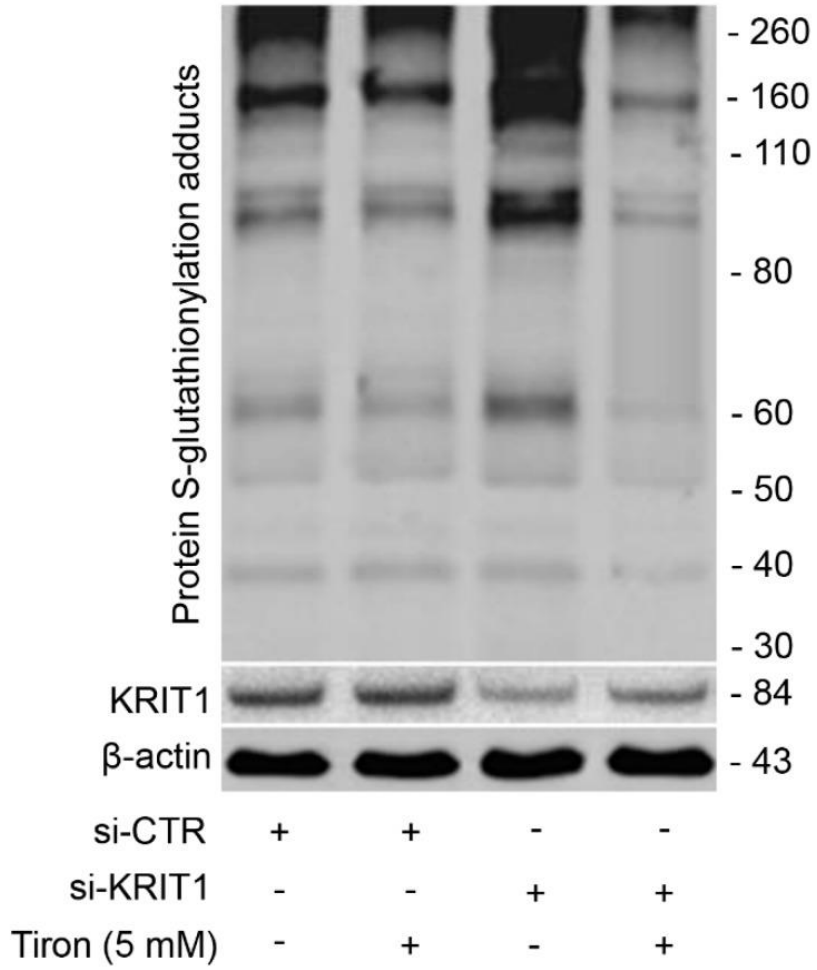

Figure 7. Redox-dependent changes in PSSG occur in human brain microvascular endothelial cells upon KRIT1 knockdown. Human brain microvascular endothelial cells (hBMEC) grown under standard conditions were transfected with either KRIT1-targeting siRNA (si-KRIT1) or a scrambled control (si-CTR). Cells were then either left untreated or treated with Tiron, lysed, and analyzed by Western blotting under nonreducing conditions with an anti-GSH antibody to detect protein S-glutathionylation adducts, and then compared with KRIT1 protein expression levels. β-actin was used as internal loading control for Western blot normalization. Results are representative of three separate experiments. Notice that KRIT1 knockdown in human brain microvascular endothelial cells leads to a significant increase in the levels of protein S-glutathionylation adducts, which are significantly reverted by cell treatment with the ROS scavenger Tiron.

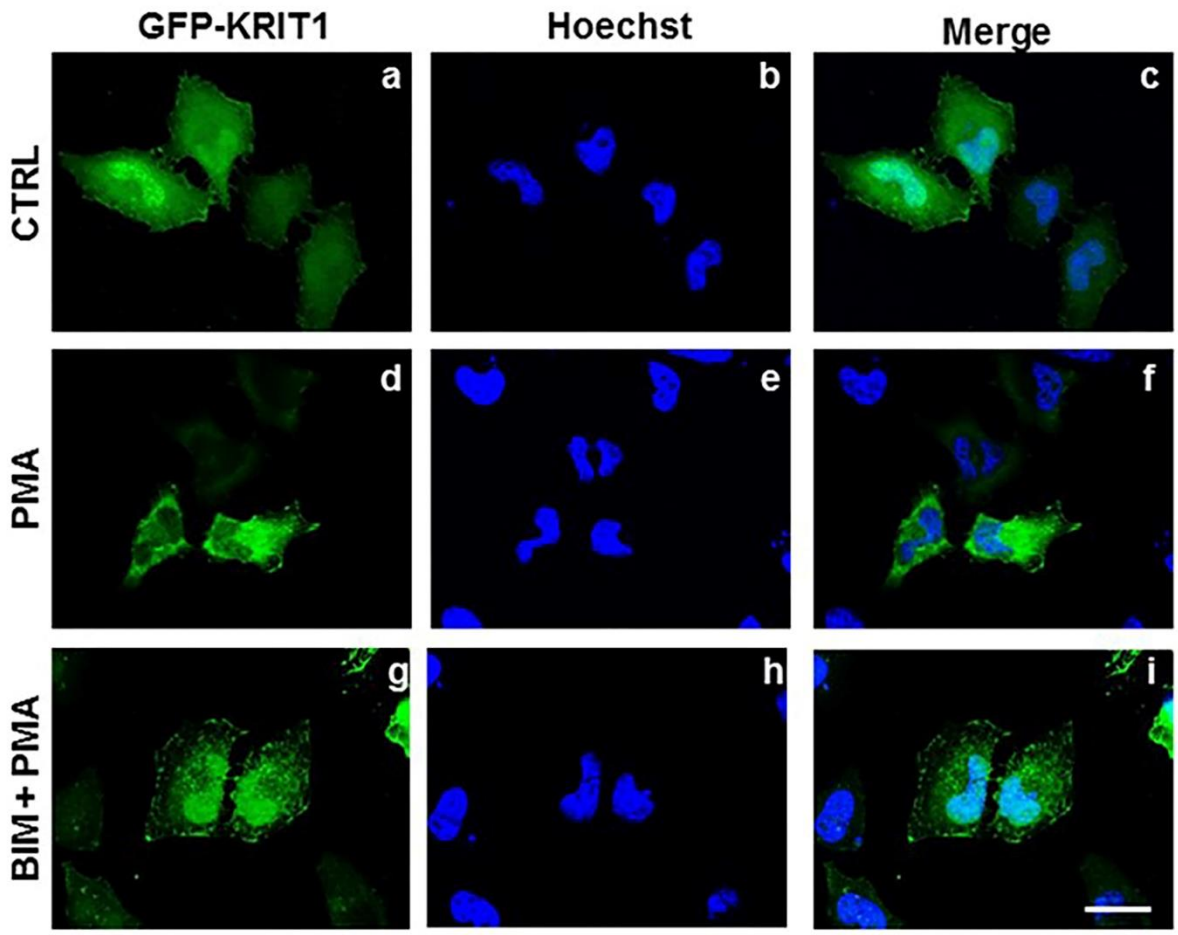

Figure 8. PKC activity regulates the nucleocytoplasmic shuttling of KRIT1. HeLa cells transiently transfected with a construct encoding GFP-KRIT1 were either vehicle-treated (DMSO vehicle alone) (CTRL, panels a-c), treated with PMA (20 ng/mL for 2 h) (PMA, panels d-f), or pre-treated with BIM (1 μM for 30 min) before PMA treatment (BIM+PMA, panels g-i), and GFP-KRIT1 subcellular distribution was assessed by fluorescence microscopy. Nuclei were visualized with the DNA-specific blue fluorescent dye Hoechst. Images are representative of several (> 3) independent experiments. Notice that, as compared to the prevalent nuclear localization of GFP-KRIT1 in vehicle-treated cells (panels a-c), cell treatment with the PKC activator PMA resulted in a drastic shift in GFP-KRIT1 subcellular distribution towards an almost exclusively cytoplasmic localization (panels d-f), which was prevented by cell pre-treatment with the PKC inhibitor BIM (panels g-i), suggesting a role for PKC activation in regulation of KRIT1 nucleocytoplasmic shuttling. Scale bar represents 15 μm.

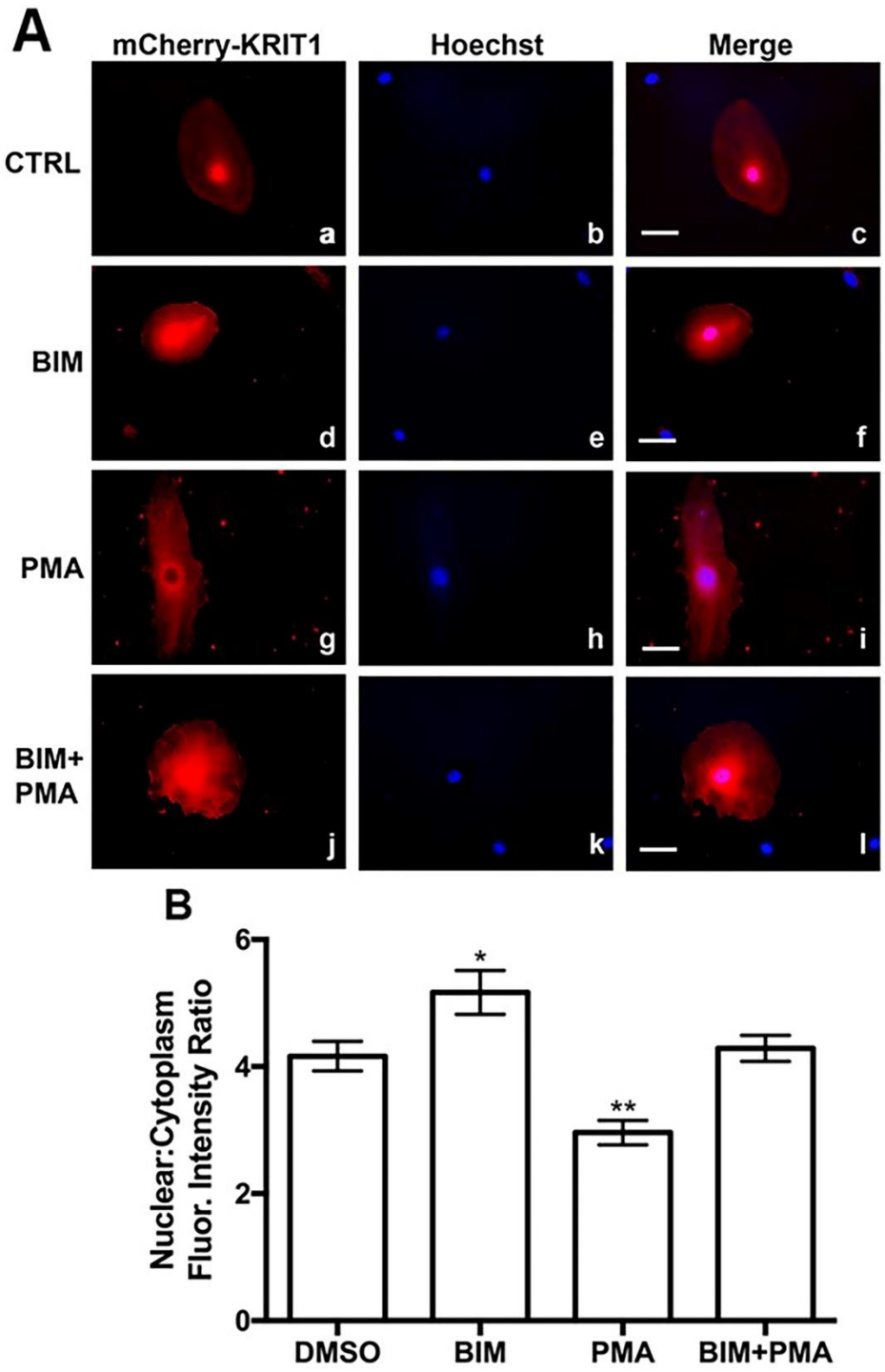

Figure 9. The PKC-dependent nucleocytoplasmic translocation of KRIT1 occurs also in endothelial cells. (A) Representative mCherry-KRIT1 fluorescence, nuclear staining (Hoechst), and merged images in adenovirally transduced human pulmonary artery endothelial cells (HPAEC). Cells were treated with DMSO vehicle (CTRL; panels a-c), 1 µM BIM for 30 min (panels d-f), 20 ng/mL PMA for 2 h (panels g-i), or pretreated for 30 min with the PKC-specific inhibitor BIM (panels j-l) before PMA administration. Subcellular localization of mCherry-KRIT1 was analyzed by epifluorescence

microscopy. Consistent with observations in HeLa cells, PMA promoted KRIT1 translocation from the nucleus to cytoplasm, while BIM treatment promoted nuclear accumulation. Scale bar represents 20 μm. (B) Quantification of nuclear/cytoplasmic fluorescence. Data shown are mean ratios +/- SEM. n=36 cells from 5 biological replicates. *$p<0.05$; **$p<0.01$ vs. vehicle.

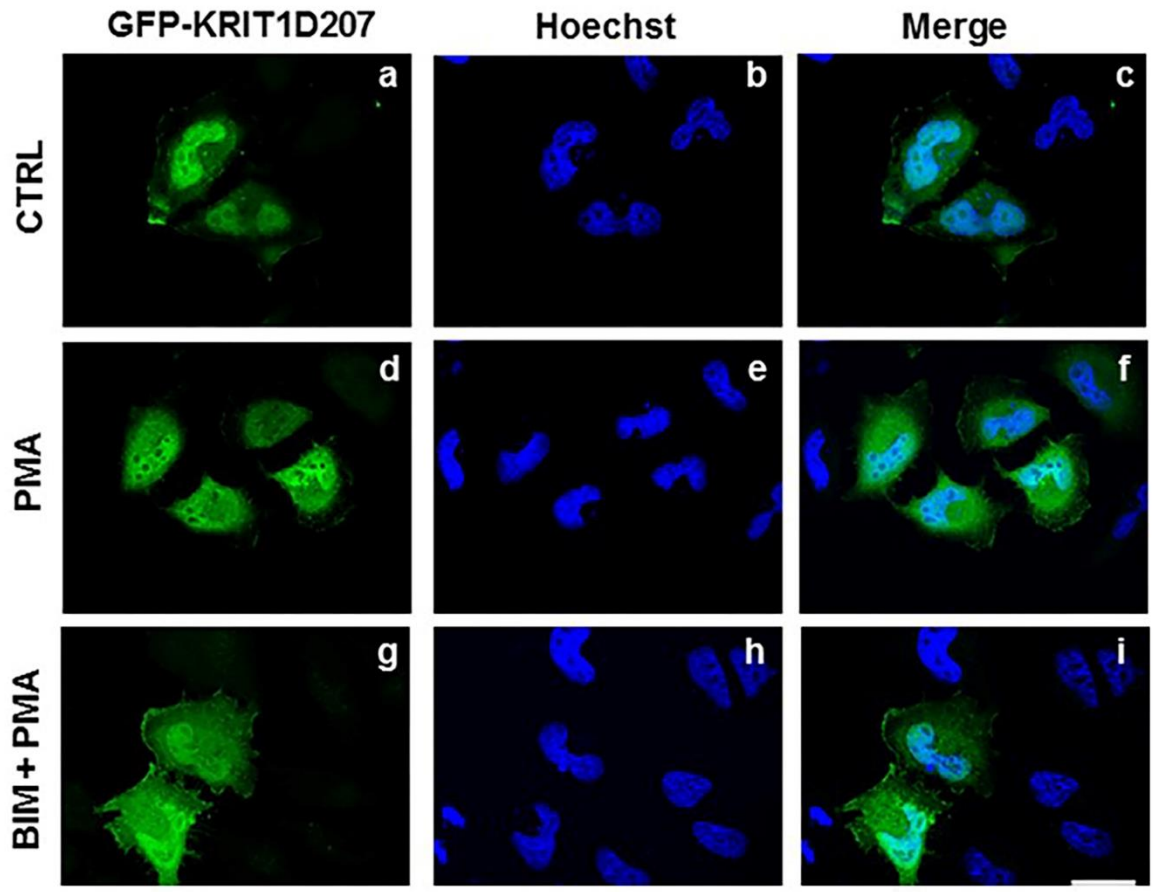

Figure 10. The N-terminal domain plays a crucial role in KRIT1 nucleus-to-cytoplasm translocation induced by PKC activation. HeLa cells transiently transfected with a construct encoding GFP-KRIT1Δ207, a GFP-tagged KRIT1 deletion mutant lacking the N-terminal domain (207 amino acids), were treated with DMSO vehicle (CTRL) (panels a-c), PMA (panels d-f), or pretreated with BIM before PMA administration (panels g-i), and the subcellular distribution of GFP-KRIT1Δ207 was assessed by fluorescence microscopy. Nuclei were visualized with the DNA-specific blue fluorescent dye Hoechst. Images are representative of several (> 3) independent experiments. Notice that the absence of the N-terminal region impaired KRIT1 impaired ability to translocate from the nucleus to cytoplasm upon PKC activation.

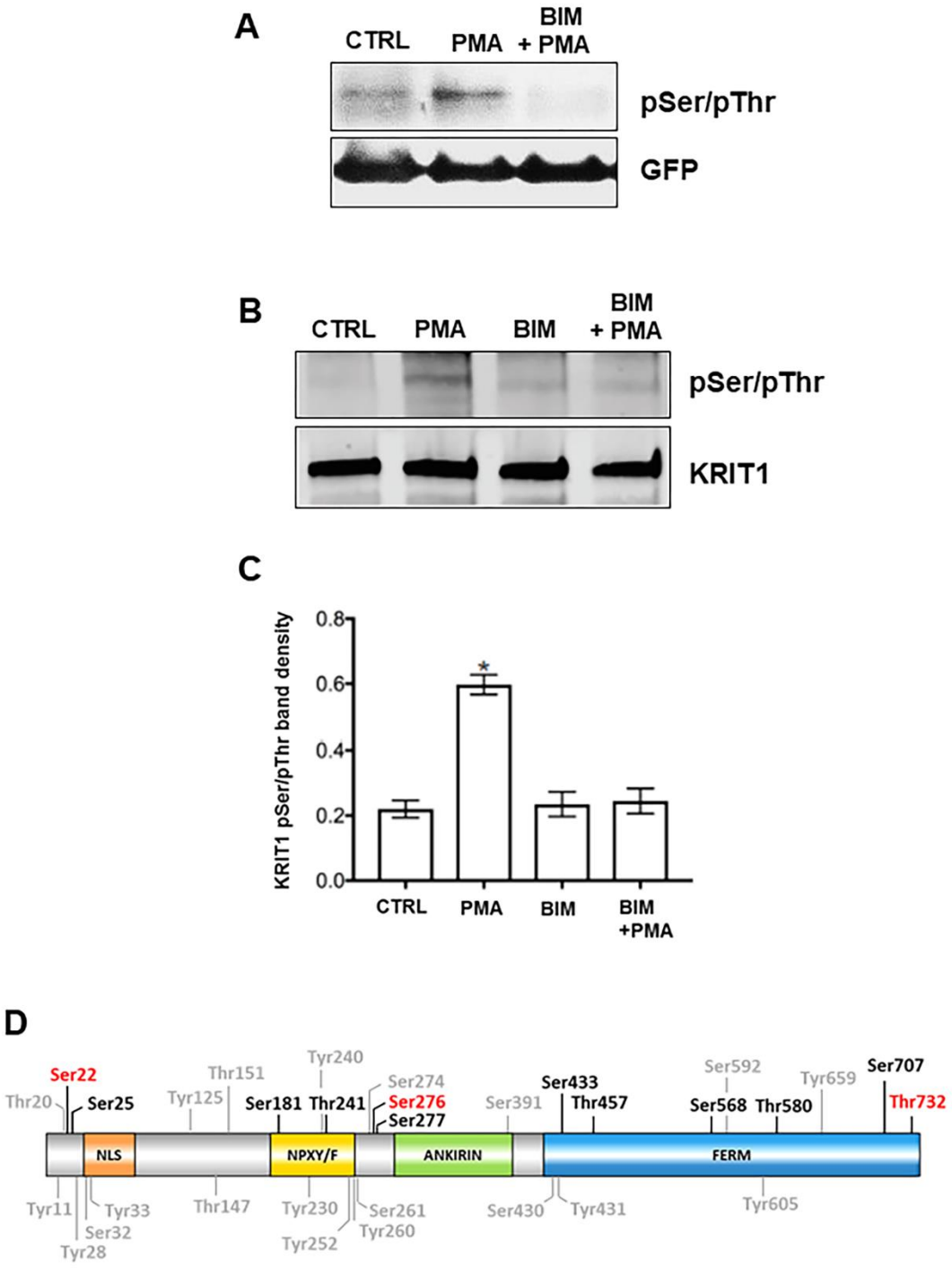

Figure 11. PMA treatment induces Ser/Thr phosphorylation of KRIT1. (A) HeLa cells transiently transfected with GFP-KRIT1 were treated with vehicle (CTRL), PMA or PMA plus BIM. Whole-cell extracts were subjected to immunoprecipitation with anti-GFP antibody and Ser/Thr phosphorylation of KRIT1 was detected with antibodies against pSer/Thr by Western blot analysis. Blots were probed for GFP-KRIT1 as loading control for immunoprecipitation. Notice that after PMA treatment a

marked phosphorylation of KRIT1 in Ser/Thr residues was detectable. BIM pretreatment completely prevented PMA-induced KRIT1 phosphorylation. (B) Representative pSer/pThr blot of transduced HPAEC lysates after immunoprecipitation with a specific anti-KRIT1 antibody. Blots were probed for total KRIT1 as loading control for immunoprecipitation. Bands shown (100 kDa) are mCherry-KRIT1, endogenous KRIT1 expression is below the antibody detection limit. Consistent with results from HeLa cells, PMA treatment induced KRIT1 Ser/Thr phosphorylation. (C) Densitometry analysis of pSer/pThr in HPAEC. Data shown are mean band density +/- SEM. n=6, *$p<0.01$ vs. vehicle. (D) General KRIT1 phosphorylation sites reported in available phosphorylation databases (Ser, Thr and Tyr residues indicated in light grey), and potential PKC-specific KRIT1 Ser and Thr phosphorylation sites predicted by our analysis with the Group-Based Prediction System (GPS) 5.0 (Ser and Thr residues indicated in black and red colors, where the red color serves to highlight residues reported also in phosphorylation databases).

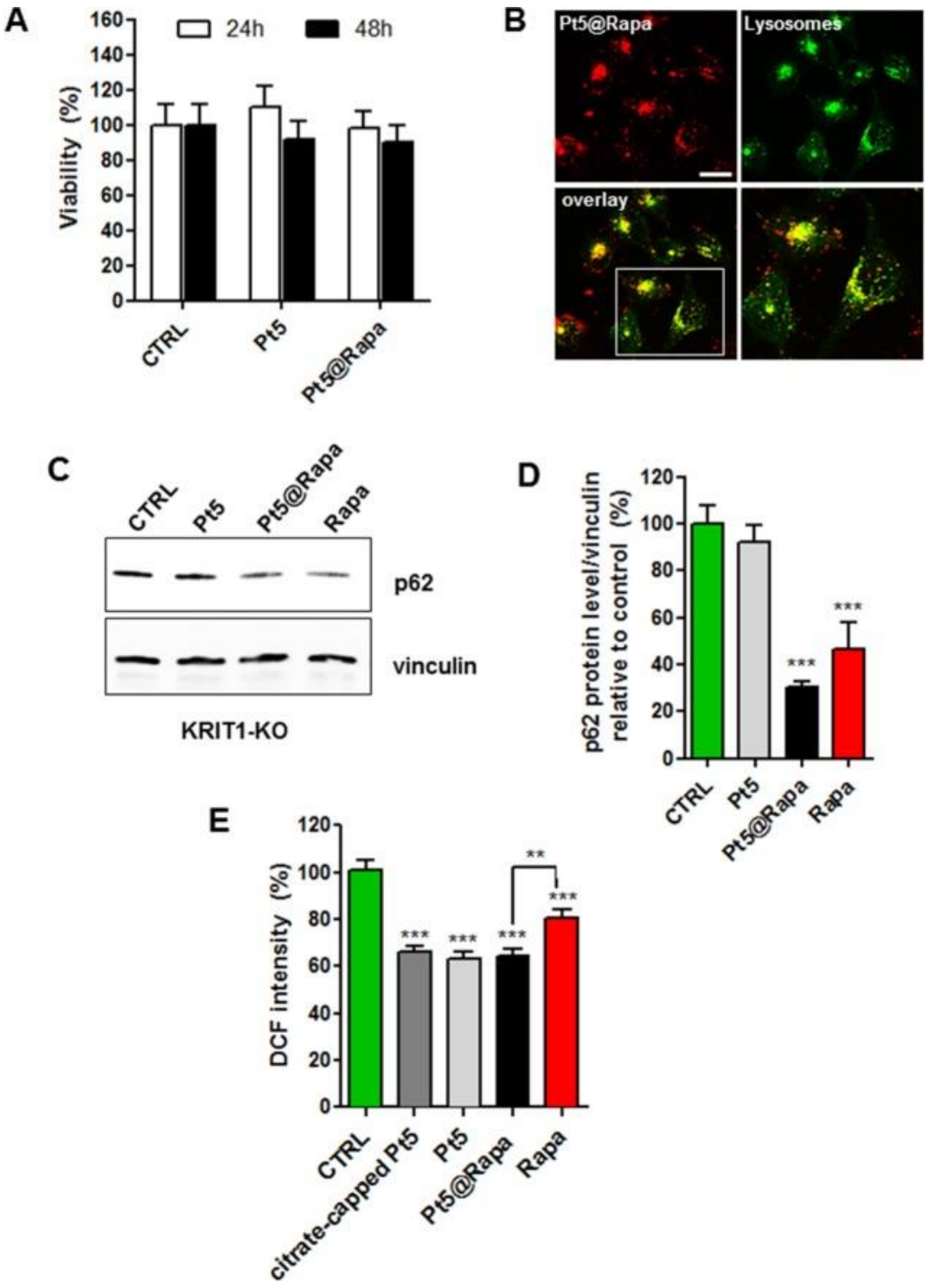

Figure 12. Pt5@Rapa NPs as an antioxidant nanocarrier for rapamycin delivery. (A) Viability of KRIT1-KO MEFs after exposure for 24 and 48 h to 50 μg/mL Pt5 or Pt5@Rapa NPs. Viability of treated cells is expressed as relative to untreated control cells (CTRL). Data are reported as mean ± standard deviation (SD). (B) Representative confocal fluorescence images of the internalization of Pt5@Rapa NPs into KRIT1-KO MEFs. Scale bar: 20 μm. Top left: fluorescent Pt5@Rapa NPs (red); top right: lysosomes stained with LysoTracker Green (green); low left: merged images; low right: magnification of the area in the white box. (C) Immunoblot analysis of p62 expression in KRIT1-KO

MEFs untreated (CTRL) or treated for 15 h with 50 μg/mL Pt5, Pt5@Rapa NPs, or 500 nM rapamycin. Vinculin was used as a loading control. (D) Quantification of p62 on vinculin in KRIT1-KO MEFs, representative of three independent Western blot experiments, is reported. (E) ROS levels in KRIT1-KO MEFs untreated (CTRL), or exposed for 15 h to 50 μg/mL of citrate-capped Pt5, Pt5, Pt5@Rapa NPs, or 500 nM rapamycin was evaluated by dichlorodihydrofluorescein diacetate (DCFH-DA) assay. DCF intensity of treated KRIT1-KO MEFs is expressed relative to untreated KRIT1-KO MEFs. At least three independent experiments were performed. Data are expressed as mean ± SD. Differences between treated samples and the control were considered statistically significant for p-values <0.05 (***$p < 0.001$).

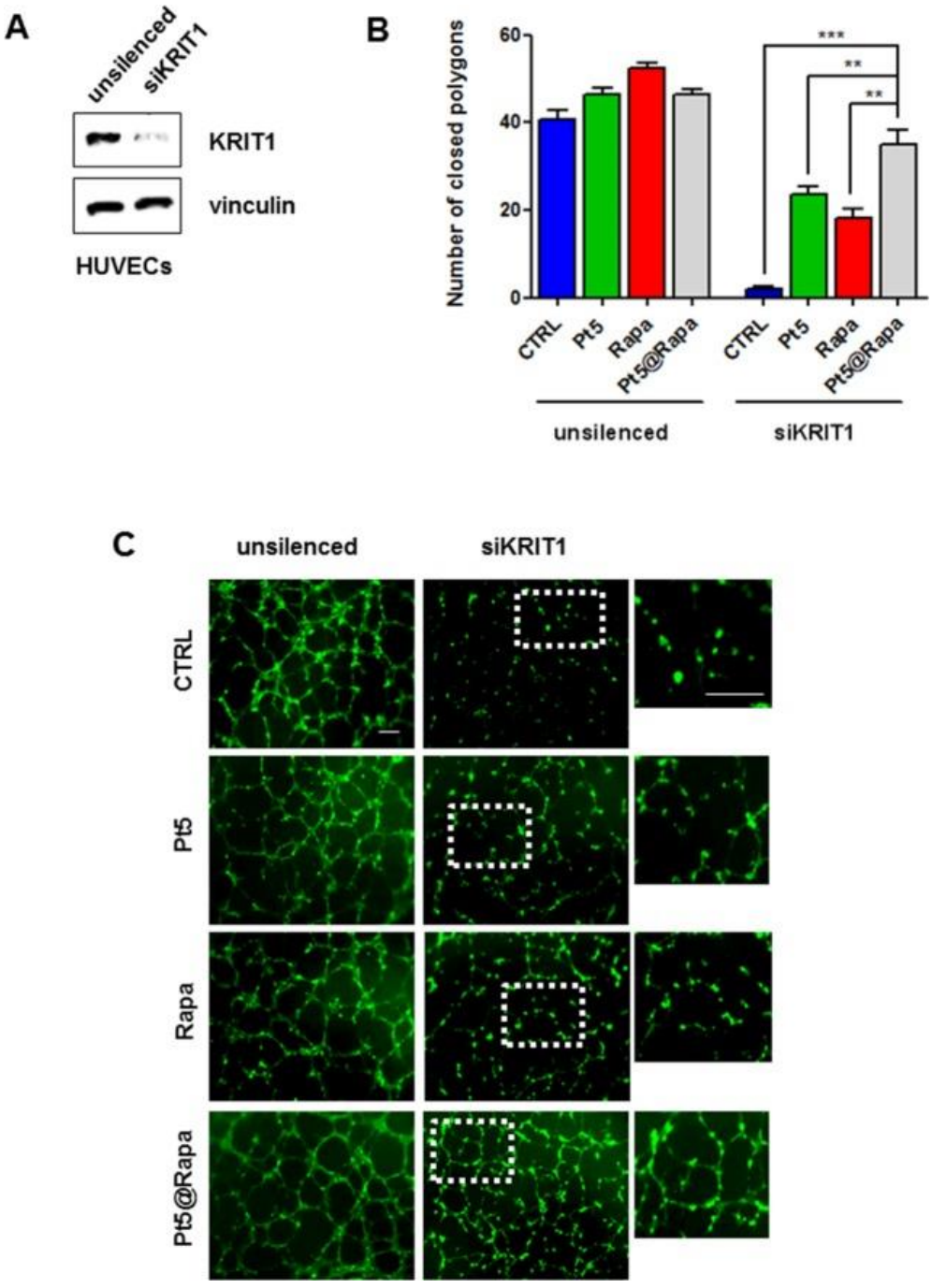

Figure 13. Pt5@Rapa NPs as angiogenesis modulator. (A) Immunoblot analysis of KRIT1 silencing in HUVECs transfected with negative control siRNA (unsilenced) or KRIT1 siRNA (siKRIT1) for 72 h. Vinculin was used as loading control. (B) Quantitative evaluation of tube formation as the number of closed polygons formed in 8 fields for each experimental condition: unsilenced or KRIT1-silenced HUVECs, left untreated (CTRL) or treated for 15 h with 50 μg/mL of Pt5 NPs, 500 nM rapamycin, or 50 μg/mL of Pt5@Rapa NPs. All the data are presented as mean ± SD. (C) Representative images of one of three independent experiments of capillary networks visualized by fluorescent calcein staining. Magnifications are reported in the inserts. Scale bars, 200 μm for full fields and 400 μm for magnified fields.

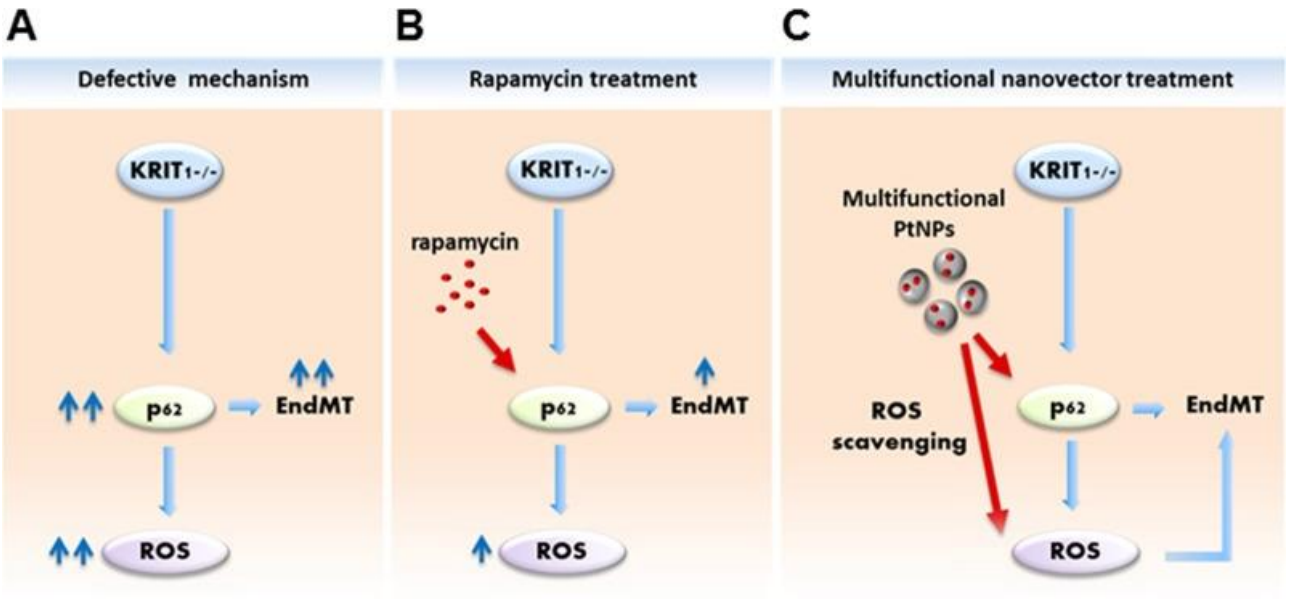

Figure 14. Schematic model of Pt5@Rapa NP mechanism of action in KRIT1-KO cells. (A) KRIT1 loss-of-function impairs autophagy, leading to the aberrant accumulation of autophagy adapter p62, which, in turn, enhances intracellular ROS and promotes the EndMT switch, the two crucial events that contribute to CCM progression. (B) Therapeutic reactivation of autophagy with rapamycin in KRIT1-KO cells decreases p62 accumulation, reduces intracellular accumulation of ROS, and inhibits the EndMT switch. (C) PtNPs-based combinatorial treatment exerts synergistic effects that enhances the efficacy of the therapeutic treatment. Pt5@Rapa NPs in KRIT1-KO cells work as multifunctional nanoplatform simultaneously acting as ROS-scavenging materials and drug nanocarriers. Pt5@Rapa NPs counterbalance the increase in intracellular ROS levels through their activity of antioxidant enzymes and deliver rapamycin into the cells to decrease the aberrant accumulation of p62. Together, these activities restore ROS homeostasis and inhibit EndMT with a higher efficacy than the treatment with rapamycin alone.

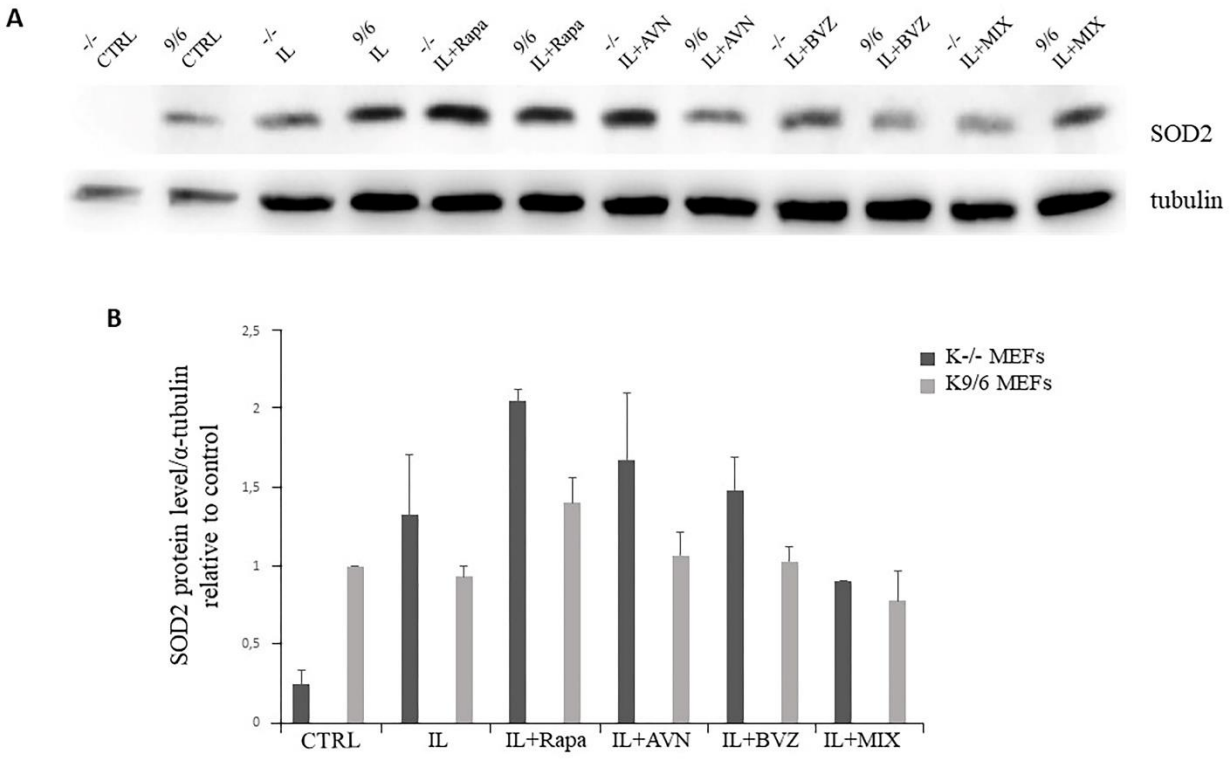

Figure 15. Lipid nanoparticles (IL) as multi-drug delivery system. (A) Immunoblot analysis of the oxidative stress marker SOD2 expression in KRIT1-KO and KRIT1+/+ MEFs untreated (CTRL) or treated for 12 hours with solid lipid nanoparticles conjugated with rapamycin, bevacizumab, avenanthramide, or with a mixture of all three compounds (herein indicated as MIX) to a final concentration of: AVN = 15 μg/mL (50 μM), RAPA = 0.46 μg/mL (500 nM), BVZ = 10 μg/mL (70 nM). After treatment cells were lysed, as described in Materials and methods, and analyzed for indicated protein by Western blot analysis. (B) The histogram represents the quantitative evaluation by densitometric analysis of SOD2 protein expression levels reported as relative protein level units referred to average value obtained for K9/6 samples. α-tubulin was used as internal loading control for WB normalization. Notice that treatment with rapamycin- and avenanthramide- loaded lipid nanoparticle significantly increase the expression level of SOD2 as compared to control cells. Data show also that lipid nanocarrier exerts an antioxidant effect partially restoring SOD2 expression level.

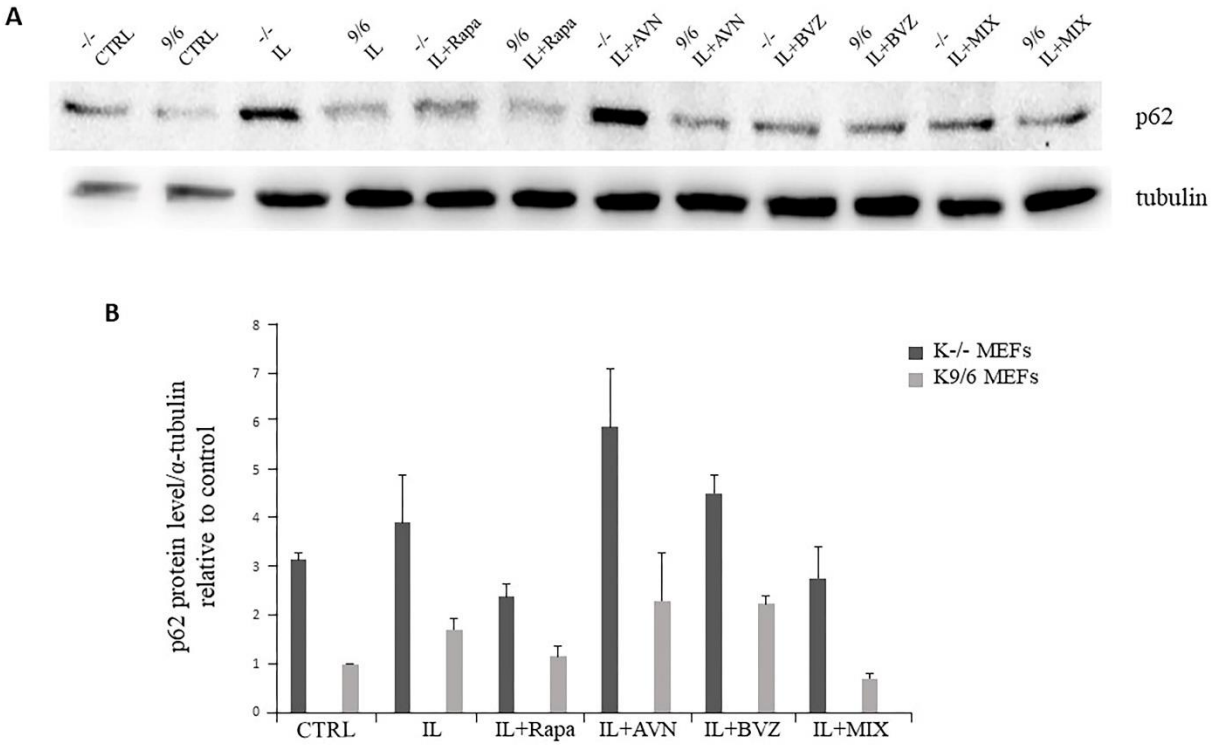

Figure 16. Treatment with lipid nanoparticles (ILs) restores autophagy in KRIT1-KO cells. (A) Immunoblot analysis of p62 expression in KRIT1-KO MEFs untreated (CTRL) treated for 12 hours with solid lipid nanoparticles conjugated with rapamycin, bevacizumab, avenanthramide, or with a mixture of all three compounds (herein indicated as MIX) to a final concentration of: AVN = 15 μg/mL (50 μM), RAPA = 0.46 μg/mL (500 nM), BVZ = 10 μg/mL (70 nM). After treatment cells were lysed, as described in Materials and methods, and analyzed for indicated protein by Western blot analysis. (B) Histograms represent the quantification by densitometric analysis of p62 protein expression levels reported as relative protein level units referred to average value obtained for K9/6 samples. α-tubulin was used as internal loading control for WB normalization. Notice that rapamycin- and mix- loaded lipid nanoparticles reactivate autophagy thus decreasing the cellular accumulation of autophagy adapter p62, while avenanthramide plays an opposite effect.

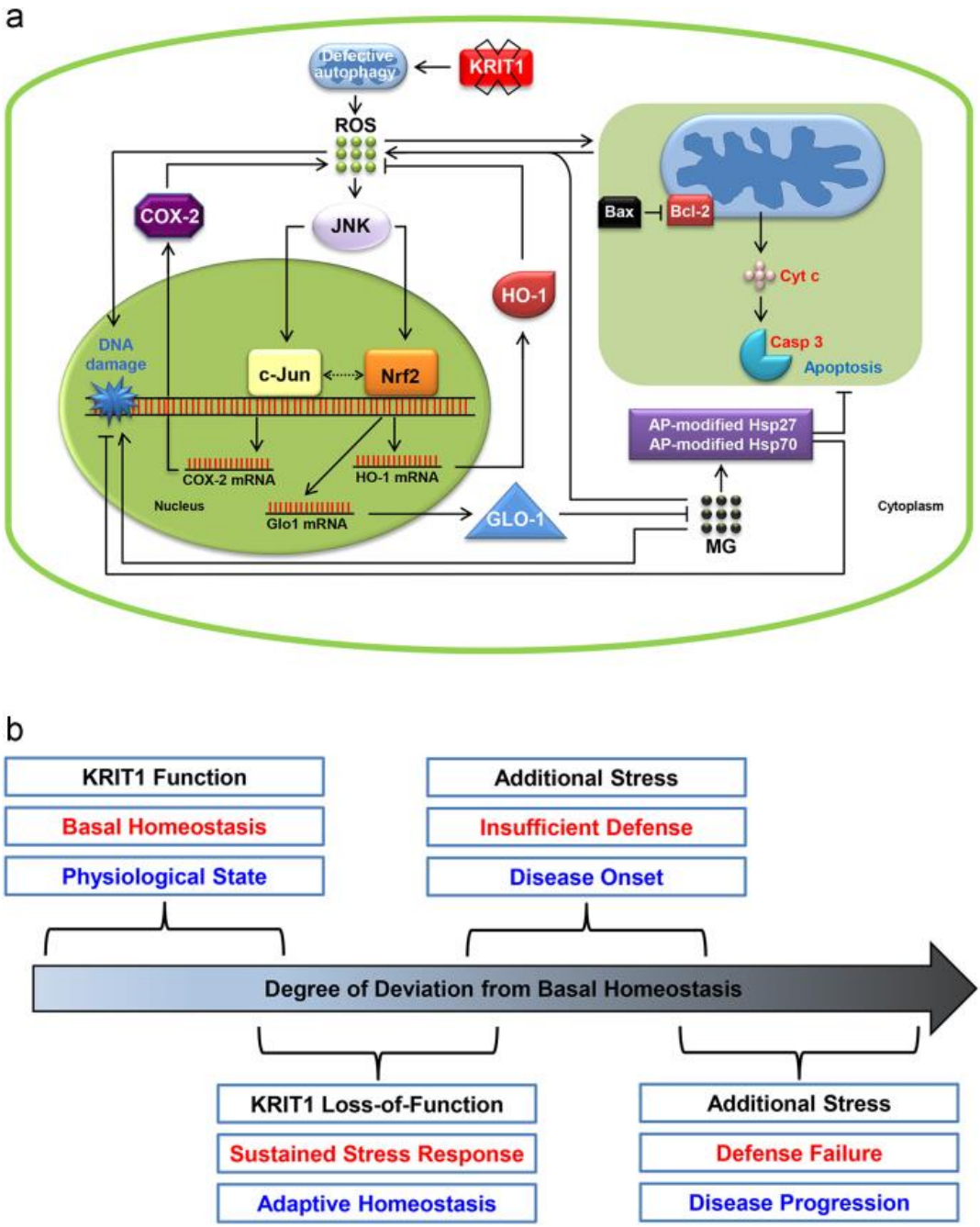

Figure 17. Schematic models representing adaptive redox responses and cellular states associated with KRIT1 loss-of-function. (A) Redox-sensitive pathways modulated by KRIT1 functions. KRIT1 loss-of-function causes a persistent activation of the major redox-sensitive transcription factors c-Jun and Nrf2 and consequent upregulation of downstream targets, including cycloxygenase-2 (COX-2), heme oxygenase-1 (HO-1) and glyoxalase 1 (GLO1). While the c-Jun/COX-2 axis promotes pro-oxidant and pro-inflammatory effects, the Nrf2/HO-1 and Nrf2/GLO1 pathways mediate adaptive antioxidant responses that counteract these effects by limiting ROS and MG intracellular accumulation, thus contributing to reduce a vicious cycle of oxidative stress and providing an adaptive defense for long-term cell survival. However, this sustained adaptive redox homeostasis occurs at the

expense of other cytoprotective mechanisms, including the MG-dependent formation of cytoprotective AP-Hsp27 protein adducts, leading to enhanced cell susceptibility to oxidative DNA damage and apoptosis, and sensitizing cells to additional stressful insults. (B) Spectrum of cellular states associated with KRIT1 loss-of-function. Cellular stress and defense responses associated with KRIT1 dysfunctions can be viewed as distinct but overlapping components of a spectrum of cellular states that ranges from basal homeostatic state, to adaptive stress response, insufficient defense, and defense failure, each of which can be defined in terms of the maintenance of molecular and cellular functions within an acceptable dynamic range. In turn, differences in expression and functional levels of stress-responsive proteins and adaptive defense mechanisms acting within the range of each cellular state may be influenced by genetic variation, resulting in inter-individual differences in adaptive stress responses and susceptibility to disease onset and progression.

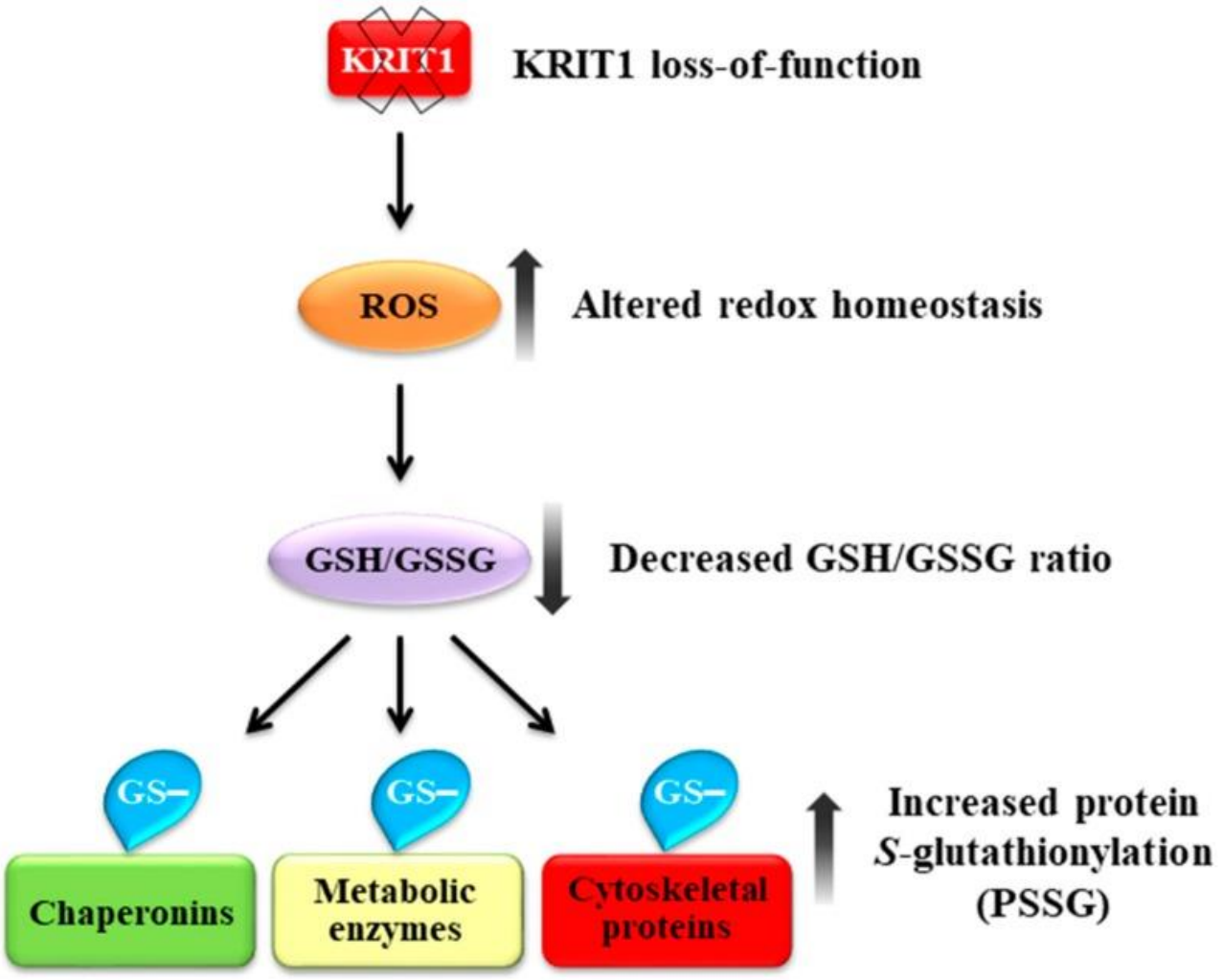

Figure 18. Schematic model representing the S-glutathionylation of distinct structural and regulatory proteins as a novel molecular signature of KRIT1 loss-of-function. The altered intracellular redox homeostasis caused by KRIT1 loss-of-function affects the glutathione (GSH) redox system, leading to a significant decrease in total GSH levels and increase in oxidized glutathione disulfide (GSSG), with a consequent deficit in the GSH/GSSG redox ratio and GSH-mediated antioxidant capacity. These effects are associated with increased S-glutathionylation of distinct proteins involved in adaptive responses to oxidative stress, including redox-sensitive chaperonins, metabolic enzymes, and cytoskeletal proteins, suggesting a novel molecular signature of KRIT1 loss-of-function that could contribute to its emerging pleiotropic effects in the pathogenesis of CCM disease.

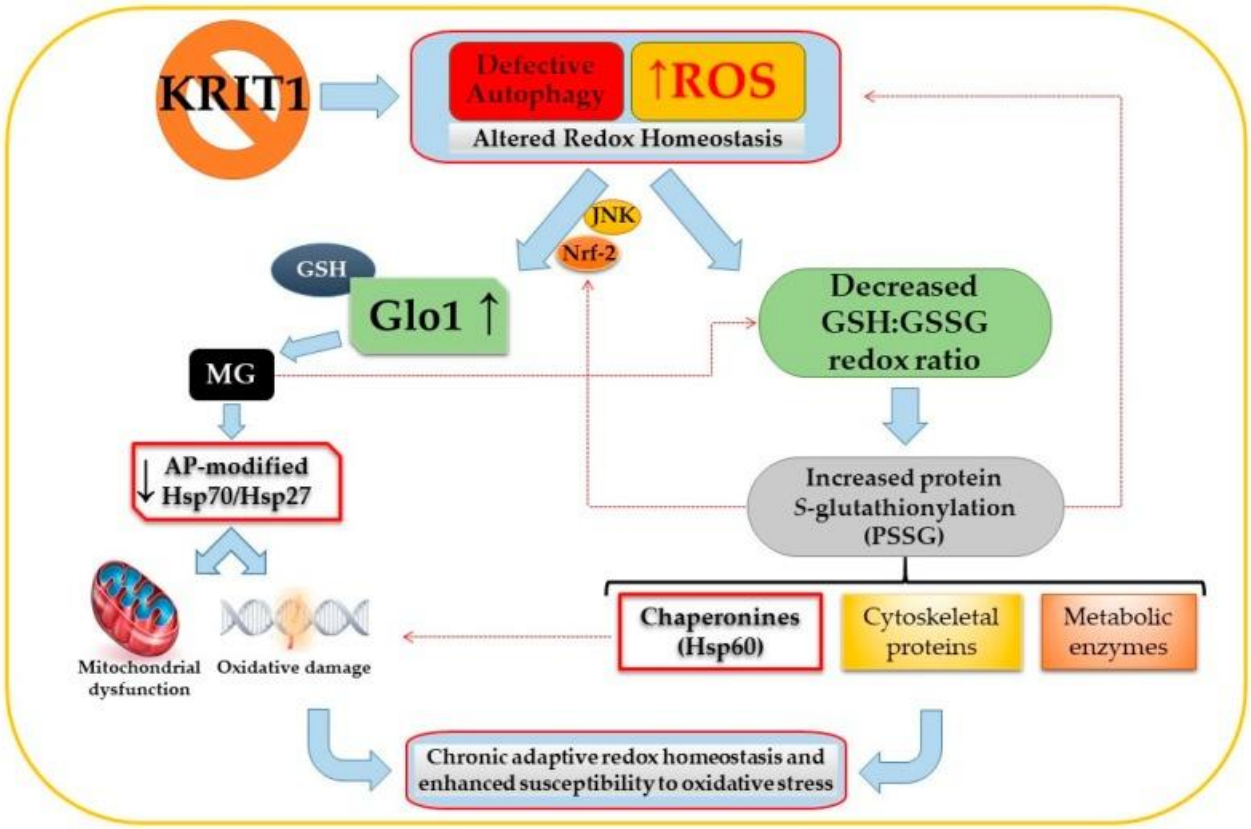

Figure 19. Potential interplay between methylglyoxal (MG)-mediated glycation and S-glutathionylation pathways induced by KRIT1 loss-of-function. The impairment of intracellular redox homeostasis caused by KRIT1 loss-of-function leads to a reactive oxygen species (ROS)-dependent sustained activation of the JNK-Nrf2 (c-Jun N-terminal kinase -nuclear factor erythroid 2-related factor) pathway and upregulation of downstream targets, including Glyoxalase 1 (Glo1). In turn, Glo1 upregulation results in decreased intracellular levels of cytoprotective MG adducts, including argpyrimidine (AP)-modified heat-shock proteins (HSP) 27 and 70, leading to an increased cell susceptibility to oxidative damage and mitochondria-dependent apoptosis. Concomitantly, KRIT1 loss-of-function affects the glutathione (GSH) redox system, causing a significant decrease in the GSH:GSSG redox ratio and an increase in the S-glutathionylation of important structural and regulatory proteins, including metabolic enzymes; cytoskeletal proteins; and chaperonines, such as the HSP60. A potential interplay between the MG-mediated glycation and S-glutathionylation pathways may also occur, including the modulation of the GSH:GSSG redox ratio by MG and the contribution of S-glutathionylation to ROS production and Nrf2 activation (hatched red lines), leading to a synergistic contribution to the chronic adaptive redox homeostasis and enhanced cell susceptibility to oxidative stress associated with KRIT1 loss-of-function mutations. Eventually, these synergistic pathological effects might therefore culminate in cerebral cavernous malformation (CCM) disease onset and severity.

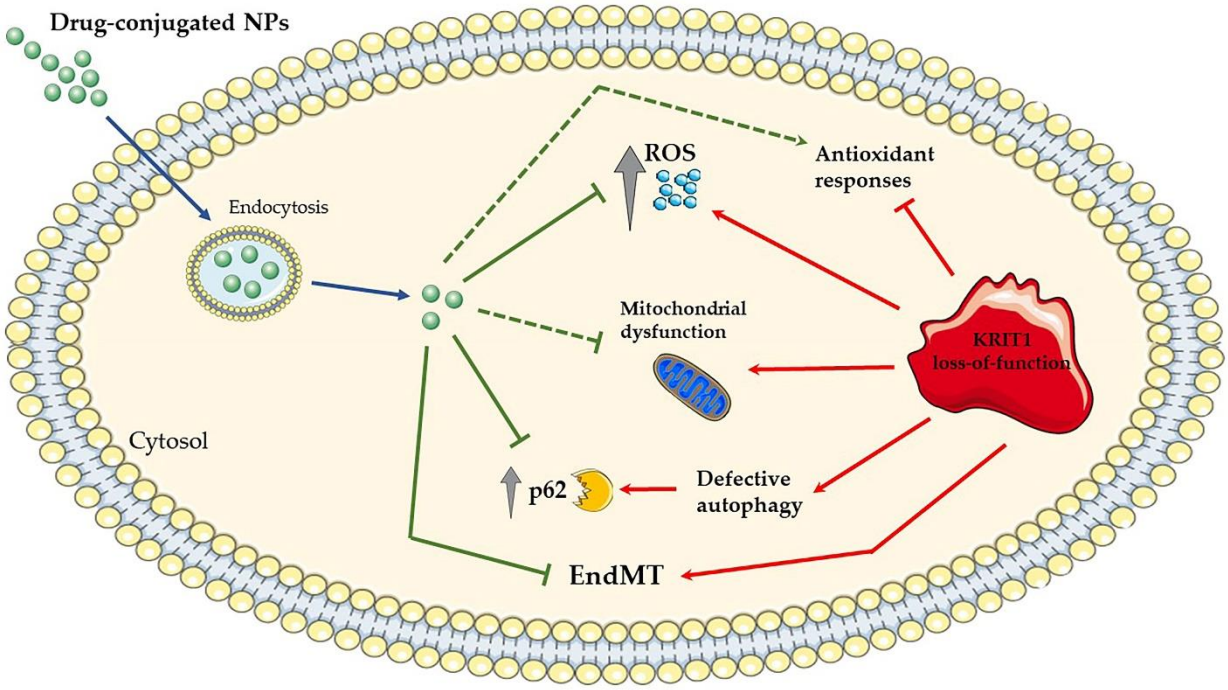

Figure 20. Schematic representation of the synergistic rescue effects of composite platinum/rapamycin nanosystems (Pt@Rapa NPs) in KRIT1-deficient cells. Red and green arrows indicate the detrimental effects of KRIT1 loss-of-function, and the beneficial multifunctional biological activities of platinum/rapamycin nanosystems, respectively. KRIT1 loss-of-function impairs redox homeostasis, mitochondrial function, and autophagy, leading to major molecular and cellular hallmarks of CCM disease pathogenesis, including the aberrant accumulation of intracellular ROS and autophagy markers, such as the p62/SQTSM1 protein, and the induction of endothelial to mesenchymal transition (EndMT), which are synergistically rescued by Pt@Rapa NPs.

Spot	SwissProt Accession	Protein description	Gene name	Mascot score	Unique peptides	Sequence coverage (%)	Mass (Da)	pI
1	P16858	Glyceraldehyde-3-phosphate dehydrogenase	Gapdh	165	3	7.8	36072	8.44
2	P16858	Glyceraldehyde-3-phosphate dehydrogenase	Gapdh	95	2	7.5	36072	8.44
3	P16858	Glyceraldehyde-3-phosphate dehydrogenase	Gapdh	100	2	7.8	36072	8.44
4	P17182	Alpha-enolase	Eno1	553	12	29.7	47453	6.37
5	P17182	Alpha-enolase	Eno1	818	15	42.2	47453	6.37
6	P17182	Alpha-enolase	Eno1	710	14	39.9	47453	6.37
7	P63038	60 kDa heat shock protein	Hspd1	856	14	34.2	61088	5.91
8	P20152	Vimentin	Vim	993	22	50.0	53712	5.06
9	P20152	Vimentin	Vim	968	21	50.4	53712	5.06
10	P14211	Calreticulin 1	Calr	163	4	8.4	48136	4.33
11	Q04447	Creatine kinase B-type	Ckb	190	4	16.5	42971	5.4
12	Q04447	Creatine kinase B-type	Ckb	179	4	16.8	42971	5.4
13	P68372	Tubulin beta-4B chain	Tubb4b	582	11	29.4	50255	4.79
14	P60710	Actin, cytoplasmic 1	Actb	185	4	17.3	42052	5.29
15	P60710	Actin, cytoplasmic 1	Actb	341	7	22.7	42052	5.29
22	P20152	Vimentin	Vim	945	22	43.8	53712	5.06
23	P20152	Vimentin	Vim	961	20	47.9	53712	5.06
24	P60710	Actin, cytoplasmic 1	Actb	276	5	16.3	42052	5.29
25	P60710	Actin, cytoplasmic 1	Actb	276	5	16.3	42052	5.29
26	Q58E70	Tpm 3 protein	Tpm3	502	10	37.9	29231	4.75
	Q6IRU2	Tropomyosin alpha-4 chain	Tpm4	308	6	27.0	28564	4.65

Table 1. Mass spectrometry analysis of tryptic digests from S-glutathionylated proteins. Spot number, SwissProt accession, protein description, gene name, Mascot score, number of unique peptides identified, sequence coverage, and theoretical mass and pI values are reported.

Acknowledgments

Firs of all, I want to thank Prof. Francesco Retta, my mentor and scientific guide, who taught me to manage my experimental life, helping me every time I needed and leading me to this fundamental step in my life carrier. For sure, I would never begin this stressful but exciting, amazing adventure without him. I also wish to gratefully acknowledge Alessandra Bordon, Gaudenzio Inverso, Luigi Battaglia, Chiara Ferraris and Valerio Benedetti, for providing help in experiments and thesis preparation, as well in helpful discussions and comments. They are all more than colleagues, and someone is really special. Moreover, I acknowledge the Italian Research Network for Cerebral Cavernous Malformation (CCM Italia), the Associazione Italiana Angiomi Cavernosi (AIAC) Onlus for fundamental collaboration and support. This work was supported by the Telethon Foundation (grant GGP15219 to SFR), and the University of Torino. Then, near the conclusion but most important at all, a deep acknowledgement to my family: Paola, Pino, Cristiana, Enrico, Alice, and Michela. Because I would never reach my goals, neither in my work neither in my life, even without just one of them. Last but not least, I want to thank my best friends Noemi, Serena, Diego, Chiara, who supports me during these years, also accidentally giving me good ideas. I would like to say much more about anyone mentioned here. This could be enough? I would talk about dreams and future if I could, but that is another story.

References

Aisiku, O., L. Dowal and S. Scarlata (2011). "Protein kinase C phosphorylation of PLCβ1 regulates its cellular localization." Arch Biochem Biophys **509**(2): 186-190.

Akerboom, T. P. and H. Sies (1981). "Assay of glutathione, glutathione disulfide, and glutathione mixed disulfides in biological samples." Methods Enzymol **77**: 373-382.

Andreeva, A. Y., E. Krause, E. C. Müller, I. E. Blasig and D. I. Utepbergenov (2001). "Protein kinase C regulates the phosphorylation and cellular localization of occludin." J Biol Chem **276**(42): 38480-38486.

Antognelli, C., A. Gambelunghe, G. Muzi and V. N. Talesa (2015). "Peroxynitrite-mediated glyoxalase I epigenetic inhibition drives apoptosis in airway epithelial cells exposed to crystalline silica via a novel mechanism involving argpyrimidine-modified Hsp70, JNK, and NF-κB." Free Radic Biol Med **84**: 128-141.

Antognelli, C., A. Gambelunghe, G. Muzi and V. N. Talesa (2016). "Glyoxalase I drives epithelial-to-mesenchymal transition via argpyrimidine-modified Hsp70, miR-21 and SMAD signalling in human bronchial cells BEAS-2B chronically exposed to crystalline silica Min-U-Sil 5: Transformation into a neoplastic-like phenotype." Free Radic Biol Med **92**: 110-125.

Antognelli, C., A. Gambelunghe, V. N. Talesa and G. Muzi (2014). "Reactive oxygen species induce apoptosis in bronchial epithelial BEAS-2B cells by inhibiting the antiglycation glyoxalase I defence: involvement of superoxide anion, hydrogen peroxide and NF-κB." Apoptosis **19**(1): 102-116.

Antognelli, C., I. Palumbo, C. Aristei and V. N. Talesa (2014). "Glyoxalase I inhibition induces apoptosis in irradiated MCF-7 cells via a novel mechanism involving Hsp27, p53 and NF-κB." Br J Cancer **111**(2): 395-406.

Antognelli, C., A. Perrelli, T. Armeni, V. Nicola Talesa and S. F. Retta (2020). "Dicarbonyl Stress and S-Glutathionylation in Cerebrovascular Diseases: A Focus on Cerebral Cavernous Malformations." Antioxidants (Basel) **9**(2).

Antognelli, C., E. Trapani, S. Delle Monache, A. Perrelli, M. Daga, S. Pizzimenti, G. Barrera, P. Cassoni, A. Angelucci, L. Trabalzini, V. N. Talesa, L. Goitre and S. F. Retta (2018). "KRIT1 loss-of-function induces a chronic Nrf2-mediated adaptive homeostasis that sensitizes cells to oxidative stress: Implication for Cerebral Cavernous Malformation disease." Free Radic Biol Med **115**: 202-218.

Antognelli, C., E. Trapani, S. Delle Monache, A. Perrelli, C. Fornelli, F. Retta, P. Cassoni, V. N. Talesa and S. F. Retta (2018). "Data in support of sustained upregulation of adaptive redox homeostasis mechanisms caused by KRIT1 loss-of-function." Data Brief **16**: 929-938.

Armeni, T., L. Cianfruglia, F. Piva, L. Urbanelli, M. Luisa Caniglia, A. Pugnaloni and G. Principato (2014). "S-D-Lactoylglutathione can be an alternative supply of mitochondrial glutathione." Free Radic Biol Med **67**: 451-459.

Ashrafizadeh, M., Z. Ahmadi, T. Farkhondeh and S. Samarghandian (2020). "Modulatory effects of statins on the autophagy: A therapeutic perspective." J Cell Physiol **235**(4): 3157-3168.

Awad, I. A. and S. P. Polster (2019). "Cavernous angiomas: deconstructing a neurosurgical disease." J Neurosurg **131**(1): 1-13.

Balcerczyk, A. and G. Bartosz (2003). "Thiols are main determinants of total antioxidant capacity of cellular homogenates." Free Radic Res **37**(5): 537-541.

Ballatori, N., S. M. Krance, S. Notenboom, S. Shi, K. Tieu and C. L. Hammond (2009). "Glutathione dysregulation and the etiology and progression of human diseases." Biol Chem **390**(3): 191-214.

Balzac, F., M. Avolio, S. Degani, I. Kaverina, M. Torti, L. Silengo, J. V. Small and S. F. Retta (2005). "E-cadherin endocytosis regulates the activity of Rap1: a traffic light GTPase at the crossroads between cadherin and integrin function." J Cell Sci **118**(Pt 20): 4765-4783.

Bansode, S. B., A. D. Chougale, R. S. Joshi, A. P. Giri, S. L. Bodhankar, A. M. Harsulkar and M. J. Kulkarni (2013). "Proteomic analysis of protease resistant proteins in the diabetic rat kidney." Mol Cell Proteomics **12**(1): 228-236.

Baranoski, J. F. and A. F. Ducruet (2019). "Nanoparticle-Facilitated Delivery of Antioxidant Therapy following Aneurysmal Subarachnoid Hemorrhage." Neurosurgery **85**(2): E174-E175.

Batra, S., D. Lin, P. F. Recinos, J. Zhang and D. Rigamonti (2009). "Cavernous malformations: natural history, diagnosis and treatment." Nat Rev Neurol **5**(12): 659-670.

Battaglia, L. and M. Gallarate (2012). "Lipid nanoparticles: state of the art, new preparation methods and challenges in drug delivery." Expert Opin Drug Deliv **9**(5): 497-508.

Battaglia, L., P. P. Panciani, E. Muntoni, M. T. Capucchio, E. Biasibetti, P. De Bonis, S. Mioletti, M. Fontanella and S. Swaminathan (2018). "Lipid nanoparticles for intranasal administration: application to nose-to-brain delivery." Expert Opin Drug Deliv **15**(4): 369-378.

Bravi, L., M. Malinverno, F. Pisati, N. Rudini, R. Cuttano, R. Pallini, M. Martini, L. M. Larocca, M. Locatelli, V. Levi, G. A. Bertani, E. Dejana and M. G. Lampugnani (2016). "Endothelial Cells Lining Sporadic Cerebral Cavernous Malformation Cavernomas Undergo Endothelial-to-Mesenchymal Transition." Stroke **47**(3): 886-890.

Brinjikji, W., A. E. El-Masri, J. T. Wald, K. D. Flemming and G. Lanzino (2017). "Prevalence of cerebral cavernous malformations associated with developmental venous anomalies increases with age." Childs Nerv Syst **33**(9): 1539-1543.

Brunetti, V., H. Chibli, R. Fiammengo, A. Galeone, M. A. Malvindi, G. Vecchio, R. Cingolani, J. L. Nadeau and P. P. Pompa (2013). "InP/ZnS as a safer alternative to CdSe/ZnS core/shell quantum dots: in vitro and in vivo toxicity assessment." Nanoscale **5**(1): 307-317.

Bryan, H. K., A. Olayanju, C. E. Goldring and B. K. Park (2013). "The Nrf2 cell defence pathway: Keap1-dependent and -independent mechanisms of regulation." Biochem Pharmacol **85**(6): 705-717.

Béraud-Dufour, S., R. Gautier, C. Albiges-Rizo, P. Chardin and E. Faurobert (2007). "Krit 1 interactions with microtubules and membranes are regulated by Rap1 and integrin cytoplasmic domain associated protein-1." FEBS J **274**(21): 5518-5532.

Cai, P., X. Zhang, M. Wang, Y. L. Wu and X. Chen (2018). "Combinatorial Nano-Bio Interfaces." ACS Nano **12**(6): 5078-5084.

Campbell, P. G., P. Jabbour, S. Yadla and I. A. Awad (2010). "Emerging clinical imaging techniques for cerebral cavernous malformations: a systematic review." Neurosurg Focus **29**(3): E6.

Carrizzo, A., M. Forte, A. Damato, V. Trimarco, F. Salzano, M. Bartolo, A. Maciag, A. A. Puca and C. Vecchione (2013). "Antioxidant effects of resveratrol in cardiovascular, cerebral and metabolic diseases." Food Chem Toxicol **61**: 215-226.

Carvalho, A. N., C. Marques, R. C. Guedes, M. Castro-Caldas, E. Rodrigues, J. van Horssen and M. J. Gama (2016). "S-Glutathionylation of Keap1: a new role for glutathione S-transferase pi in neuronal protection." FEBS Lett **590**(10): 1455-1466.

Castagna, M., Y. Takai, K. Kaibuchi, K. Sano, U. Kikkawa and Y. Nishizuka (1982). "Direct activation of calcium-activated, phospholipid-dependent protein kinase by tumor-promoting phorbol esters." J Biol Chem **257**(13): 7847-7851.

Cavalcanti, D. D., M. Y. Kalani, N. L. Martirosyan, J. Eales, R. F. Spetzler and M. C. Preul (2012). "Cerebral cavernous malformations: from genes to proteins to disease." J Neurosurg **116**(1): 122-132.

Chen, C. A., T. Y. Wang, S. Varadharaj, L. A. Reyes, C. Hemann, M. A. Talukder, Y. R. Chen, L. J. Druhan and J. L. Zweier (2010). "S-glutathionylation uncouples eNOS and regulates its cellular and vascular function." Nature **468**(7327): 1115-1118.

Chen, S. H. and G. Lahav (2016). "Two is better than one; toward a rational design of combinatorial therapy." Curr Opin Struct Biol **41**: 145-150.

Choi, A. M., S. W. Ryter and B. Levine (2013). "Autophagy in human health and disease." N Engl J Med **368**(7): 651-662.

Choquet, H., J. Nelson, L. Pawlikowska, C. E. McCulloch, A. Akers, B. Baca, Y. Khan, B. Hart, L. Morrison and H. Kim (2014). "Association of cardiovascular risk factors with disease severity in cerebral cavernous malformation type 1 subjects with the common Hispanic mutation." Cerebrovasc Dis **37**(1): 57-63.

Choquet, H., L. Pawlikowska, M. T. Lawton and H. Kim (2015). "Genetics of cerebral cavernous malformations: current status and future prospects." J Neurosurg Sci **59**(3): 211-220.

Choquet, H., E. Trapani, L. Goitre, L. Trabalzini, A. Akers, M. Fontanella, B. L. Hart, L. A. Morrison, L. Pawlikowska, H. Kim and S. F. Retta (2016). "Cytochrome P450 and matrix metalloproteinase genetic modifiers of disease severity in Cerebral Cavernous Malformation type 1." Free Radic Biol Med **92**: 100-109.

Cianfruglia, L., A. Perrelli, C. Fornelli, A. Magini, S. Gorbi, A. M. Salzano, C. Antognelli, F. Retta, V. Benedetti, P. Cassoni, C. Emiliani, G. Principato, A. Scaloni, T. Armeni and S. F. Retta (2019). "KRIT1 Loss-Of-Function Associated with Cerebral Cavernous Malformation Disease Leads to Enhanced." Antioxidants (Basel) **8**(1).

Cooper, A. D., N. G. Campeau and I. Meissner (2008). "Susceptibility-weighted imaging in familial cerebral cavernous malformations." Neurology **71**(5): 382.

Czubayko, M., P. Knauth, T. Schlüter, V. Florian and R. Bohnensack (2006). "Sorting nexin 17, a non-self-assembling and a PtdIns(3)P high class affinity protein, interacts with the cerebral cavernous malformation related protein KRIT1." Biochem Biophys Res Commun **345**(3): 1264-1272.

D'Ambrosio, C., S. Arena, G. Fulcoli, M. H. Scheinfeld, D. Zhou, L. D'Adamio and A. Scaloni (2006). "Hyperphosphorylation of JNK-interacting protein 1, a protein associated with Alzheimer disease." Mol Cell Proteomics **5**(1): 97-113.

Dalle-Donne, I., R. Rossi, G. Colombo, D. Giustarini and A. Milzani (2009). "Protein S-glutathionylation: a regulatory device from bacteria to humans." Trends Biochem Sci **34**(2): 85-96.

Dalle-Donne, I., R. Rossi, D. Giustarini, R. Colombo and A. Milzani (2007). "S-glutathionylation in protein redox regulation." Free Radic Biol Med **43**(6): 883-898.

De Luca, E., D. Pedone, M. Moglianetti, D. Pulcini, A. Perrelli, S. F. Retta and P. P. Pompa (2018). "Multifunctional Platinum@BSA-Rapamycin Nanocarriers for the Combinatorial Therapy of Cerebral Cavernous Malformation." ACS Omega **3**(11): 15389-15398.

De Luca, E., A. Perrelli, et al. (2020). "Protein Kinase Cα (PKCα) regulates the nucleocytoplasmic shuttling of KRIT1." *Submitted*.

de Souza, J. M., R. C. Domingues, L. C. Cruz, F. S. Domingues, T. Iasbeck and E. L. Gasparetto (2008). "Susceptibility-weighted imaging for the evaluation of patients with familial cerebral cavernous malformations: a comparison with t2-weighted fast spin-echo and gradient-echo sequences." AJNR Am J Neuroradiol **29**(1): 154-158.

Di Domenico, F., A. Tramutola, E. Barone, C. Lanzillotta, O. Defever, A. Arena, I. Zuliani, C. Foppoli, F. Iavarone, F. Vincenzoni, M. Castagnola, D. A. Butterfield and M. Perluigi (2019).

"Restoration of aberrant mTOR signaling by intranasal rapamycin reduces oxidative damage: Focus on HNE-modified proteins in a mouse model of down syndrome." Redox Biol **23**: 101162.

Di Napoli, M. (2004). "Benefits of statins in cerebrovascular disease." Curr Opin Investig Drugs **5**(3): 295-305.

DiStefano, P. V., J. M. Kuebel, I. H. Sarelius and A. J. Glading (2014). "KRIT1 protein depletion modifies endothelial cell behavior via increased vascular endothelial growth factor (VEGF) signaling." J Biol Chem **289**(47): 33054-33065.

Doller, A., A. Huwiler, R. Müller, H. H. Radeke, J. Pfeilschifter and W. Eberhardt (2007). "Protein kinase C alpha-dependent phosphorylation of the mRNA-stabilizing factor HuR: implications for posttranscriptional regulation of cyclooxygenase-2." Mol Biol Cell **18**(6): 2137-2148.

Doller, A., K. Schlepckow, H. Schwalbe, J. Pfeilschifter and W. Eberhardt (2010). "Tandem phosphorylation of serines 221 and 318 by protein kinase Cdelta coordinates mRNA binding and nucleocytoplasmic shuttling of HuR." Mol Cell Biol **30**(6): 1397-1410.

Draheim, K. M., O. S. Fisher, T. J. Boggon and D. A. Calderwood (2014). "Cerebral cavernous malformation proteins at a glance." J Cell Sci **127**(Pt 4): 701-707.

Draheim, K. M., C. Huet-Calderwood, B. Simon and D. A. Calderwood (2017). "Nuclear Localization of Integrin Cytoplasmic Domain-associated Protein-1 (ICAP1) Influences β1 Integrin Activation and Recruits Krev/Interaction Trapped-1 (KRIT1) to the Nucleus." J Biol Chem **292**(5): 1884-1898.

Faurobert, E., C. Rome, J. Lisowska, S. Manet-Dupé, G. Boulday, M. Malbouyres, M. Balland, A. P. Bouin, M. Kéramidas, D. Bouvard, J. L. Coll, F. Ruggiero, E. Tournier-Lasserve and C. Albiges-Rizo (2013). "CCM1-ICAP-1 complex controls β1 integrin-dependent endothelial contractility and fibronectin remodeling." J Cell Biol **202**(3): 545-561.

Finetti, F., A. Moglia, I. Schiavo, S. Donnini, G. N. Berta, F. Di Scipio, A. Perrelli, C. Fornelli, L. Trabalzini and S. F. Retta (2018). "Yeast-Derived Recombinant Avenanthramides Inhibit Proliferation, Migration and Epithelial Mesenchymal Transition of Colon Cancer Cells." Nutrients **10**(9).

Fisher, O. S. and T. J. Boggon (2014). "Signaling pathways and the cerebral cavernous malformations proteins: lessons from structural biology." Cell Mol Life Sci **71**(10): 1881-1892.

Fisher, O. S., W. Liu, R. Zhang, A. L. Stiegler, S. Ghedia, J. L. Weber and T. J. Boggon (2015). "Structural basis for the disruption of the cerebral cavernous malformations 2 (CCM2) interaction with Krev interaction trapped 1 (KRIT1) by disease-associated mutations." J Biol Chem **290**(5): 2842-2853.

Flemming, K. D. (2017). "Clinical Management of Cavernous Malformations." Curr Cardiol Rep **19**(12): 122.

Fontanella, M. (2015). Cerebral cavernous malformations (CCM). Minerva Medica, Minerva Medica.

Fontanella, M. and S. Bacigaluppi (2015). "Treatment of cerebral cavernous malformations: where do we stand?" J Neurosurg Sci **59**(3): 199-200.

Fontanella, M. M., P. P. Panciani, G. Spena, E. Roca, K. Migliorati, C. Ambrosi, C. L. Sturiale and S. F. Retta (2015). "Professional athletes and cerebral cavernomas: an obstacle to overcome." J Sports Med Phys Fitness **55**(9): 1046-1047.

Francalanci, F., M. Avolio, E. De Luca, D. Longo, V. Menchise, P. Guazzi, F. Sgrò, M. Marino, L. Goitre, F. Balzac, L. Trabalzini and S. F. Retta (2009). "Structural and functional differences between KRIT1A and KRIT1B isoforms: a framework for understanding CCM pathogenesis." Exp Cell Res **315**(2): 285-303.

Gallogly, M. M., D. W. Starke and J. J. Mieyal (2009). "Mechanistic and kinetic details of catalysis of thiol-disulfide exchange by glutaredoxins and potential mechanisms of regulation." Antioxid Redox Signal **11**(5): 1059-1081.

Galougahi, K. K., C. C. Liu, C. Gentile, C. Kok, A. Nunez, A. Garcia, N. A. Fry, M. J. Davies, C. L. Hawkins, H. H. Rasmussen and G. A. Figtree (2014). "Glutathionylation mediates angiotensin II-induced eNOS uncoupling, amplifying NADPH oxidase-dependent endothelial dysfunction." J Am Heart Assoc **3**(2): e000731.

Gastaldi, L., L. Battaglia, E. Peira, D. Chirio, E. Muntoni, I. Solazzi, M. Gallarate and F. Dosio (2014). "Solid lipid nanoparticles as vehicles of drugs to the brain: current state of the art." Eur J Pharm Biopharm **87**(3): 433-444.

Gibson, C. C., C. T. Davis, W. Zhu, J. A. Bowman-Kirigin, A. E. Walker, Z. Tai, K. R. Thomas, A. J. Donato, L. A. Lesniewski and D. Y. Li (2015). "Dietary Vitamin D and Its Metabolites Non-Genomically Stabilize the Endothelium." PLoS One **10**(10): e0140370.

Gibson, C. C., W. Zhu, C. T. Davis, J. A. Bowman-Kirigin, A. C. Chan, J. Ling, A. E. Walker, L. Goitre, S. Delle Monache, S. F. Retta, Y. T. Shiu, A. H. Grossmann, K. R. Thomas, A. J. Donato, L. A. Lesniewski, K. J. Whitehead and D. Y. Li (2015). "Strategy for identifying repurposed drugs for the treatment of cerebral cavernous malformation." Circulation **131**(3): 289-299.

Gingras, A. R., J. J. Liu and M. H. Ginsberg (2012). "Structural basis of the junctional anchorage of the cerebral cavernous malformations complex." J Cell Biol **199**(1): 39-48.

Gingras, A. R., W. Puzon-McLaughlin and M. H. Ginsberg (2013). "The structure of the ternary complex of Krev interaction trapped 1 (KRIT1) bound to both the Rap1 GTPase and the heart of glass (HEG1) cytoplasmic tail." J Biol Chem **288**(33): 23639-23649.

Giorgi, C., C. Agnoletto, C. Baldini, A. Bononi, M. Bonora, S. Marchi, S. Missiroli, S. Patergnani, F. Poletti, A. Rimessi, B. Zavan and P. Pinton (2010). "Redox control of protein kinase C: cell- and disease-specific aspects." Antioxid Redox Signal **13**(7): 1051-1085.

Giustarini, D., F. Galvagni, A. Tesei, A. Farolfi, M. Zanoni, S. Pignatta, A. Milzani, I. M. Marone, I. Dalle-Donne, R. Nassini and R. Rossi (2015). "Glutathione, glutathione disulfide, and S-glutathionylated proteins in cell cultures." Free Radic Biol Med **89**: 972-981.

Glading, A., J. Han, R. A. Stockton and M. H. Ginsberg (2007). "KRIT-1/CCM1 is a Rap1 effector that regulates endothelial cell cell junctions." J Cell Biol **179**(2): 247-254.

Glading, A. J. and M. H. Ginsberg (2010). "Rap1 and its effector KRIT1/CCM1 regulate beta-catenin signaling." Dis Model Mech **3**(1-2): 73-83.

Goitre, L., F. Balzac, S. Degani, P. Degan, S. Marchi, P. Pinton and S. F. Retta (2010). "KRIT1 regulates the homeostasis of intracellular reactive oxygen species." PLoS One **5**(7): e11786.

Goitre, L., E. De Luca, S. Braggion, E. Trapani, M. Guglielmotto, F. Biasi, M. Forni, A. Moglia, L. Trabalzini and S. F. Retta (2014). "KRIT1 loss of function causes a ROS-dependent upregulation of c-Jun." Free Radic Biol Med **68**: 134-147.

Goitre, L., P. V. DiStefano, A. Moglia, N. Nobiletti, E. Baldini, L. Trabalzini, J. Keubel, E. Trapani, V. V. Shuvaev, V. R. Muzykantov, I. H. Sarelius, S. F. Retta and A. J. Glading (2017). "Up-regulation of NADPH oxidase-mediated redox signaling contributes to the loss of barrier function in KRIT1 deficient endothelium." Sci Rep **7**(1): 8296.

Goitre, L., C. Fornelli, A. Zotta, A. Perrelli and S. F. Retta (2020). "Production of KRIT1-knockout and KRIT1-knockin Mouse Embryonic Fibroblasts as Cellular Models of CCM Disease." Methods Mol Biol **2152**: 151-167.

Gopalakrishna, R. and S. Jaken (2000). "Protein kinase C signaling and oxidative stress." Free Radic Biol Med **28**(9): 1349-1361.

Goyal, P., D. Pandey, A. Behring and W. Siess (2005). "Inhibition of nuclear import of LIMK2 in endothelial cells by protein kinase C-dependent phosphorylation at Ser-283." J Biol Chem **280**(30): 27569-27577.

Guan, J. and W. T. Couldwell (2013). "Evaluating the role of CCM1 loss-of-function-induced endothelial-to-mesenchymal transition in cavernous malformation development." World Neurosurg **80**(5): 444-446.

Guazzi, P., L. Goitre, E. Ferro, V. Cutano, C. Martino, L. Trabalzini and S. F. Retta (2012). "Identification of the Kelch family protein Nd1-L as a novel molecular interactor of KRIT1." PLoS One **7**(9): e44705.

Han, J., R. M. Weisbrod, D. Shao, Y. Watanabe, X. Yin, M. M. Bachschmid, F. Seta, Y. M. W. Janssen-Heininger, R. Matsui, M. Zang, N. M. Hamburg and R. A. Cohen (2016). "The redox mechanism for vascular barrier dysfunction associated with metabolic disorders: Glutathionylation of Rac1 in endothelial cells." Redox Biol **9**: 306-319.

Inoguchi, T., T. Sonta, H. Tsubouchi, T. Etoh, M. Kakimoto, N. Sonoda, N. Sato, N. Sekiguchi, K. Kobayashi, H. Sumimoto, H. Utsumi and H. Nawata (2003). "Protein kinase C-dependent increase in reactive oxygen species (ROS) production in vascular tissues of diabetes: role of vascular NAD(P)H oxidase." J Am Soc Nephrol **14**(8 Suppl 3): S227-232.

Iyengar, R. (2013). "Complex diseases require complex therapies." EMBO Rep **14**(12): 1039-1042.

Kar, S., A. Samii and H. Bertalanffy (2015). "PTEN/PI3K/Akt/VEGF signaling and the cross talk to KRIT1, CCM2, and PDCD10 proteins in cerebral cavernous malformations." Neurosurg Rev **38**(2): 229-236; discussion 236-227.

Karimi, M., S. Bahrami, S. B. Ravari, P. S. Zangabad, H. Mirshekari, M. Bozorgomid, S. Shahreza, M. Sori and M. R. Hamblin (2016). "Albumin nanostructures as advanced drug delivery systems." Expert Opin Drug Deliv **13**(11): 1609-1623.

Kaspar, J. W., S. K. Niture and A. K. Jaiswal (2009). "Nrf2:INrf2 (Keap1) signaling in oxidative stress." Free Radic Biol Med **47**(9): 1304-1309.

Kim, C. K., T. Kim, I. Y. Choi, M. Soh, D. Kim, Y. J. Kim, H. Jang, H. S. Yang, J. Y. Kim, H. K. Park, S. P. Park, S. Park, T. Yu, B. W. Yoon, S. H. Lee and T. Hyeon (2012). "Ceria nanoparticles that can protect against ischemic stroke." Angew Chem Int Ed Engl **51**(44): 11039-11043.

Kim, H. A., A. Perrelli, A. Ragni, F. Retta, T. M. De Silva, C. G. Sobey and S. F. Retta (2020). "Vitamin D Deficiency and the Risk of Cerebrovascular Disease." Antioxidants (Basel) **9**(4).

Kleaveland, B., X. Zheng, J. J. Liu, Y. Blum, J. J. Tung, Z. Zou, S. M. Sweeney, M. Chen, L. Guo, M. M. Lu, D. Zhou, J. Kitajewski, M. Affolter, M. H. Ginsberg and M. L. Kahn (2009). "Regulation of cardiovascular development and integrity by the heart of glass-cerebral cavernous malformation protein pathway." Nat Med **15**(2): 169-176.

Kovacic, J. C., N. Mercader, M. Torres, M. Boehm and V. Fuster (2012). "Epithelial-to-mesenchymal and endothelial-to-mesenchymal transition: from cardiovascular development to disease." Circulation **125**(14): 1795-1808.

Lendahl, U., P. Nilsson and C. Betsholtz (2019). "Emerging links between cerebrovascular and neurodegenerative diseases-a special role for pericytes." **20**(11): e48070.

Lesniewski, L. A., D. R. Seals, A. E. Walker, G. D. Henson, M. W. Blimline, D. W. Trott, G. C. Bosshardt, T. J. LaRocca, B. R. Lawson, M. C. Zigler and A. J. Donato (2017). "Dietary rapamycin supplementation reverses age-related vascular dysfunction and oxidative stress, while modulating nutrient-sensing, cell cycle, and senescence pathways." Aging Cell **16**(1): 17-26.

Li, X., R. Zhang, K. M. Draheim, W. Liu, D. A. Calderwood and T. J. Boggon (2012). "Structural basis for small G protein effector interaction of Ras-related protein 1 (Rap1) and adaptor protein Krev interaction trapped 1 (KRIT1)." J Biol Chem **287**(26): 22317-22327.

Liu, H., D. Rigamonti, A. Badr and J. Zhang (2011). "Ccm1 regulates microvascular morphogenesis during angiogenesis." J Vasc Res **48**(2): 130-140.

Liu, W., K. M. Draheim, R. Zhang, D. A. Calderwood and T. J. Boggon (2013). "Mechanism for KRIT1 release of ICAP1-mediated suppression of integrin activation." Mol Cell **49**(4): 719-729.

Loboda, A., M. Damulewicz, E. Pyza, A. Jozkowicz and J. Dulak (2016). "Role of Nrf2/HO-1 system in development, oxidative stress response and diseases: an evolutionarily conserved mechanism." Cell Mol Life Sci **73**(17): 3221-3247.

Mabray, M. C., A. Caprihan, J. Nelson, C. E. McCulloch, A. Zafar, H. Kim, B. L. Hart and L. Morrison (2019). "Effect of Simvastatin on Permeability in Cerebral Cavernous Malformation Type 1 Patients: Results from a Pilot Small Randomized Controlled Clinical Trial." Transl Stroke Res.

Macek Jilkova, Z., J. Lisowska, S. Manet, C. Verdier, V. Deplano, C. Geindreau, E. Faurobert, C. Albigès-Rizo and A. Duperray (2014). "CCM proteins control endothelial β1 integrin dependent response to shear stress." Biol Open **3**(12): 1228-1235.

Maddaluno, L., N. Rudini, R. Cuttano, L. Bravi, C. Giampietro, M. Corada, L. Ferrarini, F. Orsenigo, E. Papa, G. Boulday, E. Tournier-Lasserve, F. Chapon, C. Richichi, S. F. Retta, M. G. Lampugnani and E. Dejana (2013). "EndMT contributes to the onset and progression of cerebral cavernous malformations." Nature **498**(7455): 492-496.

Marchi, S., M. Corricelli, E. Trapani, L. Bravi, A. Pittaro, S. Delle Monache, L. Ferroni, S. Patergnani, S. Missiroli, L. Goitre, L. Trabalzini, A. Rimessi, C. Giorgi, B. Zavan, P. Cassoni, E. Dejana, S. F. Retta and P. Pinton (2015). "Defective autophagy is a key feature of cerebral cavernous malformations." EMBO Mol Med **7**(11): 1403-1417.

Marchi, S., S. F. Retta and P. Pinton (2016). "Cellular processes underlying cerebral cavernous malformations: Autophagy as another point of view." Autophagy **12**(2): 424-425.

Marchi, S., E. Trapani, M. Corricelli, L. Goitre, P. Pinton and S. F. Retta (2016). "Beyond multiple mechanisms and a unique drug: Defective autophagy as pivotal player in cerebral cavernous malformation pathogenesis and implications for targeted therapies." Rare Dis **4**(1): e1142640.

McSweeney, S. R., E. Warabi and R. C. Siow (2016). "Nrf2 as an Endothelial Mechanosensitive Transcription Factor: Going With the Flow." Hypertension **67**(1): 20-29.

Mellor, H. and P. J. Parker (1998). "The extended protein kinase C superfamily." Biochem J **332 (Pt 2)**: 281-292.

Meng, G., C. Bai, T. Yu, Z. Wu, X. Liu, J. Zhang and J. zhao (2014). "The association between cerebral developmental venous anomaly and concomitant cavernous malformation: an observational study using magnetic resonance imaging." BMC Neurol **14**: 50.

Moglia, A., L. Goitre, S. Gianoglio, E. Baldini, E. Trapani, A. Genre, A. Scattina, G. Dondo, L. Trabalzini, J. Beekwilder and S. F. Retta (2015). "Evaluation of the bioactive properties of avenanthramide analogs produced in recombinant yeast." Biofactors **41**(1): 15-27.

Moglianetti, M., E. De Luca, D. Pedone, R. Marotta, T. Catelani, B. Sartori, H. Amenitsch, S. F. Retta and P. P. Pompa (2016). "Platinum nanozymes recover cellular ROS homeostasis in an oxidative stress-mediated disease model." Nanoscale **8**(6): 3739-3752.

Moglianetti, M., D. Pedone, G. Udayan, S. F. Retta, D. Debellis, R. Marotta, A. Turco, S. Rella, C. Malitesta, G. Bonacucina, E. De Luca and P. P. Pompa (2020). "Intracellular Antioxidant Activity of Biocompatible Citrate-Capped Palladium Nanozymes." Nanomaterials (Basel) **10**(1).

Moore, S. A., R. D. Brown, T. J. Christianson and K. D. Flemming (2014). "Long-term natural history of incidentally discovered cavernous malformations in a single-center cohort." J Neurosurg **120**(5): 1188-1192.

Morse, D., L. Lin, A. M. Choi and S. W. Ryter (2009). "Heme oxygenase-1, a critical arbitrator of cell death pathways in lung injury and disease." Free Radic Biol Med **47**(1): 1-12.

Mulder, W. J., G. J. Strijkers, A. W. Griffioen, L. van Bloois, G. Molema, G. Storm, G. A. Koning and K. Nicolay (2004). "A liposomal system for contrast-enhanced magnetic resonance imaging of molecular targets." Bioconjug Chem **15**(4): 799-806.

Nass, N., K. Vogel, B. Hofmann, P. Presek, R. E. Silber and A. Simm (2010). "Glycation of PDGF results in decreased biological activity." Int J Biochem Cell Biol **42**(5): 749-754.

Newton, A. C. (2001). "Protein kinase C: structural and spatial regulation by phosphorylation, cofactors, and macromolecular interactions." Chem Rev **101**(8): 2353-2364.

Panieri, E. and M. M. Santoro (2015). "ROS signaling and redox biology in endothelial cells." Cell Mol Life Sci **72**(17): 3281-3303.

Pedone, D., M. Moglianetti, E. De Luca, G. Bardi and P. P. Pompa (2017). "Platinum nanoparticles in nanobiomedicine." Chem Soc Rev **46**(16): 4951-4975.

Perrelli, A., P. Fatehbasharzad, et al. (2020). "Precision Nanomedicine for Cerebrovascular Diseases with Emphasis on Cerebral Cavernous Malformation (CCM)." *Submitted*.

Perrelli, A., L. Goitre, A. M. Salzano, A. Moglia, A. Scaloni and S. F. Retta (2018). "Biological Activities, Health Benefits, and Therapeutic Properties of Avenanthramides: From Skin Protection to Prevention and Treatment of Cerebrovascular Diseases." Oxid Med Cell Longev **2018**: 6015351.

Perrelli, A. and S. F. Retta (2020). "Fluorescence Analysis of Reactive Oxygen Species (ROS) in Cellular Models of Cerebral Cavernous Malformation Disease." Methods Mol Biol **2152**: 451-465.

Petersen, T. A., L. A. Morrison, R. M. Schrader and B. L. Hart (2010). "Familial versus sporadic cavernous malformations: differences in developmental venous anomaly association and lesion phenotype." AJNR Am J Neuroradiol **31**(2): 377-382.

Qian, M., Q. Li, M. Zhang, X. Xu, Q. Shen, H. Chen, X. Wang, T. Liu and Y. Cheng (2020). "Multidisciplinary therapy strategy of precision medicine in clinical practice." Clin Transl Med **10**(1): 116-124.

Renz, M., C. Otten, E. Faurobert, F. Rudolph, Y. Zhu, G. Boulday, J. Duchene, M. Mickoleit, A. C. Dietrich, C. Ramspacher, E. Steed, S. Manet-Dupé, A. Benz, D. Hassel, J. Vermot, J. Huisken, E. Tournier-Lasserve, U. Felbor, U. Sure, C. Albiges-Rizo and S. Abdelilah-Seyfried (2015). "Regulation of β1 integrin-Klf2-mediated angiogenesis by CCM proteins." Dev Cell **32**(2): 181-190.

Represa, A., J. C. Deloulme, M. Sensenbrenner, Y. Ben-Ari and J. Baudier (1990). "Neurogranin: immunocytochemical localization of a brain-specific protein kinase C substrate." J Neurosci **10**(12): 3782-3792.

Retta, S. F., M. Avolio, F. Francalanci, S. Procida, F. Balzac, S. Degani, G. Tarone and L. Silengo (2004). "Identification of Krit1B: a novel alternative splicing isoform of cerebral cavernous malformation gene-1." Gene **325**: 63-78.

Retta, S. F. and A. J. Glading (2016). "Oxidative stress and inflammation in cerebral cavernous malformation disease pathogenesis: Two sides of the same coin." Int J Biochem Cell Biol **81**(Pt B): 254-270.

Retta, S. F., A. Perrelli, L. Trabalzini and F. Finetti (2020). "From Genes and Mechanisms to Molecular-Targeted Therapies: The Long Climb to the Cure of Cerebral Cavernous Malformation (CCM) Disease." Methods Mol Biol **2152**: 3-25.

Rigamonti, D. (2011). Cavernous Malformations of the Nervous System. Cambridge University Press, Cambridge University Press.

Sakamoto, H., T. Mashima, K. Yamamoto and T. Tsuruo (2002). "Modulation of heat-shock protein 27 (Hsp27) anti-apoptotic activity by methylglyoxal modification." J Biol Chem **277**(48): 45770-45775.

Salzano, A. M., G. Novi, S. Arioli, S. Corona, D. Mora and A. Scaloni (2013). "Mono-dimensional blue native-PAGE and bi-dimensional blue native/urea-PAGE or/SDS-PAGE combined with nLC-

ESI-LIT-MS/MS unveil membrane protein heteromeric and homomeric complexes in Streptococcus thermophilus." J Proteomics **94**: 240-261.

Saraiva, C., C. Praça, R. Ferreira, T. Santos, L. Ferreira and L. Bernardino (2016). "Nanoparticle-mediated brain drug delivery: Overcoming blood-brain barrier to treat neurodegenerative diseases." J Control Release **235**: 34-47.

Schalkwijk, C. G., J. van Bezu, R. C. van der Schors, K. Uchida, C. D. Stehouwer and V. W. van Hinsbergh (2006). "Heat-shock protein 27 is a major methylglyoxal-modified protein in endothelial cells." FEBS Lett **580**(6): 1565-1570.

Schmalz, D., F. Kalkbrenner, F. Hucho and K. Buchner (1996). "Transport of protein kinase C alpha into the nucleus requires intact cytoskeleton while the transport of a protein containing a canonical nuclear localization signal does not." J Cell Sci **109 (Pt 9)**: 2401-2406.

Schulz, G. B., E. Wieland, J. Wüstehube-Lausch, G. Boulday, I. Moll, E. Tournier-Lasserve and A. Fischer (2015). "Cerebral Cavernous Malformation-1 Protein Controls DLL4-Notch3 Signaling Between the Endothelium and Pericytes." Stroke **46**(5): 1337-1343.

Scoditti, E., A. Nestola, M. Massaro, N. Calabriso, C. Storelli, R. De Caterina and M. A. Carluccio (2014). "Hydroxytyrosol suppresses MMP-9 and COX-2 activity and expression in activated human monocytes via PKCα and PKCβ1 inhibition." Atherosclerosis **232**(1): 17-24.

Serebriiskii, I., J. Estojak, G. Sonoda, J. R. Testa and E. A. Golemis (1997). "Association of Krev-1/rap1a with Krit1, a novel ankyrin repeat-containing protein encoded by a gene mapping to 7q21-22." Oncogene **15**(9): 1043-1049.

Simamora, P., J. M. Alvarez and S. H. Yalkowsky (2001). "Solubilization of rapamycin." Int J Pharm **213**(1-2): 25-29.

Sivandzade, F., S. Prasad, A. Bhalerao and L. Cucullo (2019). "NRF2 and NF-κB interplay in cerebrovascular and neurodegenerative disorders: Molecular mechanisms and possible therapeutic approaches." Redox Biol **21**: 101059.

Steinberg, S. F. (2015). "Mechanisms for redox-regulation of protein kinase C." Front Pharmacol **6**: 128.

Stiegler, A. L., R. Zhang, W. Liu and T. J. Boggon (2014). "Structural determinants for binding of sorting nexin 17 (SNX17) to the cytoplasmic adaptor protein Krev interaction trapped 1 (KRIT1)." J Biol Chem **289**(36): 25362-25373.

Stockton, R. A., R. Shenkar, I. A. Awad and M. H. Ginsberg (2010). "Cerebral cavernous malformations proteins inhibit Rho kinase to stabilize vascular integrity." J Exp Med **207**(4): 881-896.

Su, V. L., B. Simon, K. M. Draheim and D. A. Calderwood (2020). "Serine phosphorylation of the small phosphoprotein ICAP1 inhibits its nuclear accumulation." J Biol Chem **295**(10): 3269-3284.

Sun, R., S. Eriksson and L. Wang (2012). "Oxidative stress induced S-glutathionylation and proteolytic degradation of mitochondrial thymidine kinase 2." J Biol Chem **287**(29): 24304-24312.

Tai, W., Z. Chen, A. Barve, Z. Peng and K. Cheng (2014). "A novel rapamycin-polymer conjugate based on a new poly(ethylene glycol) multiblock copolymer." Pharm Res **31**(3): 706-719.

Tanriover, G., B. Sozen, A. Seker, T. Kilic, M. Gunel and N. Demir (2013). "Ultrastructural analysis of vascular features in cerebral cavernous malformations." Clin Neurol Neurosurg **115**(4): 438-444.

Tapeinos, C., M. Battaglini and G. Ciofani (2017). "Advances in the design of solid lipid nanoparticles and nanostructured lipid carriers for targeting brain diseases." J Control Release **264**: 306-332.

Tatsunami, R., T. Oba, K. Takahashi and Y. Tampo (2009). "Methylglyoxal causes dysfunction of thioredoxin and thioredoxin reductase in endothelial cells." J Pharmacol Sci **111**(4): 426-432.

Teixeira, M. I., C. M. Lopes, M. H. Amaral and P. C. Costa (2020). "Current insights on lipid nanocarrier-assisted drug delivery in the treatment of neurodegenerative diseases." Eur J Pharm Biopharm **149**: 192-217.

Topham, M. K., M. Bunting, G. A. Zimmerman, T. M. McIntyre, P. J. Blackshear and S. M. Prescott (1998). "Protein kinase C regulates the nuclear localization of diacylglycerol kinase-zeta." Nature **394**(6694): 697-700.

Trapani, E. and S. F. Retta (2015). "Cerebral cavernous malformation (CCM) disease: from monogenic forms to genetic susceptibility factors." J Neurosurg Sci **59**(3): 201-209.

Um, J. Y., H. M. Kim, S. H. Han, K. H. Cho, B. S. Moon and S. H. Hong (2006). "Glutathione s-transferase gene polymorphism and ischemic cerebrovascular disease." Int J Neurosci **116**(1): 55-65.

Valovka, T., F. Verdier, R. Cramer, A. Zhyvoloup, T. Fenton, H. Rebholz, M. L. Wang, M. Gzhegotsky, A. Lutsyk, G. Matsuka, V. Filonenko, L. Wang, C. G. Proud, P. J. Parker and I. T. Gout (2003). "Protein kinase C phosphorylates ribosomal protein S6 kinase betaII and regulates its subcellular localization." Mol Cell Biol **23**(3): 852-863.

van Balkom, B. W., P. J. Savelkoul, D. Markovich, E. Hofman, S. Nielsen, P. van der Sluijs and P. M. Deen (2002). "The role of putative phosphorylation sites in the targeting and shuttling of the aquaporin-2 water channel." J Biol Chem **277**(44): 41473-41479.

Vaughan, C. J. and N. Delanty (1999). "Neuroprotective properties of statins in cerebral ischemia and stroke." Stroke **30**(9): 1969-1973.

Vieceli Dalla Sega, F., R. Mastrocola, G. Aquila, F. Fortini, C. Fornelli, A. Zotta, A. S. Cento, A. Perrelli, E. Boda, A. Pannuti, S. Marchi, P. Pinton, R. Ferrari, P. Rizzo and S. F. Retta (2019). "KRIT1 Deficiency Promotes Aortic Endothelial Dysfunction." Int J Mol Sci **20**(19).

Wang, J., J. Li, N. Cao, Z. Li, J. Han and L. Li (2018). "Resveratrol, an activator of SIRT1, induces protective autophagy in non-small-cell lung cancer via inhibiting Akt/mTOR and activating p38-MAPK." Onco Targets Ther **11**: 7777-7786.

Whitehead, K. J., A. C. Chan, S. Navankasattusas, W. Koh, N. R. London, J. Ling, A. H. Mayo, S. G. Drakos, C. A. Jones, W. Zhu, D. A. Marchuk, G. E. Davis and D. Y. Li (2009). "The cerebral cavernous malformation signaling pathway promotes vascular integrity via Rho GTPases." Nat Med **15**(2): 177-184.

Woodcock, J., J. P. Griffin and R. E. Behrman (2011). "Development of novel combination therapies." N Engl J Med **364**(11): 985-987.

Wüstehube, J., A. Bartol, S. S. Liebler, R. Brütsch, Y. Zhu, U. Felbor, U. Sure, H. G. Augustin and A. Fischer (2010). "Cerebral cavernous malformation protein CCM1 inhibits sprouting angiogenesis by activating DELTA-NOTCH signaling." Proc Natl Acad Sci U S A **107**(28): 12640-12645.

Xue, M., N. Rabbani, H. Momiji, P. Imbasi, M. M. Anwar, N. Kitteringham, B. K. Park, T. Souma, T. Moriguchi, M. Yamamoto and P. J. Thornalley (2012). "Transcriptional control of glyoxalase 1 by Nrf2 provides a stress-responsive defence against dicarbonyl glycation." Biochem J **443**(1): 213-222.

Yan, F., W. Li, H. Jono, Q. Li, S. Zhang, J. D. Li and H. Shen (2008). "Reactive oxygen species regulate Pseudomonas aeruginosa lipopolysaccharide-induced MUC5AC mucin expression via PKC-NADPH oxidase-ROS-TGF-alpha signaling pathways in human airway epithelial cells." Biochem Biophys Res Commun **366**(2): 513-519.

Yoshitomi, T. and Y. Nagasaki (2011). "Nitroxyl radical-containing nanoparticles for novel nanomedicine against oxidative stress injury." Nanomedicine (Lond) **6**(3): 509-518.

Zafar, A., S. A. Quadri, M. Farooqui, A. Ikram, M. Robinson, B. L. Hart, M. C. Mabray, C. Vigil, A. T. Tang, M. L. Kahn, H. Yonas, M. T. Lawton, H. Kim and L. Morrison (2019). "Familial Cerebral Cavernous Malformations." Stroke **50**(5): 1294-1301.

Zawistowski, J. S., I. G. Serebriiskii, M. F. Lee, E. A. Golemis and D. A. Marchuk (2002). "KRIT1 association with the integrin-binding protein ICAP-1: a new direction in the elucidation of cerebral cavernous malformations (CCM1) pathogenesis." Hum Mol Genet **11**(4): 389-396.

Zawistowski, J. S., L. Stalheim, M. T. Uhlik, A. N. Abell, B. B. Ancrile, G. L. Johnson and D. A. Marchuk (2005). "CCM1 and CCM2 protein interactions in cell signaling: implications for cerebral cavernous malformations pathogenesis." Hum Mol Genet **14**(17): 2521-2531.

Zhang, J., R. E. Clatterbuck, D. Rigamonti, D. D. Chang and H. C. Dietz (2001). "Interaction between krit1 and icap1alpha infers perturbation of integrin beta1-mediated angiogenesis in the pathogenesis of cerebral cavernous malformation." Hum Mol Genet **10**(25): 2953-2960.

Zhang, J., P. Dubey, A. Padarti, A. Zhang, R. Patel, V. Patel, D. Cistola and A. Badr (2017). "Novel functions of CCM1 delimit the relationship of PTB/PH domains." Biochim Biophys Acta Proteins Proteom **1865**(10): 1274-1286.

Zhang, J., D. Rigamonti, H. C. Dietz and R. E. Clatterbuck (2007). "Interaction between krit1 and malcavernin: implications for the pathogenesis of cerebral cavernous malformations." Neurosurgery **60**(2): 353-359; discussion 359.

Zhang, R., X. Li and T. J. Boggon (2015). "Structural analysis of the KRIT1 ankyrin repeat and FERM domains reveals a conformationally stable ARD-FERM interface." J Struct Biol **192**(3): 449-456.

Zhuang, X. X., S. F. Wang, Y. Tan, J. X. Song, Z. Zhu, Z. Y. Wang, M. Y. Wu, C. Z. Cai, Z. J. Huang, J. Q. Tan, H. X. Su, M. Li and J. H. Lu (2020). "Pharmacological enhancement of TFEB-mediated autophagy alleviated neuronal death in oxidative stress-induced Parkinson's disease models." Cell Death Dis **11**(2): 128.

Zitka, O., S. Skalickova, J. Gumulec, M. Masarik, V. Adam, J. Hubalek, L. Trnkova, J. Kruseova, T. Eckschlager and R. Kizek (2012). "Redox status expressed as GSH:GSSG ratio as a marker for oxidative stress in paediatric tumour patients." Oncol Lett **4**(6): 1247-1253.